

Department of Physics and Astronomy

University of Heidelberg

Master thesis

in Physics

submitted by

Elsa Wilken

born in Hamburg

2018

Retrieval Advances of BrO/SO₂ Molar Ratios from NOVAC

This Master thesis has been carried out by Elsa Wilken

at the

Institute for Environmental Physics, University of Heidelberg,

Germany

under the supervision of

Prof. Ulrich Platt

Optimierte Bestimmung des Molaren BrO/SO₂ Verhältnisses aus NO-VAC Daten

Die Messung der absoluten Menge und des Verhältnisses von Vulkanischen gas Emissionen geben Einsicht in magmatische Prozesse. Das Network for Observation of Volcanic and Atmospheric Change (NOVAC) verfügt über ein System an automatisierten UV-Spektrometern, welche die Gas Emissionen der Vulkane aufzeichnen. Der Ausstoß von BrO und SO₂ kann mithilfe von Differenzieller optischer Absorptionsspektroskopie (DOAS) aus den aufgenommenen Spektren bestimmt werden wobei die optische Absorption in der Fahne mit einem Hintergrundspektrum verglichen wird. Dies setzt voraus, dass das Hintergrund Spektrum nicht durch Vulkanische Gase beeinträchtigt ist. Typischerweise wird das Hintergrund Spektrum für einen Scan ein Höhenwinkel gewählt welcher als außerhalb der Fahne liegend identifiziert wird. Es hat sich jedoch gezeigt, dass auch diese Spektren noch durch Vulkanische Emissionen verunreinigt sein können. Als alternative Referenzspektren könnten 1) ein theoretisches Solar Atlas Spektrum oder 2) ein nicht verunreinigtes referenz Spektrum des selben Messgeräts dienen. Option 1) hat den Nachteil einer verringerten Messgenauigkeit, da Instrumenteneffekte hier modelliert werden müssen. Option 2) setzt voraus, dass das Referenzspektrum unter ähnlichen Wetter- und Strahlungsbedingungen aufgenommen wurde. Wir verwenden die erste Methode um Kontaminierung zu identifizieren und greifen für die Bestimmung der Gas Konzentration auf die zweite Methode zurück um eine hohe fit Qualität sicher zu stellen. Stellen unsere Methode für NOVAC Daten von den Vulkanen Tungurahua und Nevado Del Ruiz vor.

Retrieval advances of BrO/SO₂ molar ratios from NOVAC:

Measurements of magnitude and composition of volcanic gas emissions allow insights in magmatic processes. Within the Network for Observation of Volcanic and Atmospheric Change(NOVAC) automatically scanning UV-spectrometers are monitoring gas emission at volcanoes. The emissions of BrO and SO₂ can be retrieved from the recorded spectra by applying Differential Optical Absorption Spectroscopy(DOAS) and comparing the optical absorption of the volcanic plume to the background. Therefore, the background spectrum must not be affected by volcanic influence. Classically, the background spectrum is taken from the same scan but from an elevation angle which has been identified to be outside of the volcanic plume. However, experience shows those background spectra can still be contaminated by volcanic gases. Alternatively reference spectra can be derived from 1) a theoretical solar atlas spectrum or 2) a volcanic-gas-free reference spectrum recorded by the same instrument. 1) comes with a drawback of reduced precision, as the instrumental effects have to be modeled and added to the retrieval. For 2), the alternative reference spectrum should be recorded at similar conditions with respect to meteorology and radiation. We use the first option to check for contamination and the second to evaluate the spectra to maintain a god fit quality. We present our approach and its results when applied on NOVAC data from Tungurahua and Nevado Del Ruiz.

Contents

1	Introduction	6
I	Theoretical background	9
2	Volcanism and volcanic chemistry	10
2.1	Volcanism	10
2.2	Volcanic gases and their impact on the climate	10
2.3	Volcanic degassing	12
2.4	Volcanic plume chemistry	12
2.4.1	Sulphur species	12
2.4.2	Bromine oxide	13
2.5	Using the BrO/SO ₂ ratio to study volcanic activity	15
3	Remote sensing of volcanic gases	21
3.1	Differential Optical Absorption Spectroscopy (DOAS)	23
3.1.1	Technical implementation of the DOAS approach	24
II	Evaluation of the data of Tungurahua and Nevado Del Ruiz	27
4	Network for Observation of Volcanic and Atmospheric Change	28
4.1	Measurement routine	30
5	Evaluation routine	32
5.1	Conventional evaluation routine	32
5.2	Contamination problem	36
6	BrO evaluation and its limitations	42
6.1	BrO error dependence on external parameters	43
6.1.1	Temporal difference	44
6.1.2	Temperature	50
6.1.3	Daytime	52
6.1.4	Colorindex	54
6.1.5	Elevation Angle	58
6.1.6	Exposure time	61

6.2	BrO dependence on external parameters	71
7	Contamination based method	75
7.1	Fit data	77
7.2	Other approaches	80
7.2.1	Nearest neighbor approach	80
7.2.2	Iterative approach	82
8	Comparison with NOVAC evaluation	83
8.1	Tungurahua	85
8.2	Nevado Del Ruiz	87
8.3	BrO/SO ₂ time series	89
9	Issues of our method	93
9.1	Contamination of the plume	93
10	Conclusion	95
III	Appendix	97
A	Lists	103
A.1	List of Figures	103
A.2	List of Tables	109
B	Bibliography	113

1 Introduction

Volcanic activities on Earth have always shaped the earth surface and influenced atmospheric processes. Volcanoes are often particularly recognized by their dramatic consequences of a major volcanic eruption. But volcanoes influence our lives in more than this way. Volcanic gases can effect the weather (timescales of days to weeks) or the climate (timescales of months to years) Schmidt and Robock (2015). Examples are the lake eruption in Iceland (1783-1784) followed by a very hot summer and a cold winter in central Europa Thordarson and Self (2003) and the Tambora eruption, indonesia in 1815 which caused the "year without summer" in 1816.

Considering the plate tectonics of earth most volcanoes are caused by diverging or converging of the continental plates and therefore located at the margins of the continental plates. Another possibility for occurrence of volcanoes is the the interior of continental or oceanic shelves. Schmincke (2000)

The most abundant volatile species released during a volcanic eruption are water vapour (H_2O ; relative amount of the plume: 50%-90%) and carbon dioxide (CO_2 ; relative amount of the plume: 1%-40%) Platt and Bobrowski (2015). But the short effects of those two gases are rather low since there effect on atmospheric composition is negligibly due to the high abundance of atmospheric H_2O and CO_2 . But on timescales of the age of the earth the volcanic emission of H_2O and CO_2 are the source of our current atmosphere. Schmidt et al. (2015)

A typically volcanic plume consists of many different gases alongside H_2O and CO_2 sulfur dioxide (SO_2) contributes with 1%-25% to the plume, hydrogen sulfide (H_2S) with 1%-10% and hydrogen chloride with (HCl) 1%-10%. Furthermore there are trace gases for example carbon disulfide (CS_2), carbon sulfide (COS) carbon monoxide (CO) hydrogen fluoride (HF) and hydrogen bromide (HBr) Platt and Bobrowski (2015)

A decrease of stratospheric ozone (O_3) has been observed after the eruption of El Chickon in 1982 and the eruption of mount Pinatubo 1991. A depletion stratospheric O_3 results in ozone holes. The depletion comes from volcanic aerosols which serve anthropogenic chlorine/bromine into more reactive forms Solomon et al. (1998). Volcanic gases can alter the radiative balance of the earth in timescales relevant for climate change due to scatter and absorption of solar radiation Schmidt et al. (2015).

The gas composition of the volcano plume change with activity and could be a indication for the processes inside the earth.

In this work we are particularly interested in the ratio of BrO and SO_2 . The halogen sulfur ratio is a proxy for volcanic processes. Therefore we make the assumption

that the ratio of BrO and SO₂ contains informations about its degassing source depth. A change in BrO/SO₂ prior to eruption was observed at Etna and Nevado del Ruiz.

To gain further knowledge about the volcanoes the Network for Observation of Volcanic and Atmospheric Change (NOVAC) was installed. NOVAC is a Network of DOAS Instruments located next to about 30 volcanoes in America, Africa and Europe. At every Volcano there are two to four DOAS Instruments installed, recording record back-scattered solar radiation spectra at different viewing angles.

NOVAC is a network which produces a large amount of data and we have the chance to evaluate long time periods which is a unique opportunity to study correlations of the trace gases.

Since the conditions at volcanoes are rough, the instruments need to be rather simple to keep the maintenance cheap and to assure a longer lifetime of the instruments. So we need to waive on temperature stabilization even at the expense of the quality of the data.

One possibility to measure the volcanic trace gases is to use Differential Optical Absorption Spectroscopy [Platt and Stutz \(2008\)](#). DOAS exploit the wavelength dependency of the absorption of light. Here the gas emissions can be retrieved from the quotient of the absorption signal of the volcanic plume and a reference region. This will be explained in a further chapter.

The reference region, is usually treated as free of volcanic trace gases. If the reference region is for any reason contaminated by volcanic trace gases, the reference spectrum has to be replaced by a volcanic-gas-free reference. Alternative spectra could be for example a theoretical solar atlas spectrum or a volcanic-gas-free reference spectrum recorded in the temporal proximity(eg. a day before) by the same instrument. The first option comes with the drawback of reduced precision, as the instrumental effects have to be modeled and added to the retrieval. The reduction in precision is acceptable for the SO₂ retrieval, but not suitable for a BrO retrieval because then most data would be below the detection limit. For the second option, the alternative reference spectrum should have been recorded at similar conditions with respect to meteorology and radiation as well as in the temporal proximity due to instrumental changes with time and ambient conditions. We combined both options in order to achieve both, enhanced accuracy but still maximum possible precision of the SO₂ and BrO retrievals. We present an algorithm which finds the optimal reference spectrum automatically. As first step, a possible SO₂ contamination of the standard reference is checked by a comparison with the theoretical solar atlas. If a contamination is detected, as second step, the algorithm picks a volcanic-gas-free reference (beforehand automatically checked for contamination) from another scan.

In this work we are mainly dealing with data from Tungurahua in Ecuador in the timespan of 01.08.2008 to 30.07.2009. Later on, we will also show the results of

Nevado del Ruiz a volcano located in Colombia.

Part I

Theoretical background

2 Volcanism and volcanic chemistry

2.1 Volcanism

The high thermal energy in the deep interior of the earth is mostly well separated from the earth's surface by the earth's crust. A volcano is geological structure that allows magma to reach the earth's surface. Such a phenomenon can occur in various ways. In the following paragraphs the different types of volcanoes are described.

Mid-ocean ridge volcanism The mid-ocean ridge volcanism can be traced back to tectonic processes of oceanic plates. The spreading of two plates, that are pulled apart, leads to a thinning of the oceanic earth crust. This way solid material from the upper mantel (lower than 100 km) can ascend to depths of approximately 50 km. As the pressure at this depth is much lower, the mantle material starts to melt to basaltic magma that fills the gap between the two plates.

Continental rift zone volcanism Similar to mid-ocean ridge volcanism continental rift zone volcanism results from two continental plate are pulled apart.

Subduction zone volcanoes Subduction zone volcanoes occur if an oceanic plate converges under another plate (oceanic or continental). This way the descending plate penetrate into the lower mantle. At a depth of 80-150 km the water of this plate evaporates and rises and causes the mantle material above to melt. The resulting water-rich magma mainly consists of andesite. Subduction zone volcanoes are known for their violent eruptions caused by the low viscosity magma.

Hot-spot volcanoes Hot-spot volcanoes occur on continental or oceanic plates. This type of volcanoes arises from a hot spot at the coremantle boundary inside Earth that leads to a plume in the mantle where solid material can rise. This material melts to basaltic magma at a depth of 100-150 km. Through a futher rise also other types of magma (e.g. rhyolitic, more-viscous magma) can arise.

2.2 Volcanic gases and their impact on the climate

Volcanoes emit various gases (see table 2.1) in the atmosphere. This can occur due to volcanic eruptions or due quiet degassing. Gas emitted by quiet degassing remains in the troposphere while eruptions can inject volcanic gases up to the stratosphere Robock (2000). The larger lifetime in the stratosphere and a larger sensitivity of



Figure 2.1: Influence of volcanic eruptions and quiet degassing on earth climate.
Redrawn on the basis of [Robock \(2000\)](#)

the stratospheric chemistry to volcanic gases leads to an higher impact on the earth climate of these gases. Volcanic gases have a large influence on the earth climate especially CO₂ and SO₂ or more specific its oxidation product sulfur acid. The relevance of CO₂ for the climate is a subject of many discussions about the climate change compared to CO₂ in the atmosphere, the share of volcanic CO₂ is rather low.

Even though the SO₂ emissions during eruptive episodes are up to one order higher than during quite degassing episodes, Halmer et al. (2002) estimated that quiescent degassing contributes 40% of the accumulated SO₂ between 1972 to 2000.

Halmer et al. (2002) estimated the mean annual SO₂ emitted from volcanoes from 1972 to 200 as 7.5 to 10.5TgSyr⁻¹, while the anthropogenic SO₂ amount for 2000 is estimated as 55TgSyr⁻¹ (IPCC, 2013). Despite the less SO₂ occurring from volcanoes the impact may be higher as the impact of the anthropogenic SO₂. Graf et al. (1997) supposed that the volcanic SO₂ has a higher impact on the climate since it reaches up to the stratosphere while the anthropogenic SO₂ is mostly located in planetary boundary layer. In the lower troposphere sulphuric acid has a lifetime of about a week whereas the lifetime in the stratosphere is about a year (IPCC, 2013). Sulphuric acid in the atmosphere increases the earth albedo due to direct backscattering radiation. Additional the condensation on sulphuric acid particles leads to finer droplets thus to more stable and more white clouds this increases the albedo as

well (Twomey, 1974). volcanic particles can be surfaces for heterogeneous reaction. The result is a depletion of stratospheric Ozone, and thus a more high energetic solar flux on the earth surface. Large particles may backscatter IR radiation from the earth surface and the lower atmosphere, leading to a small reduction of the net cooling of the lower troposphere. In the upper troposphere or stratosphere absorption of IR or UV radiation results in a net heating in the stratosphere and a cooling at the earth surface. Figure 2.1 shows the above described effects and their localization in the atmosphere. The dominating radiative effect of volcanic gases is a cooling of the earth atmosphere due to more backscattered radiation, more diffusive scattering(Robock, 2000). IPCC (2013) records a volcanic radiative forcing of $-0.11Wm^{-1}$ between 2008 and 2011. For comparison the radiative of CO₂ is estimated as $1.68Wm^{-1}$.

2.3 Volcanic degassing

2.4 Volcanic plume chemistry

Volcanoes are emitter of many gases and aerosols particles, which are rising and forming the volcanic plume. The Temperature where the gases and aerosols are emitted is approximately 500°C Gerlach (2004). Due to the high temperatures the gas raises, cools down and mix up with ambient air. This process leads to many chemical reactions. The large amount of aerosols catalyses heterogeneous reactions. The volcanic gases are listed in Table 2.1.

In the following the chemical reactions of the plume constituents BrO and SO₂ will be discussed. This are the gases observed in this thesis.

Species	H ₂ O	CO ₂	SO ₂	H ₂ S	COS	SC ₂	HCl	HBr	HF
% / vol	50	1	1	1	10^{-4}	10^{-4}	1		
	-	-	-	-	-	-	-	?	<
	90	40	25	10	10^{-2}	10^{-2}	10		10^{-3}
Tg / year	?	75		1.5	1	0.005	0.007	0.4	0.0078
				50	2.8	0.1	0.096	11	0.1
									6

Table 2.1: Volcanic gas constituents at the emission vent and global estimated source strength. Adapted from Textor et al. (2004)

2.4.1 Sulphur species

Sulphur species are the third most abundant gases in volcanic plumes, hereby contributes SO₂ with about 25% and H₂S with 1 to 10%. Only H₂O and CO₂ have a

larger share on the volcanic gases in the plume Table 2.1.

Outside of the volcanic plume the SO₂ amount is with approximately 1ppb negligible, in contrast the SO₂ amount inside the plume can easily reach 1ppm ? When H₂S escapes from the volcano vent, it enters the oxidizing conditions in the atmosphere. The conversion of H₂S into SO₂ starts with:



The SH radical goes through a series of reactions, leading to the SO₂ formation ? SO₂ is removed from the atmosphere by dry or wet deposition. At homogeneous reactions the lifetime is from 1-3 weeks Robock (2000). Heterogeneous reactions such as take place on particles or liquid phases leads to much faster depletions. But this was yet not observed by volcanic plume measurements.

Further discussions of the stability of SO₂ in the atmosphere can be found at Lübcke (2014).

However SO₂ can be seen as stable several ours after the release of the volcanic vent. The long lifetime alongside of the negligible amount of SO₂ in the atmospheric background makes SO₂ a good tracer of the volcanic plume. Therefore relatively to other trace gases SO₂ may be used to examine their evolution independent of the plume dispersion.

One attempt to use SO₂ to examine other trace gases was made by Bobrowski et al. (2007). They found a higher BrO/SO₂ ratio at the edges of volcano plumes (Mt. Etna on Sicily, Italy, in August–October 2004 and May 2005 and Villarica in Chile in November 2004) and concluded that the BrO amount is higher at the edges due to the insufficient mixing with ozone rich air inside of the plume (see 2.2).

In this thesis it is supposed that SO₂ is stable on time-scales occurring with ground based remote sensing measuring of about 20 minutes.

2.4.2 Bromine oxide

The amount of Bromine in volcanic plumes is rather low compared to SO₂. The first time Bromine monoxid (BrO) was observed at a volcano was 2013 at the soufrière hills by Bobrowski et al. (2003). Since then many others were able to detect BrO using ground based remote sensing measurement techniques (DOAS: see Section 3.1) for example: Bobrowski and Platt (2007), Bobrowski et al. (2007), Vogel (2011) and Lübcke et al. (2014)

The main Bromine formation which is released from the volcano is HBr. BrO is formed due to mixing with the ozone rich atmosphere at ambient temperatures Bobrowski et al. (2007).

Due to the raising of hot air in the volcano vent , ambient air is pulled into the vent. There temperatures of 600°C to 1200°C prevent the formation of BrO. Only Br is formed. BrO occur after further cooling and mixing while rising. When the temperature cooles down to ambient conditions the so called "Bromine Explosion"

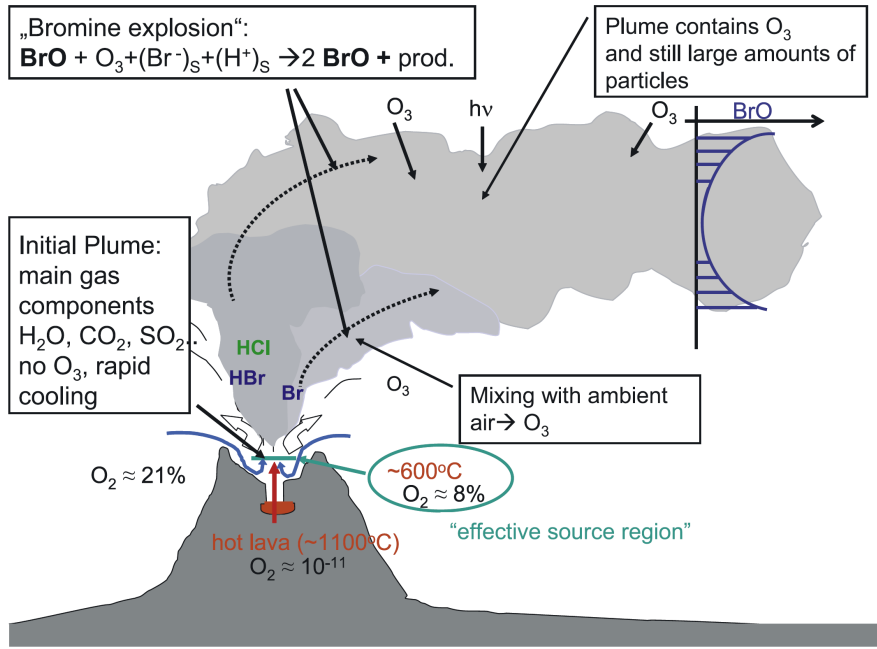
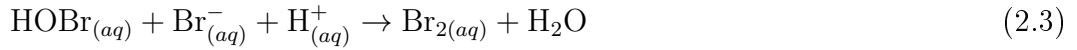


Figure 2.2: schematic sketch of a Bromine Explosion. Release of HBr at the volcanic vent. Mixing with ambient air in the effective source region leads to Br formation. This resulting Bromine species react to BrO with ozone from the plume. Adapted from Bobrowski et al. (2007)

causes a non linear formation of BrO. The "Bromine Explosion" is illustrated in Figure 2.4 and can be described with the following reaction cycle:



The gaseous HBr emitted by the volcano is split heterogeneously into H^+ and Br^- (eq. (2.1)). Inside of an aerosol it forms with HOBr Br_2 and H_2O (eq. (2.3)). Br_2 evaporates to the gaseous phase and splits photolytically into 2Br. Including an ozone molecule (O_3) the two Br react to 2BrO. The last step of the circle visualized in Figure 2.4 with blue lines is the reaction of a BrO with H_2O to an HOBr molecule condensing into the liquid phase and thus closing the circle. The non linear explosion occurs due to the formation of two BrO particles from one HBr from



Figure 2.3: BrO/SO₂ ratio as a function of the distance from the volcanic vent with a constant wind speed of 10 m/s. From Lübcke (2014)

the volcano.

The BrO formation is slightly diminished due to self reaction of BrO molecules marked with the red lines in fig. 2.4. The 2BrO react with themselves and form Br₂ or may split photolytically into 2Br.

The BrO concentration reaches a maximum approximately 5 minutes after emission and then remains constant for the next 25 minutes Lübcke et al. (2014).

2.5 Using the BrO/SO₂ ratio to study volcanic activity

Volcanic degassing is influenced by many factors, which can be exploited to study volcanic activity by using the gas composition of the volcano plume. Therefore remote sensing should be an additional tool for forecasting of volcanic activity next to classical monitoring techniques like seismographic and deformation measurements. Inside of volcanoes volatiles are in solution in magmatic melt. The Henry law Equation (2.10) describes the necessary conditions for gas formation:

$$P = K_H \cdot c \quad (2.10)$$

Here P is the partial pressure at equilibrium of the solute, c is the concentration and K_H is the Henry constant which is anti proportional to the solubility α ($\alpha = \frac{1}{K_H}$). If the partial pressure of the gas solute (in this case a magmatic gas constituent) exceeds the pressure of the surrounding solvent, a formation of gaseous bubbles occur. Otherwise, if the partial pressure of the gas in the solution is below the surrounding

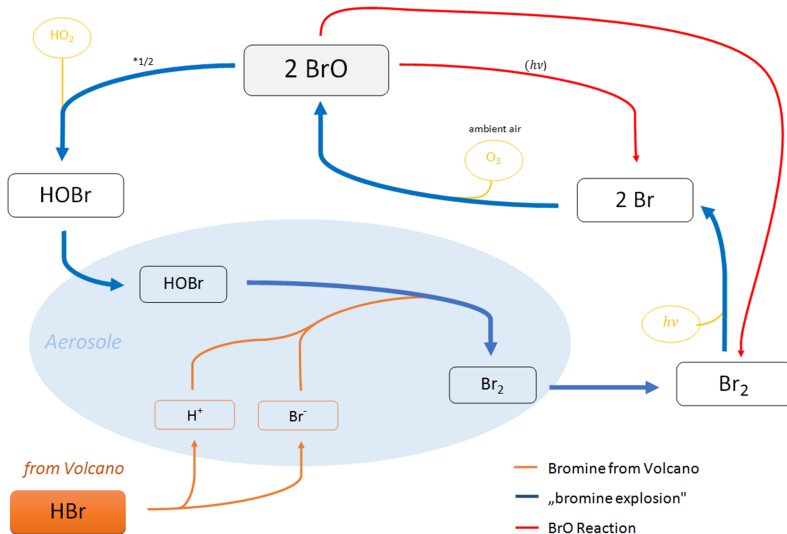


Figure 2.4: Bromine reactions inside of a volcanic vent. The release of HBr at the volcanic vent is drawn in orange. Inside of aerosols heterogeneous dissociation with HOBr forms Br₂. Then Br₂ splits photolytically into single Br radicals. BrO results through a reaction with O₃ upon mixing with ambient air. Reactions with H₂O forms HOBr creating an autocatalytic cycle. The reaction cycle along the blue lines are called Bromine explosion. From Warnach (2015)

pressure the formation of gas bubbles stops.

The solubility α depends on the temperature, the chemical composition and on the solvent (here magma). Whereas the partial pressure of the constituent depends on the surrounding pressure. The pressure below the volcanic vent increases with depth, this leads to a correlation between the partial pressure of the constituents and the depth. The result is, that the gas starts exsolving at a certain depth depending on the partial pressure of the constituent. Thus the gas bubble formation increases with rising magma. But at a certain depth the percentage of solved gas is different for each volcanic gas. The result is, that the composition of the gases changes with depth. So gas ratios contain information about its originating source depth.

Prior to volcanic eruptions the magma starts raising since the gas is mostly less dense than the magma, it raises faster and could be therefore a indicator for its origin source depth thus a indicator for the volcanic activity.

Figure 2.5 shows the ratios of H₂O / CO₂, S/Cl, CO₂/S as a function of the pressure respectively on the depth. Noguchi and Kamiya (1963) found decrease Cl/S prior to eruptive periods Pennisi and Le Cloarec (1998) observed lower Cl/S ratio during eruptive periods than not eruptive periods at Mt. Etna. Burton et al. (2007) found CO₂/SO₂ and SO₂/hCl ratios 3-5 times higher during explosions compared to quiet degassing episodes. the authors compared these data to gas formation simulations for different degassing source depth they concluded that these eruptions were driven

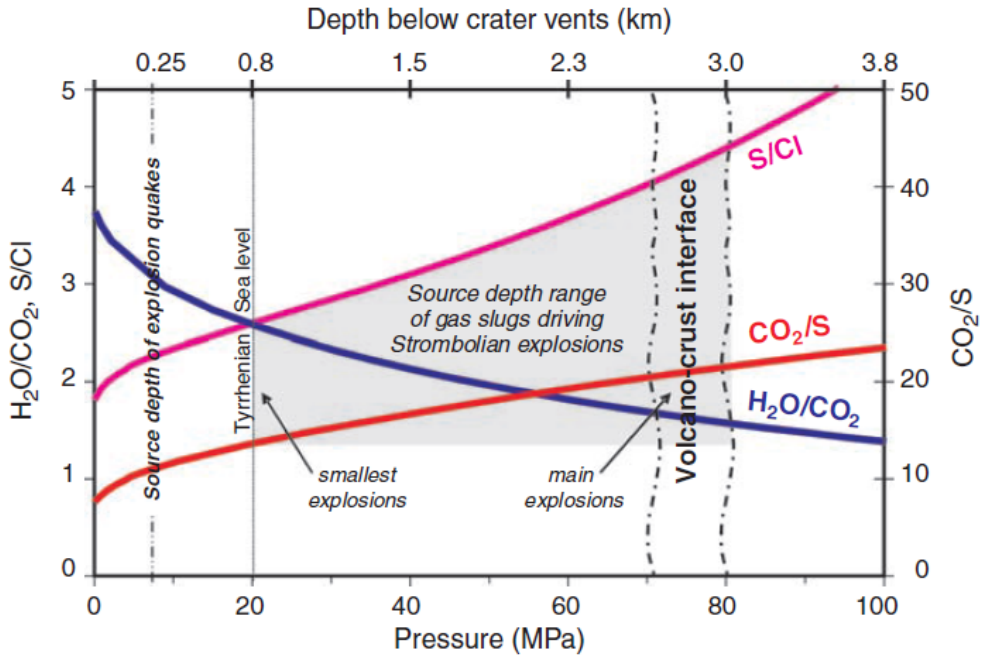


Figure 2.5: Dependency of the ratios of different volcanic trace gases on depth. Data originate from Stromboli volcano. From Lübcke (2014) reproduced from Burton et al. (2007)

by gas slugs from deeper levels where the ratios were higher while quiet degassing originates from shallow magma

Especially halogen-sulfur ratios are interesting as possible tracer for the volcanic activity since the ambient air concentrations are negligible BrO/SO_2 curves equivalent as in Figure 2.5 are yet not available due to lack of bromine solubility curve but the following observations were made: Changes of BrO/SO_2 were found by Bobrowski and Giuffrida (2006): multiple eruptions between 2006 and 2009 highest ratios 2-3 month before the eruptions the ratio then decreased and was lowest during eruptive phase. Therefore it could be concluded that bromine exsolves earlier, at lower depth than sulphur. Lübcke et al. (2014) found decrease of BrO 5 month prior to the eruption 2012 at Nevado Del Ruiz can also be attributed to an earlier exsolution of bromine during rising magma. Despite the lack of the solubility curve of BrO until now, the BrO/SO_2 has a great potential for investigations of the volcanic activity. The first reason is, that both gases can be measured with remote sensing by DOAS instruments. For examples ground based measurements by Bobrowski et al. (2007), Lübcke (2014) or satellite based measurement by ? or ?. The advantage of remote sensing techniques is the possibility of measuring during eruptions which is with in situ measurements not always possible. Secondly due to the NOVAC network (See 4) continuous measurements are possible.

Another reason for the research on BrO/SO_2 ratios at volcanoes is the constance of

the ratio from 5 to at least 30 minutes after release (Bobrowski et al., 2007);(Lübcke, 2014). As well as the constance from 5 to 20 km off the volcano see 2.3. This ensures that the data measured from different positions or at different conditions are comparable.

This chapter motivated the research on the BrO/SO₂ ratio as a tracer for volcanic activity.

Tungurahua

Tungurahua is a steep-sided andesitic-dacitic subduction zone volcano located in the Ecuadorian Andes (Lat: 1.467°S; Long:78.442°W). 2014 Tungurahua was one of the most active volcanoes in southern America, since then the activity was decreasing. Tungurahua is 5023m high and is one of the defining volcanoes of the eastern volcanic rows in Ecuador (Hall et al., 1999).

The modern volcano was formed by a sequentially construction of three major edifices on a basement of metamorphic rocks. It has a total diameter of 12 km. Tungurahua I was roughly located at the same place as today and was build up in the mid-Pleistocene, mainly by andesitic and dacitic lava flows as well as interbedded tephra. Tungurahua II was formed in the past 14,000 years as a result of the collapse of the initial edifice.

3000 years ago the Tungurahua II edifice collapse. The collapse of Tungurahua II produced a large debris-avalanche deposit and a horseshoe-shaped caldera which is open to the west side. Tungurahua III the current glacier caped stratovolcano was constructed in this caldera ([Glo](#)).

The current ongoing long term eruption started in October 1999. The eruptive phase was preceded by hydrothermal tremors between 1994 and 1997 (?). From September 1998 to July 1999 an increase of seismic activity like volcano tectonic earthquakes indicates the raising of magma. This eruptive phase is characterized by alternating periods of high and low volcanic activity.

At Tungurahua three instruments described in Table 2.2, with data recorded in the time span from July in 2008 to August in 2009 are used in this thesis. **Tabelle muss noch besser erklahrt werden, was ist das alles? was nicht erklähr wird, sollte raqusgeloescht werden**

Nevado Del Ruiz

Nevado Del Ruiz is a glacier-covered, subduction zone volcano which is located in the Central Cordillera of Colombia, 140 km west of Bogota (Lat: 4.892°N; Long:75.324°W). Nevado De Ruiz has a hight of 5389 m and covers an area of more than 200 km². Three major edifices has been constructed since the beginning of the Pleistocene, consisting of andesitic and dacitic lavas and pyroclastics ([Glo](#)). The current cone is build within the caldera of older edifice and consists of a cluster of lava domes. The crater on the summit the name is Arenas crater, with a diameter

Instrument	D2J2140_0	I2J8546_0	I2J8548_0
compass	90.0	30.0	360.0
tilt	0.0	0.0	0.0
latitude	-1.453584	-1.543492	-1.404719
longitude	-78.513047	-78.517179	-78.494777
altitude	2609.980	2782.352	2911.253
volcano	Tungurahua	Tungurahua	Tungurahua
site	pillate	bayushig	huayrapata
observatory	igepn	igepn	igepn
serial	D2J2140	I2J8546	I2J8548
spectrometer	S2000	S2000	S2000
instrumenttype	gothenburg	gothenburg	gothenburg
version	2.1	2.1	2.1
softwareversion	1.40	1.40	1.40
compiledate	Jun 27 2008	Jun 27 2008	Jun 27 2008

Table 2.2: Technical data of the instruments installed at the Tungurahua volcano.

of 1 km and a depth of 240 m. The last big eruption was in 1985. This was South America's deadliest eruption.

In this thesis the data of two NOVAC Instruments (see Table 2.3) in the time from the end of 2009 to the end of 2011 are used.

Instrument	D2J2200_0	D2J2201_0
compass	115.0	59.0
tilt	0.0	0.0
latitude	4.900917	4.876183
longitude	-75.335134	-75.353408
altitude	4866.500	4494.259
volcano	Nevado Del Ruiz	Nevado Del Ruiz
site	bruma	alfombrales
observatory	ingeominas	ingeominas
serial	D2J2200	D2J2201
spectrometer	S2000	S2000
instrumenttype	gothenburg	gothenburg
version	2.2	2.2
softwareversion	1.82	1.82
compiledate	Feb 19 2009	Feb 19 2009

Table 2.3: Technical data of the instruments installed at the Nevado Del Ruiz volcano.

3 Remote sensing of volcanic gases

In this thesis we are interested in the volcanic trace gases SO₂ and BrO, both measured with the Differential Optical Absorption Spectroscopy (DOAS) a remote sensing technique proposed by [Platt and Stutz \(2008\)](#)

Beer-Lambert Law

The Lambert-Beer law describes the attenuation of light when traveling through a material.

This section will give an overview about the reasons for decreasing light intensity when going through a medium.

The Lambert-Beer law describes the attenuation of light when traveling through a material.

, Atoms and Molecules exists in several energy states, depending on the different electron configuration. Moreover Molecules have additionally rotation and vibration states, also enclose to the energy states. If a photon matches the energy gap between two possible energy states, this includes, that the lower energy state is occupied and the selection rules are fulfilled the molecule could absorb the photon, remaining in a higher energy state.

The additional photon energy could be loosed by collision with another molecule or by emission. But since the direction of the emitted photon is mostly not the same direction of the absorbed photon the intensity I₀ of the light before passing the medium is higher than the intensity I after traveling the distance L through the medium.

This can be described as:

$$I(L, \lambda) = I_0(\lambda) \cdot \text{expt} \left(- \int_0^L \sigma(\lambda, p, T) \cdot c(l) dl \right) \quad (3.1)$$

where $c(l)$ is the location-dependent concentration of the trace gas of interest. $\sigma(\lambda, p, T)$ is the absorption cross section, $\sigma(\lambda, p, T)$ is unique for each molecule and depends on pressure p and on the temperature T.

An important quantity used in many optical remote sensing techniques is the optical density τ . The optical density is a measure for the weakening of radiation when going through a material. τ can be calculated using the lambert beer law:

$$\tau = -\ln \left(\frac{I(\lambda)}{I_0(\lambda)} \right) = \sigma \cdot S \quad (3.2)$$

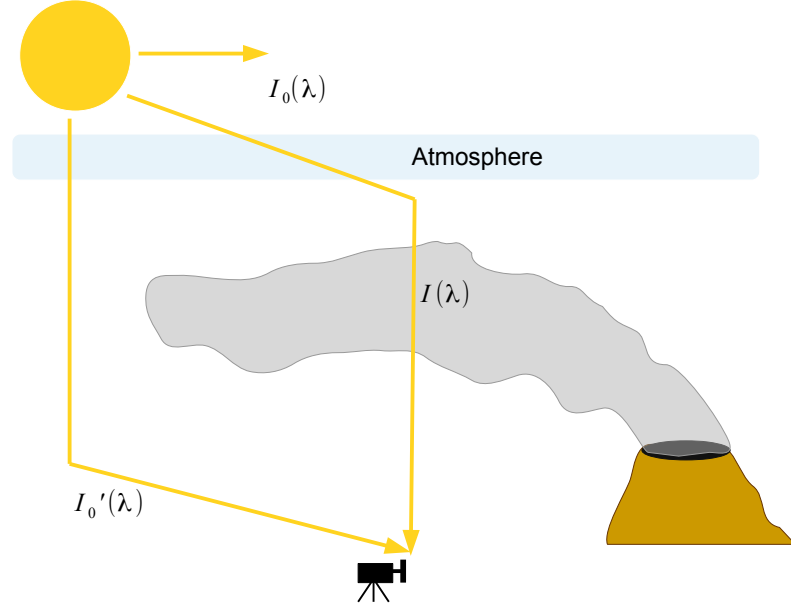


Figure 3.1: Schematic sketch of the DOAS measurement of volcanic plume constituents. The column density of the plume constituent of interest is retrieved by comparing the spectrum $I(\lambda)$ which is measured through the plume with the spectrum $I'_0(\lambda)$ measured outside of the plume.

Hereby is S the column density. The column density is the concentration of the trace when integrating along the light path, the dimension of S is therefore the number of molecules divided by an area: $\frac{\text{molec}}{\text{cm}^2}$.

$$S = \int_0^L c(l) dl \quad (3.3)$$

When measuring at a volcano, that means measuring in the atmosphere the situations gets more complex, since we need to deal with several absorbers and scattering processes have to be taken into account. One possibility is to treat scattering effects as pseudo absorbers with the respective extinction coefficients for Rayleigh (ϵ_R) and Mie (ϵ_M) scattering

$$I(L, \lambda) = I_0(\lambda) \cdot \exp \left(- \int_0^L \sum_j \sigma_j(\lambda, p, T) \cdot c_j(l) + \epsilon_R(\lambda, l) + \epsilon_M(\lambda, l) dl \right) \quad (3.4)$$

The first term of Equation (3.4) in the exponential function, multiple absorbers j are considered, the corresponding concentration depends on the position l of the light path. The last two terms in describe the extinction due to Rayleigh and Mie scattering in the atmosphere.

Inelastic scattering (for example the Ring effect) and effects due to turbulences in the atmosphere are neglected here.

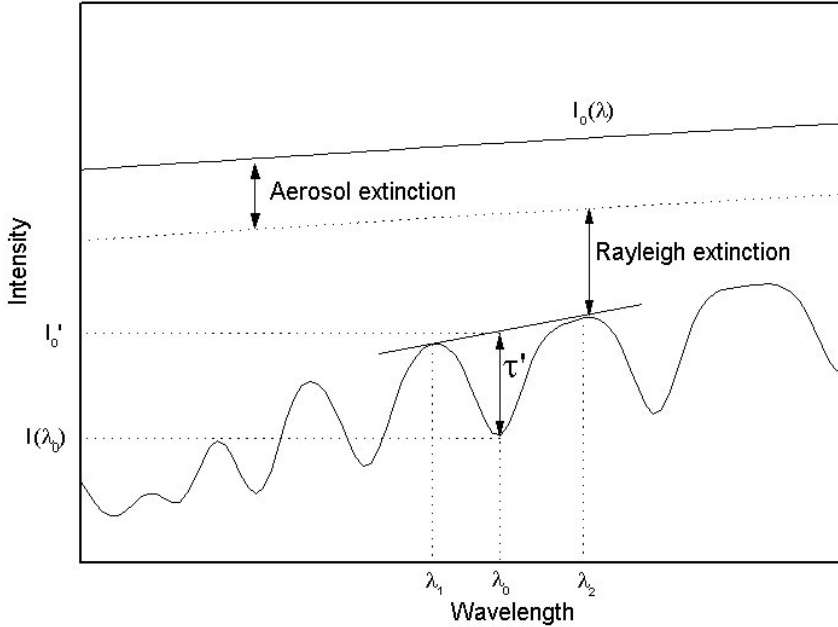


Figure 3.2: Basic idea of the DOAS principle: Light attenuate due to broad band and narrow band effects. The broad band extinction is caused by aerosols and Raylight scattering ($I_0 \rightarrow I'$). The measured intensity I is formed by narrow band effects due to differential absorption structures by trace gases with the optical density τ' . Adapted from Kern (2009)

3.1 Differential Optical Absorption Spectroscopy (DOAS)

It is impossible to distinguish between various broad-band effects, like scattering in the atmosphere or instrument effects which influence the measured spectra (Lübcke, 2014). Therefore Equation (3.4) cannot be applied to real measurements.

Differential Optical Absorption Spectroscopy (DOAS) was invented in the late 1970s by Perner and Platt (1979). This section will give an overview about the DOAS technique. More detailed information can be found in the work of Platt and Stutz (2008)

Differential Optical Absorption Spectroscopy uses the fact, that absorption can be divided into broad-band parts and narrow-band parts. Broad band parts are effects that only changes weakly with the wavelength, i.e. scattering and instruments effects have a broad-band structure. The narrow band part includes effects that strongly depends on the wavelength. Within the DOAS-Method only narrow-band absorption features of molecules are used to obtain their column densities. The absorption cross section of trace gases j have broad-band ($\sigma_b(\lambda)$) and narrow band

$(\sigma'(\lambda))$ features, only the narrow-band structures are used in DOAS.

$$\sigma(\lambda) = \sigma_b(\lambda) + \sigma'(\lambda) \quad (3.5)$$

With this considerations the Lambert-Beer law Equation (3.4) can be rewritten dividing the exponential part into a narrow-band part and a broad-band part:

$$I(\lambda, L) = \overbrace{I_0(\lambda) \cdot \exp \left(- \int_0^L \sum_j \sigma_{b,j}(\lambda, p, T) \cdot c_j(l) + \epsilon_R(\lambda, l) + \epsilon_M(\lambda, l) dl \right)}^{=I'_0(\lambda)} \cdot \exp \left(- \int_0^L \sum_j \sigma'_j(\lambda, p, T) \cdot c_j(l) dl \right) \quad (3.6)$$

The so defined $I'_0(\lambda)$ differs from $I_0(\lambda)$ only by broad band effects. With $I'_0(\lambda)$ a differential optical density τ' can be defined:

$$\tau' = \ln \left(\frac{I'_0(\lambda)}{I(\lambda)} \right) = \int_0^L \sum_j \sigma'_j(\lambda) \cdot c_j(l) dl = \sum_j \sigma'_j(\lambda) \cdot S_j \quad (3.7)$$

The optical density can now be calculated by using the difference of the column density S_M in the measurement spectrum to the column density S_R of a reference spectrum. From Equation (3.6) we know:

$$I_{P,R} = I'_0 \cdot \exp(-S_{P,R} \cdot \sigma(\lambda)) \quad (3.8)$$

In general the obtained column density S_M is called differential slant column density: "dSCD". If the reference spectrum does not contain the trace gas of interest (is not contaminated with trace gases) that means $S_R = 0$, S_M is called the slant column density (SCD). With Equation (3.8) the optical density can be derived by:

$$\tau(\lambda) = -\ln \left(\frac{I_M}{I_R} \right) = \sigma(\lambda) \cdot (S_M - S_R) \quad (3.9)$$

3.1.1 Technical implementation of the DOAS approach

The theory explained above only describes the ideally situation. In real measurements more problems occur due to instrument limitations inelastic scattering causing the Ring effect and due to impacts of external parameters like temperature. In the following a short overview about these problems and their consequences for our retrieval is given. Further information can be found in Lübecke (2014).

Optical and spectral resolution of the spectrometer

The resolution of the spectrometer is finite, thus, the detector receives a spectrum $I^*(\lambda)$ which can be retrieved with a convolution of the incident spectrum $I(\lambda)$ with the instrument function $H(\lambda)$:

$$I^*(\lambda) = I(\lambda) * H(\lambda) = \int I(\lambda - \lambda') \cdot H(\lambda - \lambda') d\lambda' \quad (3.10)$$

For the evaluation all σ_j of the trace gases of interest need to have the same spectral resolution as the instrument used for recording the spectra. In this work we will use high resolution cross sections and convolute them with the instrument function H :

$$\sigma^*(\lambda) = \sigma(\lambda) * H(\lambda) \quad (3.11)$$

The instrument function H can be approximated by using the spectral lines of a mercury lamp since the width of those lines is only a few pm, they could be treated as delta peaks when comparing it to the resolution of the spectrometers.

Effects of the detector

The detector only has discrete pixels, therefore a wavelength interval is mapped to a pixel i .

$$I'(i) = \int_{\lambda(i)}^{\lambda(i+1)} I^*(\lambda') d\lambda' \quad (3.12)$$

For the retrieval the relationship between the detector channels and the wavelength of the spectrum need to be known. The wavelength to pixel mapping (WMP) for a detector with q channels can be calculated as:

$$\lambda(i) = \sum_{k=0}^{q-1} \gamma_k \cdot i^k \quad (3.13)$$

Hereby, γ_0 is a shift of the spectrum and γ_1 is a squeeze (respectively stretch) of the spectrum. The wavelength to pixel mapping can be discovered by using a mercury lamp again and compare pixel-position with the well known wavelength of the individual HG-lines of the mercury lamp.

The wavelength to pixel mapping depends on the instrument temperature as well as on the ambient pressure (Lübecke et al., 2014).

Ring effect

As mentioned above inelastic scattering causes the Ring effect (named after Grainger and Ring, 1962). The Ring effect is observable through a filling of the Fraunhofer lines in spectra of scattered solar radiation, (e.g. if the sunlight travels through the earth atmosphere). When compared to direct sunlight measurements (e.g. outside of the earth atmosphere). ([Bussemer \(1993\)](#),[Solomon et al. \(1987\)](#)) proposes that the Ring effect is a result of rotational Raman scattering mainly of O_2 and N_2 in the atmosphere. [Solomon et al. \(1987\)](#) suggested to treat the Ring effect as a pseudo-absorber.

Part II

Evaluation of the data of Tungurahua and Nevado Del Ruiz

4 Network for Observation of Volcanic and Atmospheric Change

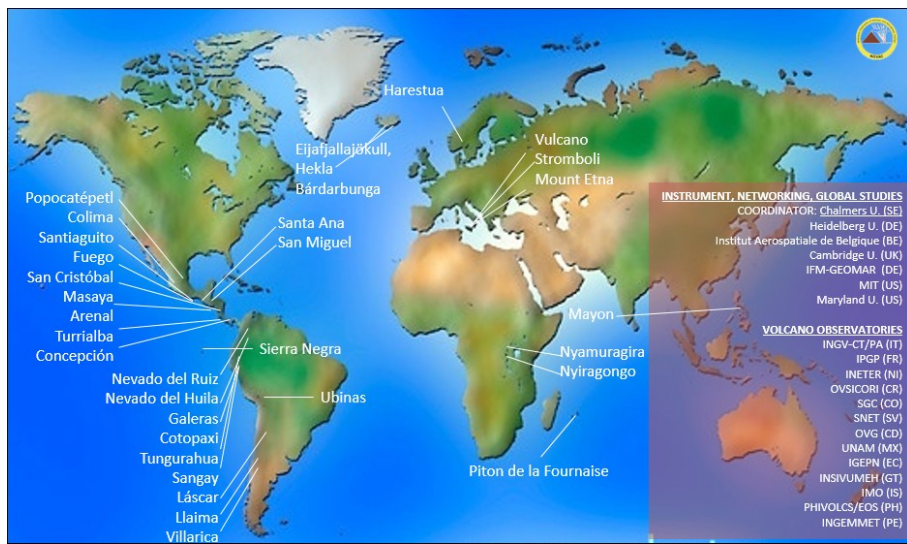


Figure 4.1: Global map of the volcanoes monitored by NOVAC. Used with friendly permission of Santiago Arellano.

The Network for Observation of Volcanic and Atmospheric Change (NOVAC) is a network of instruments monitoring volcanoes over the whole world. NOVAC was installed to gain another tool for risk assessment, for gas emissions and geophysical researches.

NOVAC was originally funded by the European Union on the first October in 2005. The aim of NOVAC is to establish a global network of stations for the quantitative measurement of volcanic gas emissions. At the beginning, NOVAC encompassed observatories of 15 volcanoes in Africa America and Europe, including some of the most active and strongest degassing volcanoes in the world. Although the EU-funding has stopped, the network has been constantly growing since it was founded. In 2017 more than 80 instruments are installed at over 30 volcanoes in more than 13 countries. Figure 4.1 shows a map, with all volcanoes of the Network for Observation of Volcanic and Atmospheric Change.

The great advantage of the data monitored in NOVAC is the fact that NOVAC provides continuous gas emission data over many years. This ensures statistically meaningful results for the data evaluation.

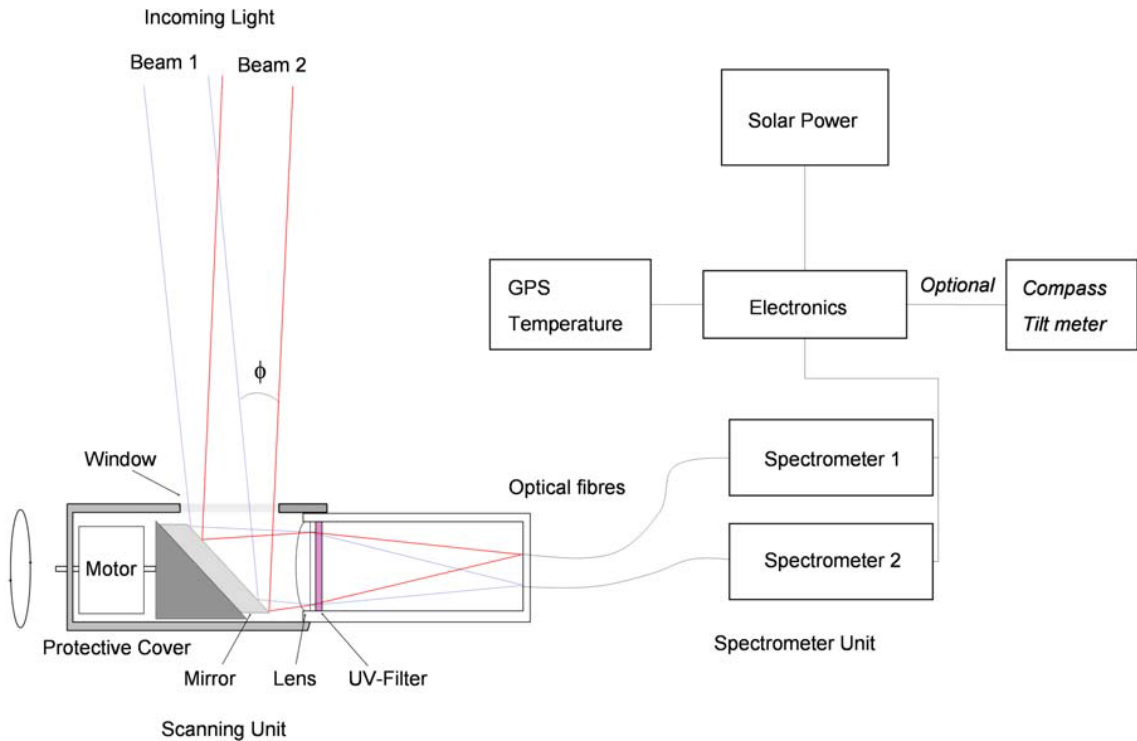


Figure 4.2: schematic sketch of a NOVAC instrument. From Galle et al. (2010)

The instruments used in NOVAC are scanning UV-spectrometer named Mini Doas instruments.

The Mini DOAS instrument represents a major breakthrough in volcanic gas monitoring as it is capable of real-time semi-continuous unattended measurement of the total emission fluxes of SO₂ and BrO from a volcano. Semi-continues in this case means that the measurement is only possible during daytime and if the sunlight is sufficient.

The basic Mini DOAS system consists of a pointing telescope fiber-coupled to a spectrograph. Ultraviolet light from the sun, scattered from aerosols and molecules in the atmosphere, is collected by means of a telescope with a quartz lens defining a field-of-view of 12 mrad. NOV

The spectrometers measure in the UV region in a wavelength range of 280 to 420 nm. In this range the differential structures of SO₂ and BrO are dominant.

The NOVAC-instruments need to be very robust to stand the conditions around volcanoes. Therefore the design of the instruments is rather simple, this means the instruments do not have internal stabilisation features like temperature stabilization to keep the measurement independent of external parameters.

This comes with a reduced precision of the data, but the huge amount of data produced by NOVAC compensates for this limitation.

4.1 Measurement routine

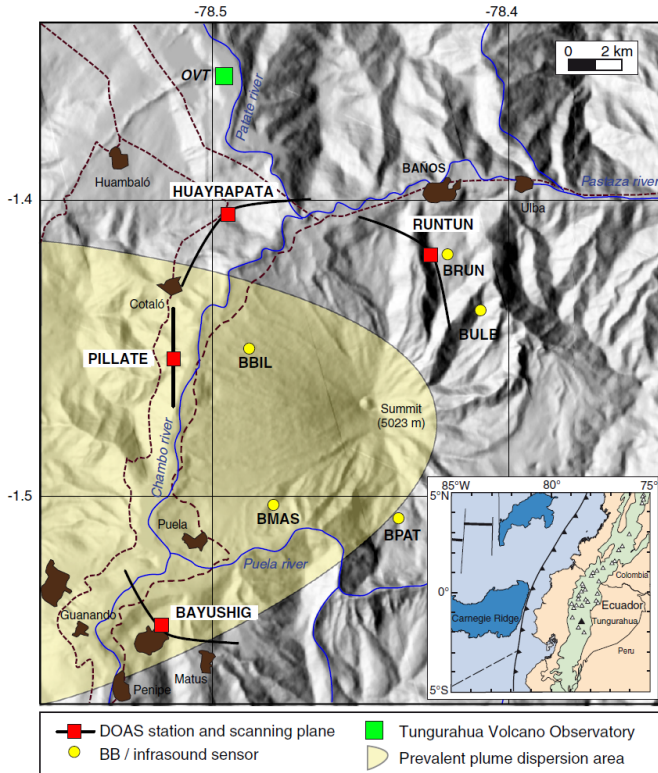


Figure 4.3: Topographic Map of the Tungurahua Volcano. The predominant plume direction is shaded in yellow. Four NOVAC stations are shown as red squares, the corresponding scanning geometry is sketched with black lines. From [Hidalgo et al. \(2015\)](#).

The instruments are set up five to ten km downwind of the volcano. To cover most of the occurring wind directions two to five instruments are installed at each volcano. Ideally, the measurement plane is orthogonal to the plume, to get the best measurement results. In reality, the measurement plane might be rotated.

For the calculations of gas data from the DOAS retrieval a scan of the Plume and a scan without any volcanic trace gases (reference spectrum) is needed. This is done without any knowledge of the plume location by scanning the whole sky. The measurement routine starts with a spectrum in zenith direction: the pre-reference. The exposure time of the pre-reference will be used for the whole scan. Afterwards, the dark current spectrum is recorded for the correction of the dark current and offset.

Then the instrument turns automatically to the side, recording spectra at the elevation angle from -90° to 90° with steps of 3.6° .

The instruments records 53 spectra per Scan, the pre-reference, the dark current

spectrum and 51 spectra at different elevation angles. One hole measurement takes 6 to 15 minutes.

5 Evaluation routine

This chapter outlines the algorithm which is used for the evaluation of the spectroscopic data recorded in NOVAC. The problem of contamination of the reference is explained and possible solutions are presented.

5.1 Conventional evaluation routine

The fitting routine used for this thesis is based on the DOASIS software ([Kraus, 2006](#)). The equations of the DOAS retrieval of this work are slightly different from Equation (3.7) and therefore described in the following. Equation (3.4) can be rewritten as:

$$\begin{aligned} \ln(I(\lambda, L)) &= \ln(I_0) + P(\lambda) - \int_0^L \sum_j \sigma_j(\lambda, p, T) \cdot c_j(l) dl \\ &= \ln(I_0) + P(\lambda) - \sum_j \sigma_j(\lambda, p, T) \cdot S_j \end{aligned} \quad (5.1)$$

The polynomial $P(\lambda)$ accounts for all broad-band effects which approximates the scattering effects of the atmosphere as well as broad band absorptions.

The task of the DOAS retrieval is to find a model function $F(\lambda)$ that minimizes χ^2 :

$$\chi^2 = \sum_{i=\lambda_1}^{\lambda_2} (\ln(I(i)) - F(i))^2 \quad (5.2)$$

While $F(\lambda)$ can be expressed on the basis of Equation (5.1):

$$F(\lambda) = \ln(I_0) + P(\lambda) - \sum_j \sigma_j(\lambda) \cdot S_j \quad (5.3)$$

The DOAS fitting routine uses a combination of a standard least-squares fit and a Levenberg-Marquardt algorithm to minimize χ^2

Prior to the DOAS fitting, the spectra need to be calibrated, this done by using a wavelength to pixel mapping function (WMP) developed by ?. The WMP uses a solar atlas spectrum that is concorded with the Hg line of the single instruments, hereby an initial calibration based on the Hg lines is given as a first parameter. The calibration is done by fitting the Fraunhofer lines of the recorded spectrum on the

convolved Solar Atlas spectrum. The Rayleigh scattering is considered by adding a Ring spectrum as well as a wavelength dependent Ring spectrum (proportional to λ^4) (?). Mie scattering and broadband absorption structures were accounted due to adding a third order polynomial to the retrieval well as an offset polynomial to correct for stray-light influence (Lübcke et al., 2014).

The SO₂ evaluation is performed for a wavelength range between 314.8 nm and 328 nm. Including a SO₂ absorption cross section recorded at a temperature of 298K (Vandaele et al., 2009) and a O₃ absorption cross section recorded at 221K (Burrows et al., 1999).

The BrO evaluation is performed for a wavelength range between 330.6 nm and 352.7 nm (found by Vogel (2011)). The sum in Equation (5.3) includes for the BrO evaluation the following absorption cross sections: BrO at 298K (Fleischmann et al., 2004), the SO₂ and O₃ absorption cross sections described above, O₄ (Hermans et al., 2003), NO₂ at 298K (Vandaele et al., 1998) and CH₂O at 298K (Meller and Moortgat, 2000).

The choice of the wavelength range as well as the considered trace gases used in the fits is based on studies on the optimal evaluation wavelength range in a combination of real measurement data and theoretical studies for BrO and SO₂, made by Vogel (2011).

The spectra of the trace gases were convoluted by using the 334.15 nm line of a mercury lamp.

A further effect influencing the evaluation is the I_0 effect, in order to account for the I0-effect (Platt and Stutz, 2008) an iterative approach was used. Further informations can be found at (Wagner et al., 2002), Lübcke et al. (2014), Vogel (2011)). To further correct for small inaccuracies of the WMP, the FRS and both Ring spectra as one set, and all trace gases absorption cross sections as another set, are allowed to be shifted, and first order squeezed against the measurement spectrum.

NOVAC provides spectral data for roughly 50 different elevation angles. For the DOAS evaluation a reference and a measurement spectrum is needed. Obtaining the complete amount of volcanic gases is only possible in the case of the availability of references which are free of volcanic gases of interest(this will be discussed more detailed in Section 5.2). The column density of BrO and SO₂ of the measurement spectrum relatively to the reference spectrum can be calculated Equation (5.2) and 5.3.

In the following we describe the technical implementation of the DOAS approach using the data of NOVAC instruments:

The first step is to correct each spectrum of the scan for dark current and offset using the dark spectrum. The next task is to locate the spectra in and outside of the volcanic plume. First a "pre-reference" (the spectrum recorded at an elevation angle of 0°) is used to perform the evaluation of the scan spectra recorded at every elevation angle. For every spectrum of the scan the SO₂ differential slant column density (dSCD) with respect to the pre-reference is calculated using Equation (5.3) by the DOASIS fit routine.

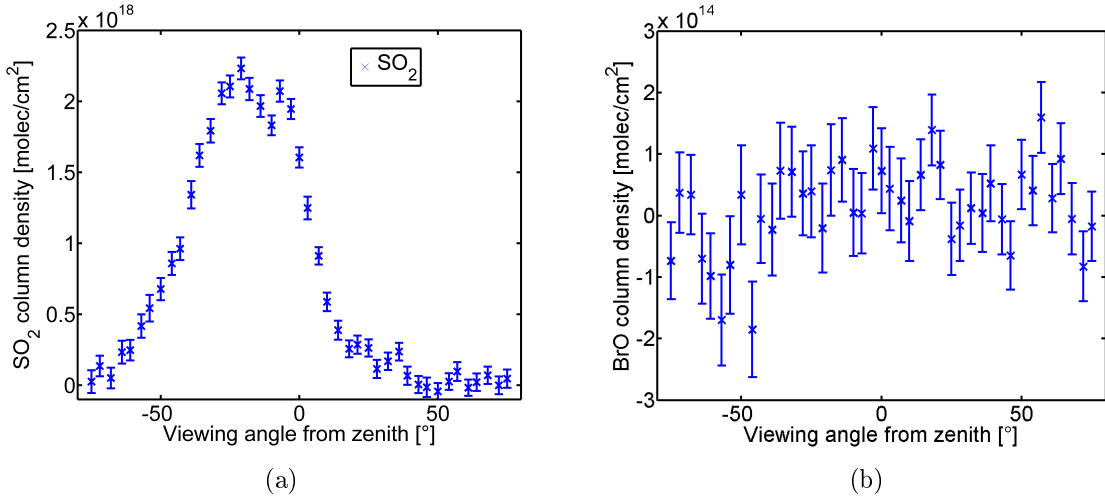


Figure 5.1: (a) SO_2 SCD as a function of the elevation angle with error bars computed by the DOASIS fitting routine. (b) BrO SCD as a function of the elevation angle with error bars computed by the DOASIS fitting routine. Taken from Warnach (2015)

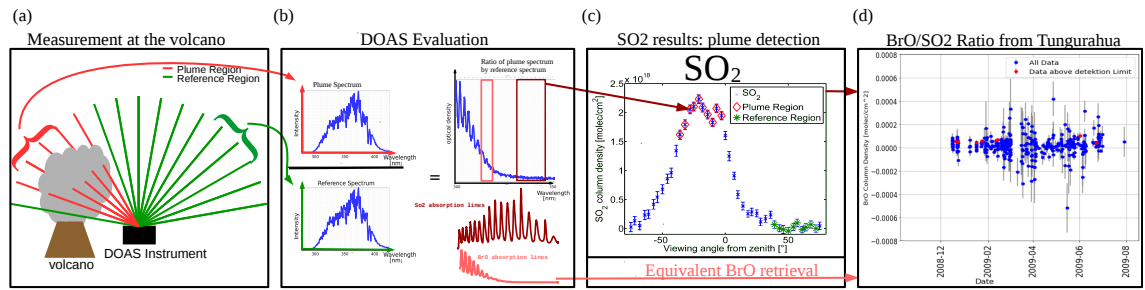


Figure 5.2: NOVAC Evaluation: (a) Measurement at the volcano (b) Evaluation of the spectral data with the DOAS routine using the absorption cross sections of BrO and SO₂. (c) Finding the location of the plume and reference (d) (taken from Warnach (2015)) Computation of the ratios BrO/SO₂ at Tungurahua. Bild noch ändern, letztes bild andere stil, verwechseln SO₂ und BrO absorbtion

The result is SO₂ dSCDs as a function of the elevation angle. This way the elevation angle corresponding to the maximum and the minimum of the SO₂ column density can be determined. The location of the SO₂ maximum defines the location of the plume. The assumption is that the minimum of the SO₂ curve corresponds to a region outside of the plume which is true in most cases. The background SO₂ amount in the earth atmosphere around Tungurahua is usually negligible (see Section 2.4.1) so we take it as a region of zero SO₂.

We use a gauss fit of the SO₂-elevation-angle-curve to define the plume region. The sum over all plume spectra is taken, which are in the elevation angle interval of the gauss peak plus minus one sigma, to increase the photon statistic and to reduce the residuum. If the gauss curve is too wide, what this means in specific is that more than 10 spectra are added within the gauss evaluation. The running mean is calculated and the 10 spectra with the highest SO₂ amount are used for the retrieval. As reference we use the sum of the 10 spectra with the lowest SO₂ amount.

The absolute slant column densities (SCD's) of BrO and SO₂ can now be calculated with the previously defined reference and plume spectrum. In Figure 5.1 (a) an example SO₂ SCD as a function of the elevation angle is shown. The SO₂ curve has a maximum at the position of the plume at an elevation angle of approximately -30° to 0° and a reference region at an elevation angle of 40° to 70°. Figure 5.1 (b) illustrates that extrema of the BrO curve are not as distinct as it is the case for the SO₂ curve.

Since the BrO column density is much lower than the SO₂ column density, and just lies slightly above the detection limit, the plume is hard to detect using the BrO column density as it is shown in fig. 5.1 (b). Therefore we evaluate BrO only in the plume location determined by using SO₂.

In a further step multiple reference and plume spectra of successive measurements are added to further increase the fit quality. Figure 5.2 visualizes the different steps described above in the retrieval of the BrO/SO₂ ratios.

Figure 5.3 (b) shows the routine of adding multiple spectra of consecutive measuring times. In the following the spectra resulting from the multi adding technique will be referred to as "Multi Add Spectra". The algorithm for co-adding is visualized in Figure 5.3 (b) was invented by [Vogel \(2011\)](#) and [Lübcke et al. \(2014\)](#).

Taking the BrO/SO₂ molar ratios if the column densities are close to zero yields unpredictable and unrealistic results. Thus, spectra measured in a thin volcano plume need to be excluded. This could be achieved by setting a BrO or/and an SO₂ threshold. A reasonable BrO threshold needs to be at least in the order of the DOAS fit error. However this could lead to elevated BrO/SO₂ ratios, since the BrO error is often close to the detection limit. Thus, all low BrO column densities are excluded from the evaluation ([Lübcke et al., 2014](#)), as an effect the ratios are systematic to high. The other possibility is to set an SO₂ threshold. In this thesis an SO₂ threshold (plume limit) of $7 \cdot 10^{17} \frac{\text{molec}}{\text{cm}^2}$ is used for the selection of spectra for the evaluation of the BrO/SO₂ ratio. $7 \cdot 10^{17} \frac{\text{molec}}{\text{cm}^2}$ is a high threshold for the column density. However, this approach assures that only strongly significant gas amounts are accounted ([Lübcke et al., 2014](#)). Choosing the SO₂ threshold in this way leads

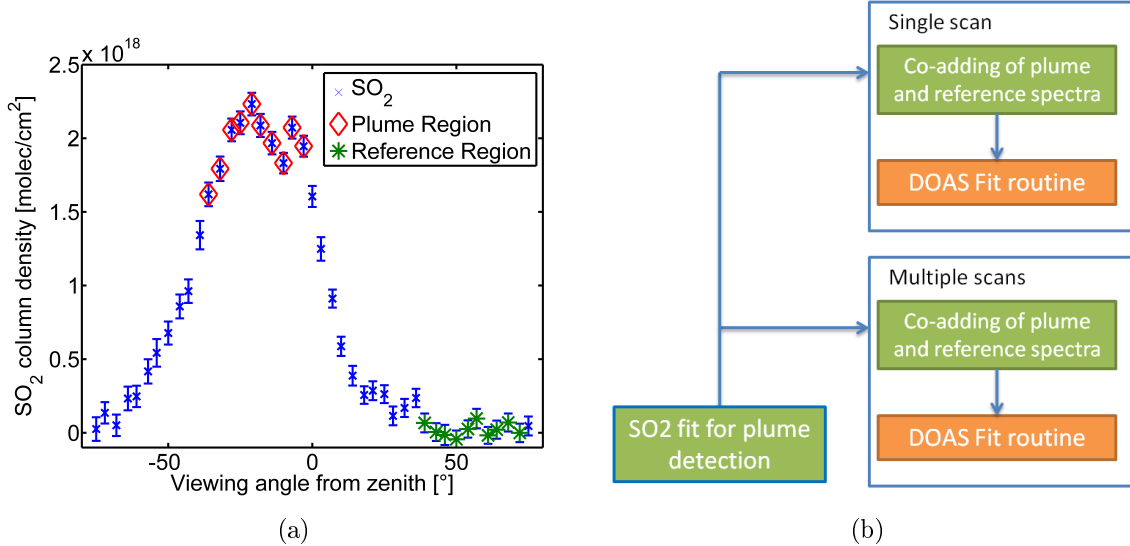


Figure 5.3: (a) SO_2 SCD as a function of the elevation angle. The co-added plume region is marked with red diamonds, and the co added reference region with green stars. From Warnach (2015). (b) Flow chart of the BrO and SO_2 evaluation. From Lübcke (2014).

to consistent observations for strong degassing, but low degassing events are rather excluded in the evaluation.

Ich würde hier noch erwähnen für welche Ratios wir mit diesem Plume Limit sensitiv sind (siehe Appendix in Dinger et al, 2018).

Increasing a plume limit leads to a decrease of usable data. The ratio of usable data as a function of the plume limit is shown in Figure 5.4. An exponential decrease of data can be observed. The plot is based on the data of Tungurahua. Plume limits below $7 \cdot 10^{17}$ are shaded in yellow. A plume limit of $7 \cdot 10^{17}$ leads to a ratio of usable data of approximately 10%.

5.2 Contamination problem

The conventional Evaluation is based on the assumption, that the reference is free of volcanic gases. This assumption was checked by using a volcanic gas free a high resolution solar atlas spectrum (see below) to evaluate the reference ?; Salerno et al. (2009). In some reference spectra an amount of SO_2 different from zero is found. Thus we can conclude, that there are some references which contain a non-negligible amount of volcanic trace gases. In rare (ca. 10% of the data) scenarios, the volcanic plume covers the whole scan region. This could happen if for example the volcanic plume of the day before extends over the hole scan area as a consequence of windless conditions. In consequence, the reference is contaminated with volcanic trace gases. Thus, the gas amount is underestimated by the NOVAC-evaluation: In Figure 5.5

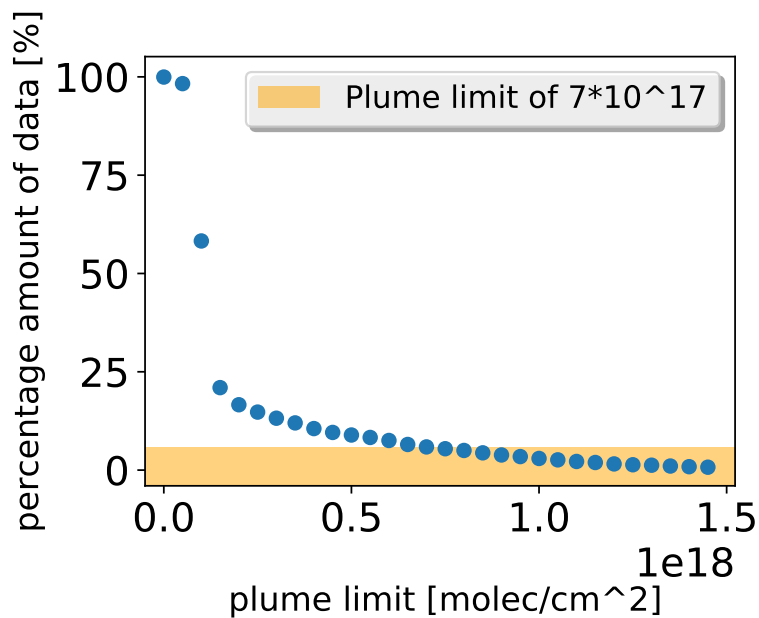


Figure 5.4: The decrease of the amount of data above the plume limit as a function of the plume limit. The plume limits below the actual plume limit of $7 \cdot 10^{17}$ are marked with a yellow shade.
noch dazu: In Prozent sieht das in der Tat schrecklich aus, relevant für eine Zeitreihenanalyse ist aber eher die (absolute) Anzahl der Tage mit (Multi-Scan-)Daten. Vielleicht als zweites Bild daneben?!

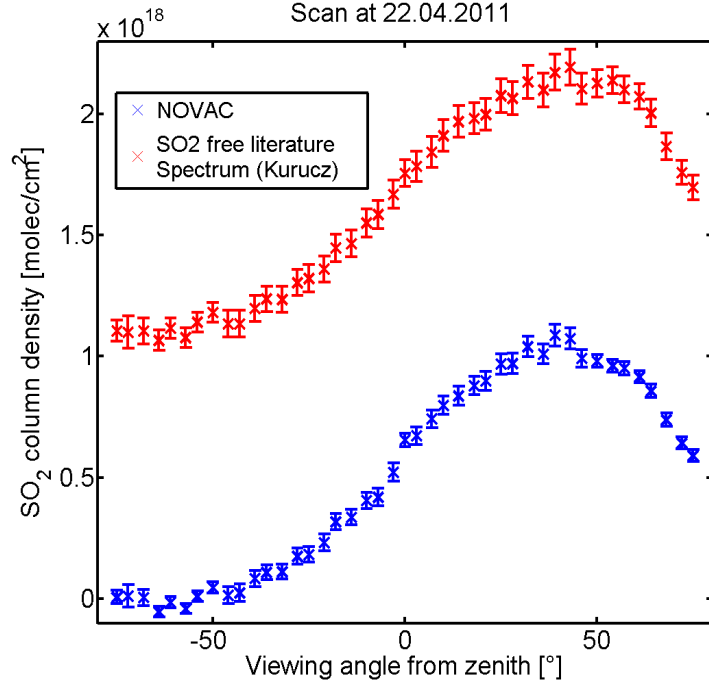


Figure 5.5: Scan with a contaminated reference spectrum from April 2011. From Warnach (2015)

we see an example from April 2011 (Tungurahua) where the reference region is contaminated by volcanic trace gases. The blue SO₂ curve shows the calculations with the NOVAC-evaluation, but since there is still SO₂ in the reference region, the assumption, that the SO₂ amount could be set to zero in the reference region is wrong. The red curve shows the real SO₂ curve, which lies significantly above the NOVAC -curve.

If the reference region for any reason is contaminated by volcanic trace gases, there are two possibilities: excluding the contaminated data from the evaluation or the reference spectrum has to be replaced by a volcanic-gas-free reference. Alternative spectra are a theoretical solar atlas spectrum or a volcanic-gas-free reference spectrum recorded by the same instrument at another time.

A further possibility is to assume, that contamination only occurs for SO₂, but not for BrO due to the smaller lifetimes of BrO, thus it is possible to use the Solar atlas spectrum for the SO₂ evaluation, but the reference, recorded by the NOVAC-instrument at the same time for the BrO retrieval. Hereby the assumption, that BrO is not contaminated need to be proved.

In the following we will discuss the two alternative reference spectra.

Evaluation using a Solar Atlas spectrum

An alternative for choosing the region with the lowest column density as reference region is to use a theoretical high resolution solar atlas spectrum as reference (Chance and Kurucz, 2010). ist das richtig?? The use of a theoretical solar atlas spectrum as a reference which is completely volcanic-trace-gases-free was first proposed by Salerno et al. (2009) and evolved by (Lübcke et al., 2014). The advantage of using a solar atlas spectrum as reference is, that we know that it is not affected by past or current volcanic gas emissions. Thus, it allows for a retrieval of the absolute trace gas SCDs in the volcanic gas plume. The disadvantage is, that using a solar atlas spectrum comes along with a drawback of precision: The spectral resolution of the theoretical solar atlas spectrum is much higher than of the NOVAC instruments. Therefore the instrument functions would need to be perfectly modeled and added to the retrieval. This is not straight forward, because the instrumental line-shape varies over the wavelength region and is also mathematically often not perfectly described by a simple approach like Gauss, lorentz,..etc.

The reduction of precision is acceptable for the SO₂ retrieval but not suitable for a BrO retrieval because then most data would be below the detection limit.

Possible contaminations can be checked by a theoretical solar atlas spectrum to evaluate the SO₂ amount in the reference.

Evaluation using a spectrum of the same instrument

An alternative reference spectrum could be a volcanic-gas-free reference spectrum recorded by the same instrument at a different time. When using such a reference several problems occur:

As described in Chapter 4 the instruments used in NOVAC do not include features like temperature stabilization. Due to that the measurements are not independent of external parameters. So we need to choose a reference recorded at similar conditions with respect to meteorology and radiation as well as in the temporal proximity due to instrumental changes with time and ambient conditions. Ideally the external conditions should be equal to the conditions at the time when the plume was recorded.

When performing the evaluation with the Solar Atlas Spectrum as reference, finding the instrument function occur to be a central challenge. If the instrument function for the solar atlas spectrum is found the functions is typically used for a few years. This could lead to higher errors due to an gradual worse matching instrument function. Using the reference of the same instrument but recorded at another day, leads also to problems caused by different instrument functions, but compared to the calculated instrument function used for the evaluation with the solar atlas spectrum those differences in the instrument function could be smaller.

In this work we combine both options in order to achieve both, enhanced accuracy but still maximum possible precision of the SO₂ and BrO retrievals. So we use the solar atlas spectrum to check for contamination and a reference spectrum recorded in temporal proximity by the same instrument as reference.

If contamination occurs it is possible to choose a new reference from a list of gas free alternative references. *wurde das schon mal gesagt???* In theory, for ideal instruments all references should lead to the same results for the gas retrievals. But instruments are imperfect (see Chapter 4) thus the reference need to be chosen carefully in order to ensure reliable results.

As discussed above it might occur, that the reference is contaminated for example by the plume of the day before. *das verstehe ich jetzt nicht - ich meine wenn wir jetzt das solar atlas spectrum nehmen ueberschaetzen wir ja , weil wir fahne von gestern und heute als eine einzige Fahne zusammen addieren... unterschaetzung haben wir wenn der bei zum beispiel kleiner windgeschwindigkeit -> breite fahne das instrument in keiner richtung fahnen freien himmel sieht - oder bei hoher windgeschwindigkeit und instrument nah am berg die fahne so runtergedreucht wird das das instrument in der fahne steht..: Florian : @ Nicole zur Überschätzung: wenn wir annehmen, dass die alte, bodennahe Fahne überall die gleiche Dicke hat und die neue Fahne eher im Zenit steht, dann ist der Anteil der alten Fahne zum neuen Gesamt signal kleiner als der alten Fahne zum neuen Referenzsignal. D.h. Überschätzung ja, aber weniger als simple Addition.* If that happens, we underestimate the gas amount by using a contaminated reference. But another possibility is, that the plume itself is also contaminated. This might be the case if the volcanic gas of the volcano is not taken away by the wind, but accumulates at the instrument. If this is the case, using an other reference would lead to an overestimation of the column density of gases. With the data retrieved by the NOVAC instruments it is very difficult to discover whether the plume is contaminated or not.

Figure 5.6 shows the strength of contamination as function of the mean SO₂ amount of the day before. The strength of contamination is measured as the difference between the evaluation for SO₂ with a contaminated reference recorded at the same time as the plume spectrum was recorded and using a gas free reference. The data where fitted with a linear function. The left plot shows data from the Tungurahua volcano. In the right plot the data of Nevado Del Ruiz are visualized. Even though both plots show a slight increase of contamination strength with the mean amount of SO₂ of the day before, the increase is not significant.

hier waere es gut noch andere parameter zu testen - wie in Luebcke et al, zum beispiele als funktion von Wind geschwindigkeit... Für NdR kann ich die Meteorologischen Daten ab 2014 beisteuern.

However this thesis is build on the assumption, that the plume is free of additional contamination *Nicole hat hier noch fragen, was ?*. In the following we discuss how to automatically determine an optimal reference from another scan.

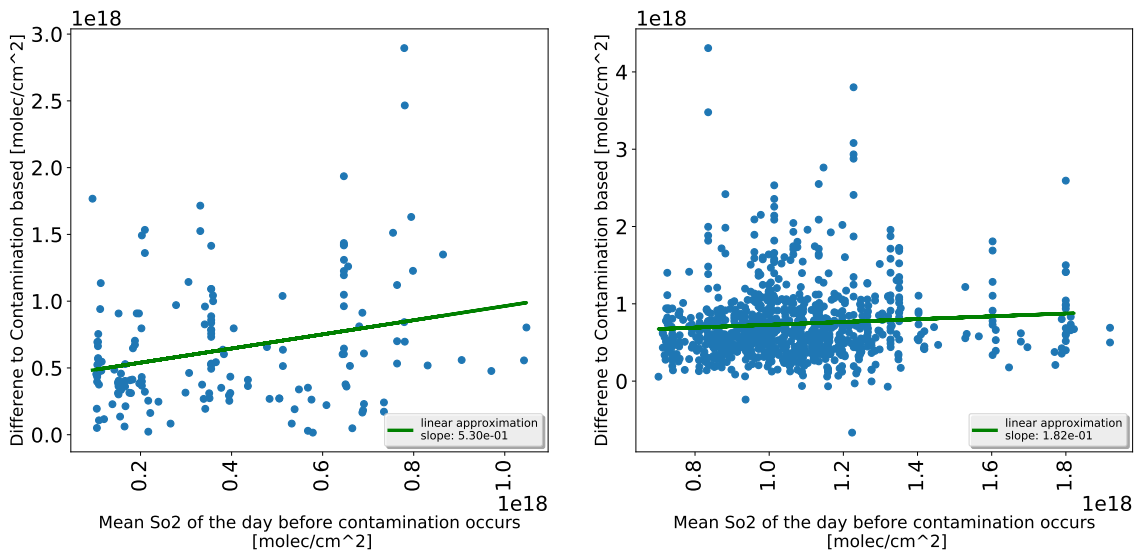


Figure 5.6: The strength of contamination as function of the mean SO₂ amount of the day before. The strength of contamination is defined as the difference in SO₂ SCD when evaluation with an alternative reference, or neglect the contamination. Left: data from Tungurahua. Right: data from Nevado Del Ruiz. Wie wurde mean SO₂ bestimmt? Wie sieht es bei max SO₂ aus? (Und eigentlich müsse man ja eher die SO₂ Emissionen anschauen. Die wir aber nicht (so einfach) kennen.)

6 BrO evaluation and its limitations

This chapter discusses the evaluation of the BrO Column densities, calculated from the spectra recorded by the spectroscopic instruments of NOVAC. The quality of the BrO retrieval hereby is defined by the BrO retrieval error.

Figure 6.1 shows the BrO "Multi Add" retrieval error distribution, which is centered around $1.1e^{13}$ to $1.4e^{13}$. The instruments of Nevado del Ruiz are coloured blue, while the the instruments of Tungurahua are coloured in yellow to red.

The evaluation of the data from NOVAC are parted into the evaluation of SO₂ and the evaluation of BrO. While the retrieving of SO₂ is relatively easy due to the high amount of SO₂ in the plume (magnitude of SO₂ at Tungurahua $\approx 1e^{18}$), the BrO evaluation is much more problematic (as it can be seen in Figure 5.1). The magnitude of BrO SCD is around $\approx 1e^{14}$.

This results in a larger uncertainty of the BrO SCD. Most of the BrO data (98.3% of the data) are below the detection limit of $\text{BrO}_{\text{err}}/\text{BrO}_{\text{value}} < 1/4$. In comparison SCD's of SO₂ in almost all cases (99.5% of the data) are above the detection limit. Choosing a different reference than the reference measured at the same time as the plume in 99% of the cases results in an increasing of the absolute error. Thus a BrO error which is smaller than the "Same Time Error" is often not possible to retrieve. However, for a contaminated same-time-reference the relative error might decrease due to the underestimation of the gas amount.

Due to the large uncertainty of BrO relative to SO₂ the optimization of the BrO error is of particular importance. Therefore, the reference is chosen with respect to the BrO error to maximize the quality of the BrO/SO₂ ratio.

The amount of gas free alternative references is around 1500 per year. To make an optimal choice, it is necessary to examine the conditions which influence the BrO retrieval.

Every spectrum is measured under certain conditions. These measuring conditions generally are not equal for the plume and the reference. References for which the surrounding conditions e.g temperature or cloudiness are equivalent with the surrounding conditions of the plume measuring lead to a small error.

In the following, we take a closer look at the dependence of the BrO error on external parameters.

Data used for the analysis

For this analysis, every plume reference pair of the observed time span is used. Thus 1000 recorded "multi add" spectra result in 1000^2 possible plume reference pairs and

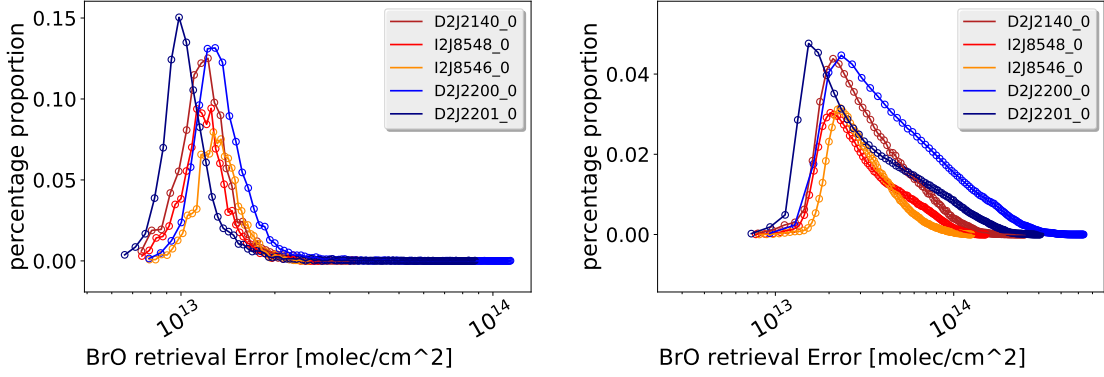


Figure 6.1: BrO error distribution shown for all instruments considered in this thesis. The left plot shows the BrO distribution for the "same time retrieval", the right plot shows the BrO error distribution for the evaluation with a reference from another time, where the temporal difference between plume and reference is not longer than two weeks. The peaks for the single instrument are located at: D2J2140_0: 1.2e+13; I2J8548_0: 1.3e+13; I2J8546_0: 1.4e+13; D2J2200_0: 1.4e+13; D2J2201_0: 1.1e+13

the corresponding differences in the external parameter and their associated BrO error.

6.1 BrO error dependence on external parameters

The measurement and evaluation of the spectra monitored with NOVAC depends on the surrounding conditions like temperature or cloudiness (Lübcke, 2014). Thus, the surrounding conditions need to be taken into account for choosing a new reference.

The better the surrounding conditions for the reference coincide with the conditions for the plume measurement, the lower is the BrO error.

The surrounding conditions that are considered in this thesis are:

- Temporal difference between measuring the plume and the reference,
- Temperature,
- Colorindex,
- Exposure time,
- Elevation angle,

- Daytime

The analysis of these external parameters are performed for spectra recorded at Tungurahua and Nevado del Ruiz. At Tungurahua three instruments with data recorded in the time span from July in 2008 to August in 2009 are used. Nevado del Ruiz contributes with two instruments in the time from the end of 2009 to the end of 2011.

6.1.1 Temporal difference

Due to instrument drifts the fit quality decreases with the time difference between recording the plume and the reference. This could be a result of a wavelength shift over time observed by Warnach (2015). As a result of the observed wavelength shift, the instrument function of the plume, does not match with the instrument function of the reference, thus the retrieving errors increase. Warnach (2015) suggests that the drift is caused by a hysteresis effect. Figure 6.2 shows the wavelength shift as a function of the time for six NOVAC instruments located at Tungurahua in the time between 2008 to 2014. In this thesis for the analysis data of Tungurahua between 2008 to the mid of 2009 are used. Figure 6.2 shows a rather steep drift in this time interval. Warnach (2015) observed a decrease of the shift after initial negative drift after the first two years at Pillate. Thus, it is observed that the temporal difference becomes less important for old instruments.

When using reference and plume spectra of the same time, these effects are cut out since the shift is equal for the plume and reference spectrum. For an increasing temporal difference between reference and plume measurement time the fit quality decreases and so does the BrO error.

To examine the effect of the temporal difference on the retrieved BrO error, for all reference-plume pairs the corresponding BrO error is calculated. Due to the large amount of reference plume pairs within one year, it takes more than a month (Hardware details: Intel(R) Core(TM) i5-4570 CPU @ 3.20Ghz 64 Bit operating system, amount of kernels: 4) to evaluate the corresponding BrO error for every possible reference-plume pair of one instrument. We did this for the D2J2140_0 instrument installed at Tungurahua:

In Figure 6.3 the BrO error as a function of the time difference between recording the plume and the reference is shown. The running mean is plotted with a black line.

In Figure 6.3 (a) it can be seen that a large temporal difference results in an increase of the BrO error of up to 600%. BrO errors of such magnitudes are too large for our purposes. Therefore, it is useful to set a maximal temporal difference, to prevent too large BrO error and to reduce the calculation time. In Figure 6.3 (a) it can be seen that the evolution of the BrO error with the temporal difference is symmetric around zero. Thus it is not necessary to distinguish between positive or negative temporal differences. Figure 6.3 (b) shows the evolution of the BrO error for a maximal absolute temporal difference of 120 hours. It is only possible to record

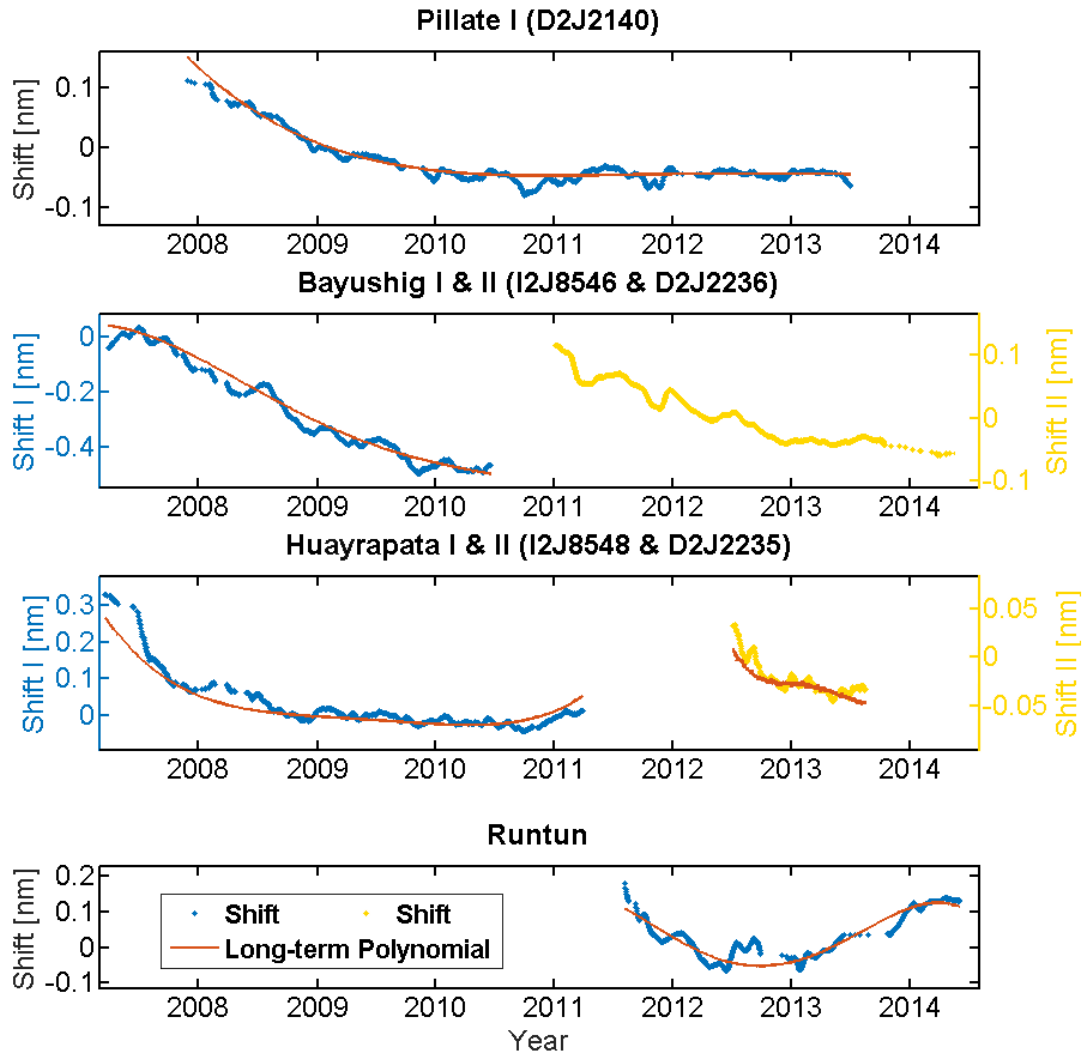


Figure 6.2: Wavelength shift over the time. The shift is shown for six NOVAC-instruments from Tungurahua. The red and yellow dots show the running mean over 20 days. Red line indicates a temperature independent long term polynomial. Source: Warnach (2015)

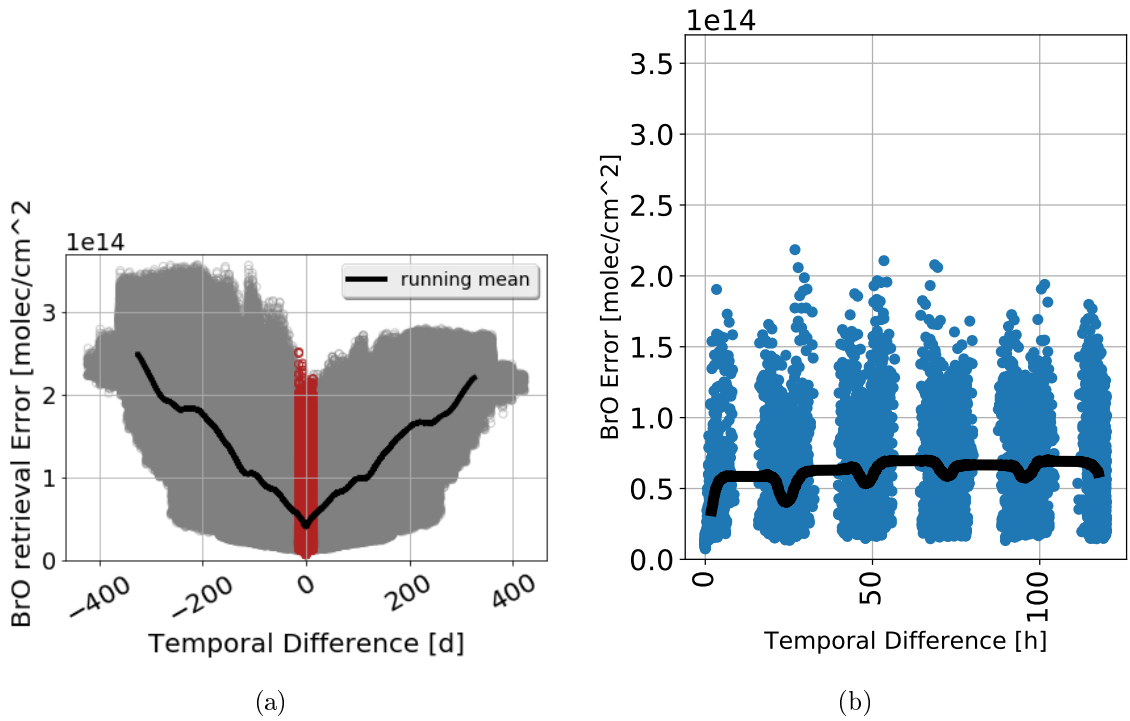


Figure 6.3: The BrO error as a function of the temporal difference shown for the Pilat instrument from Tungurahua (2008-2009). (a) Temporal differences up to 400 days. (b) Temporal differences up to 120h. The periodical BrO error evolution indicates the impact of the daytime

data during daytime. This causes the lack of data in the night time. A periodic decrease of the BrO error can be seen. This is a result of a decrease of the BrO error when the surrounding conditions coincide. In this case the daytime coincidence causes the BrO error decrease. This effect is analysed in detail in Section 6.1.3.

The maximal temporal difference should be large enough to ensure a sufficient amount of references to be able to pick a reference with similar conditions. However, the maximal temporal difference should be small enough to prevent too large BrO errors due to long term shifts.

To evaluate the maximal time difference, for which we still get reliable results for every plume, where the "same time reference" is contaminated, the alternative reference is chosen, which leads to the minimal BrO error.

In Figure 6.4 a histogram with the probability of picking the best reference as a function of the time difference is plotted. Obviously, the best results are achieved, if the day of measuring the plume is the same day as measuring the reference. A Gaussian fit is used to fit the data of the histogram. We allow all time differences within two sigma area. Thus, the maximal time difference is 14 days.

By restricting the temporal difference to 14 days, the amount of possible gas free

Instrument	D2J2140_0	I2J8546_0	I2J8548_0	D2J2200_0	D2J2201_0
Mean	84.6	163.7	217.1	284.0	225.6
Std	35.8	29.9	64.8	69.5	41.2
Min	8	113	97	64	63
Max	169	214	399	433	297

Table 6.1: Amount of possible references when restricting the time span between plume and reference to two weeks. Here in the "Mean" and "Std" row for each instrument the average restriction is shown with the corresponding standard deviation. The "Min" and "Max" rows show the extend of restriction in the extreme cases (minimum and maximum amount of available references / restriction ratio).

references decreases to an average of 195 alternative references per contaminated plume (see table 6.1). Hereby every plume has potential alternative reference spectra. The minimum amount of references is 8.

If a continuously evaluation is required, this means the spectra are evaluated directly after the recording, the number of suitable gas free references halves since only references recorded before the plume are available.

For the following analysis of the remaining external parameters all temporal differences are below 14 days.

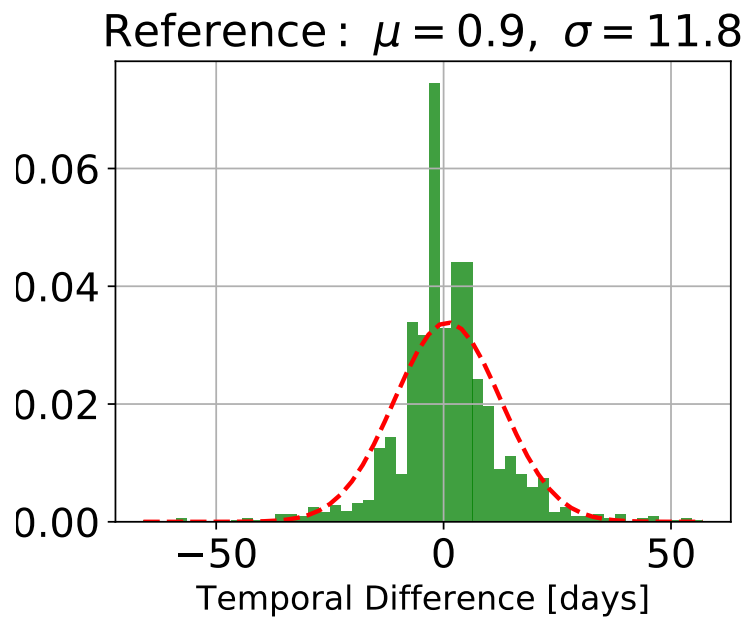


Figure 6.4: Histogram showing the frequency of getting the best reference as function of the temporal difference between plume and reference measuring. A Gaussian-like distribution is retrieved. The red dotted line visualizes a Gaussian fit for the shown histogram.

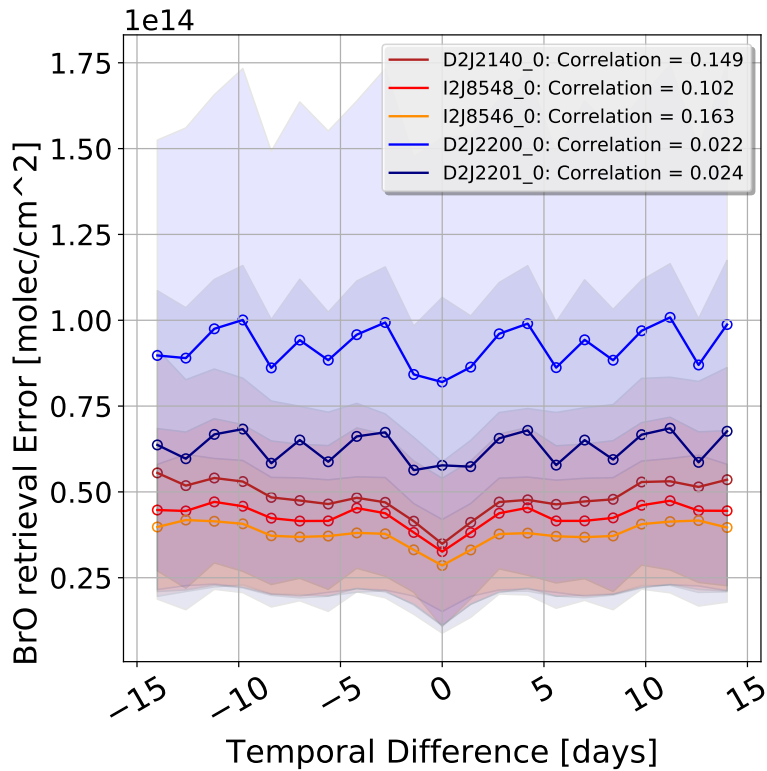


Figure 6.5: The BrO measurement error as a function of the temporal difference in days between the reference and the plume is shown for each of the individual instruments at Tungurahua and Nevado del Ruiz. The instruments at Nevado del Ruiz are coloured in blue, while the instruments at Tungurahua are coloured in red colour tones. To evaluate the plume spectra all reference spectra with a temporal distance of no longer than two weeks are used. An increase of the BrO error with the absolute difference in temperature is observable. This is quantified by a correlation between the BrO retrieval error and the absolute temporal difference. The plots reveal a symmetry around the axis with zero temperature difference.

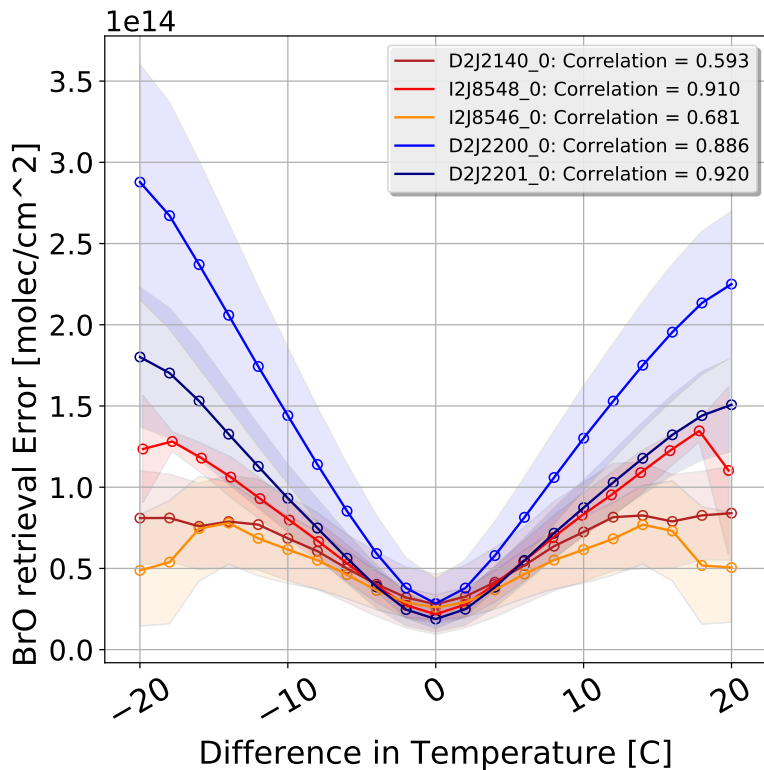


Figure 6.6: The BrO measurement error as a function of the difference of temperature between the reference and the plume is shown for each of the individual instruments at Tungurahua and Nevado del Ruiz. To evaluate the plume spectra all reference spectra with a temporal distance of no longer than two weeks are used. An increase of the BrO error with the absolute difference in temperature is observable. This is quantified by a correlation between the BrO retrieval error and the absolute difference in temperature. The plots reveal a symmetry around the axis with zero temperature difference.

6.1.2 Temperature

The instrument design of the NOVAC instruments compromises between accuracy and robustness as explained in Chapter 4. In particular, there are no internal thermal stabilizations installed as an attempt to reduce the instruments power consumption. This can influence the recorded spectra.

Each pixel of the spectrometer, which is used for the DOAS experiment, collects photons of a certain wavelength range.

The calibration for the wavelength to pixel mapping (WMP) is commonly done with a mercury lamp or by the comparison with the high defined Kuruz spectrum. As the WMP depends on the optical alignment of the spectrometer, which itself depends on the temperature, it is not constant. Changes in the spectrometers temperature

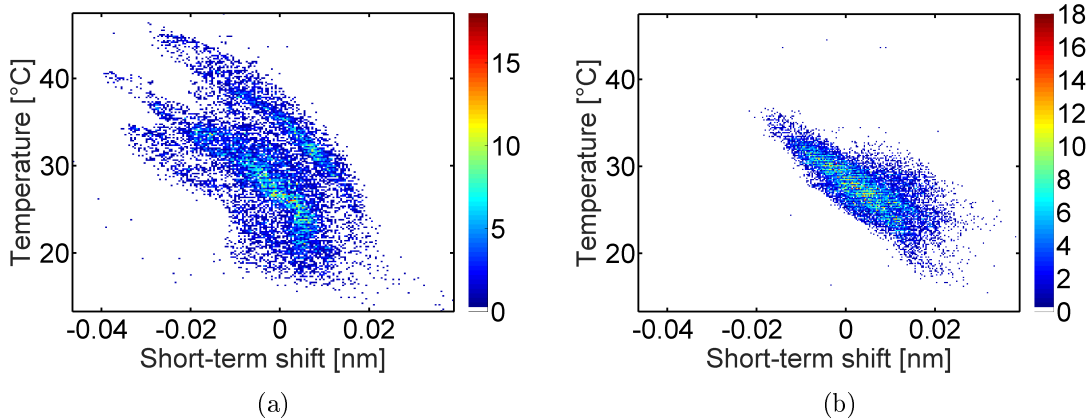


Figure 6.7: Short term wavelength as a function of the instrument temperature for Pillate 1. The coloring of the scatter points indicate the temporal evolution. (a) initial period prior to January 2010 (b) after 2010. Source: Warnach (2015).

can cause changes in the instrument line function and shifts in the WMP ((Pinardi et al., 2007)). Moreover, Warnach (2015) show that, short term shifts are related to the instrument temperature (see Figure 6.7).

The above discussed temperature dependence of the WMP causes a reduction of the fit quality with increasing instrument temperature difference between plume and reference. Thus, the BrO error also increases with the temperature difference. Compared to the other external parameters the temperate difference has the largest impact on the BrO error.

In Figure 6.6 the BrO error is plotted against the temperature difference between the plume and the reference spectrum. The blue dots show the mean BrO error at the specific temperature difference, the standard deviation is illustrated with gray error bars. The mean BrO deviation for the sametime evaluation is additionally marked with a red point. The plots reveal a symmetry around axis with zero temperature difference. To quantify the dependency between the BrO error and the difference in temperature the data are fitted with a polynom of the first order. Because of the observed symmetry around zero the absolute temperature difference is used for the fit. The computed fitting parameters slope and zero point for each instrument are shown in Section 6.1.2.

The zero points at Tungurahua vary from $1.6 \cdot 10^{13} \frac{\text{molec}}{\text{cm}^2}$ to $2.58 \cdot 10^{13} \frac{\text{molec}}{\text{cm}^2}$. The variation at Nevado del Ruiz ranges from $9.07 \cdot 10^{12} \frac{\text{molec}}{\text{cm}^2}$ to $1.38 \cdot 10^{13} \frac{\text{molec}}{\text{cm}^2}$.

Also the correlation between the BrO error and the absolute temperature difference is shown. Here the correlation is calculated using the python library Numpy. The correlation ranges from 0.593 for the instrument D2J2140_0 to 0.92 for D2J2201_0 and exhibits a large variation between the instruments.

Instrument	D2J2140_0	I2J8546_0	I2J8548_0	D2J2200_0	D2J2201_0
Slope	4.10e+12	3.93e+12	6.50e+12	1.24e+13	8.17e+12
Correlation	0.593	0.681	0.910	0.886	0.920
Zero point	2.58e+13	2.23e+13	1.60e+13	1.38e+13	9.07e+12
ΔT_2	6.3	5.7	2.5	1.1	1.1

Table 6.2: The BrO measurement error as a function of the difference of temperature between the reference and the plume is fitted with a first order polynomial for each of the individual instruments at Tungurahua and Nevado del Ruiz. This table shows the fitting parameters slope and zero point. Moreover, the correlation between the BrO error and the absolute temperature difference is shown. For the temperature difference this correlation with an average of 0.797 is the highest compared to the other external parameters. In the ΔT_2 row the temperature difference for which the error doubles compared to a temperature difference of zero is shown. This is already the case for a difference of $3.3^\circ C$

The ΔT_2 row in the table shows the temperature difference for which the error doubles compared to a temperature difference of zero. If restricting the temperature difference to the mean ΔT_2 over all instruments ($Mean(\Delta T_2) = 3.3$) the amount of possible references decrease as shown in Table 6.3. Excluding references with temperature differences above $Mean(\Delta T_2) = 3.3$ restricts the amount of potential references to 46.8% for D2J2140_0 to 82.3% for D2J2200_0.

The advantage of restricting the accepted temperature difference is a better control of the choice of the best reference. The disadvantage is that the amount of possible references decreases. Thus, it could occur that a reference is dismissed, which has a large temperature difference but is very similar in the remaining parameters.

6.1.3 Daytime

During the day a lot of external parameters like temperature, solar altitude etc. change. In particular, the solar altitude could have an impact on the fit quality since the light path of the sun is much longer in the morning or evening compared to the noon. Therefore, the scattering effects and the Fraunhofer structures are different for both spectra.

In Figure 6.8 the BrO error is plotted against the daytime difference between the plume and the reference spectrum. The plots are similar to the plots for the temperature: The blue dots show the mean BrO error at the specific daytime difference, the standard deviation is illustrated with gray error bars. The mean BrO deviation for the sametime evaluation is additionally marked with a red point.

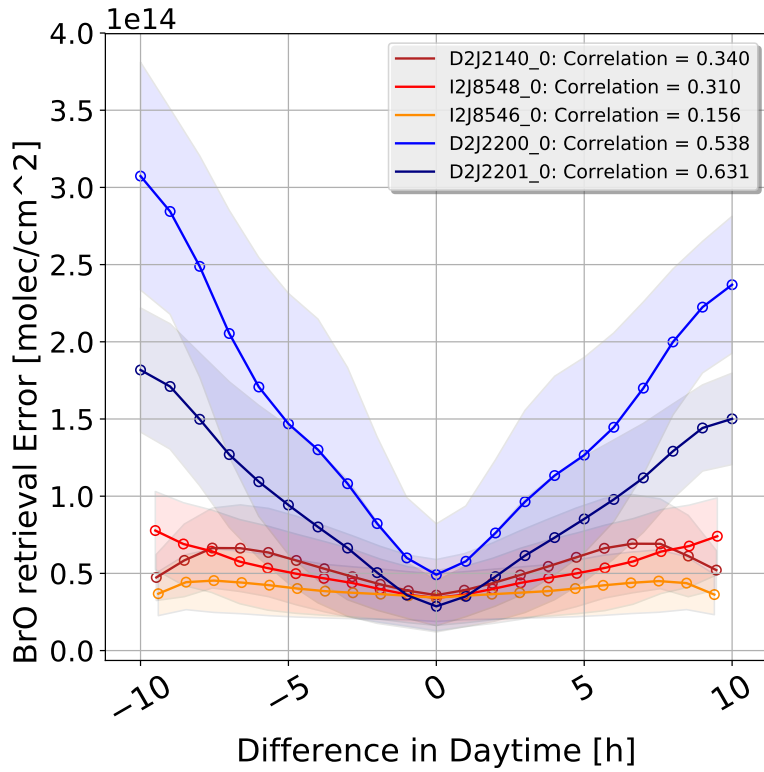


Figure 6.8: The BrO measurement error as a function of the difference of daytime between the reference and the plume is shown for each of the individual instruments at Tungurahua and Nevado del Ruiz. To evaluate the plume spectra all reference spectra with a temporal distance of no longer than two weeks are used. An increase of the BrO error with the absolute difference in daytime is observable. This is quantified by a correlation between the BrO retrieval error and the absolute difference in daytime. The plots reveal a symmetry around axis with zero daytime difference.

Instrument	D2J2140_0	I2J8546_0	I2J8548_0	D2J2200_0	D2J2201_0
Mean	39.6/46.8%	119.3/72.9%	158.2/72.9%	233.6/82.3%	151.6/67.2%
Std	24.7/68.9%	50.4/168.6%	76.0/117.2%	84.5/121.6%	72.6/176.2%
Min	1/12.5%	8/7.1%	12/12.4%	3/4.7%	6/9.5%
Max	130 /76.9%	213 /99.5%	386/96.7%	414 /95.6%	296 /99.7%

Table 6.3: This table shows the absolute amount and the ratio (to Table 6.1) of remaining references if restricting the temperature difference to the mean ΔT_2 over all instruments ($Mean(\Delta T_2) = 3.3^\circ C$). Here in the "Mean" and "Std" row for each instrument the average restriction is shown with the corresponding standard deviation. The "Min" and "Max" rows show the extend of restriction in the extreme cases (minimum and maximum amount of available references / restriction ratio).

As for the temperature the plots reveal a symmetry around the axis of zero daytime difference.

To quantify the dependency between the BrO error and the difference in daytime the data are fitted with a polynom of the first order. Because of the observed symmetry around zero the absolute daytime difference is used for the fit. The computed fitting parameters slope and zero point for each instrument are shown in Section 6.1.3.

As it can be seen in Section 6.1.3, the zero points at Tungurahua vary from $3.28 \cdot 10^{13} \frac{molec}{cm^2}$ to $3.43 \cdot 10^{13} \frac{molec}{cm^2}$. The variation at Nevado del Ruiz ranges from $2.24 \cdot 10^{13} \frac{molec}{cm^2}$ to $4.01 \cdot 10^{13} \frac{molec}{cm^2}$.

The correlations ranges from 0.156 for the instrument I2J8546_0 to 0.631 for D2J2201_0 and exhibits a large variation between the instruments.

The ΔDT_2 row in the table shows the daytime difference for which the error doubles compared to a daytime difference of zero.

If restricting the daytime difference to the mean ΔT_2 over all instruments with significant impact of the daytime, ($Mean(\Delta DT_2) = 4.75h$) the amount of possible references decrease as shown in Table 6.5. The mean ($Mean(\Delta DT_2)$) is calculated without taking the I2J8546_0 into account due to the low correlation of 0.156. Using the I2J8546_0 instrument as well would lead to an $Mean(\Delta DT_2)$ of 8.6h, thus, the restriction would not have any influence, since the maximal time difference is limited to the time where the sun is shining.

Excluding references with daytime differences above 4.75h restricts the amount of potential references to 85.1% for D2J2140_0 to 96.8% for D2J2200_0. In extreme cases a restriction down to 51.3% of the entire set of references can occur.

6.1.4 Colorindex

Clouds have a strong influence on the atmospheric radiative transfer and thus affect the interpretation and analysis of DOAS (Wagner et al., 2014). Clouds can be iden-

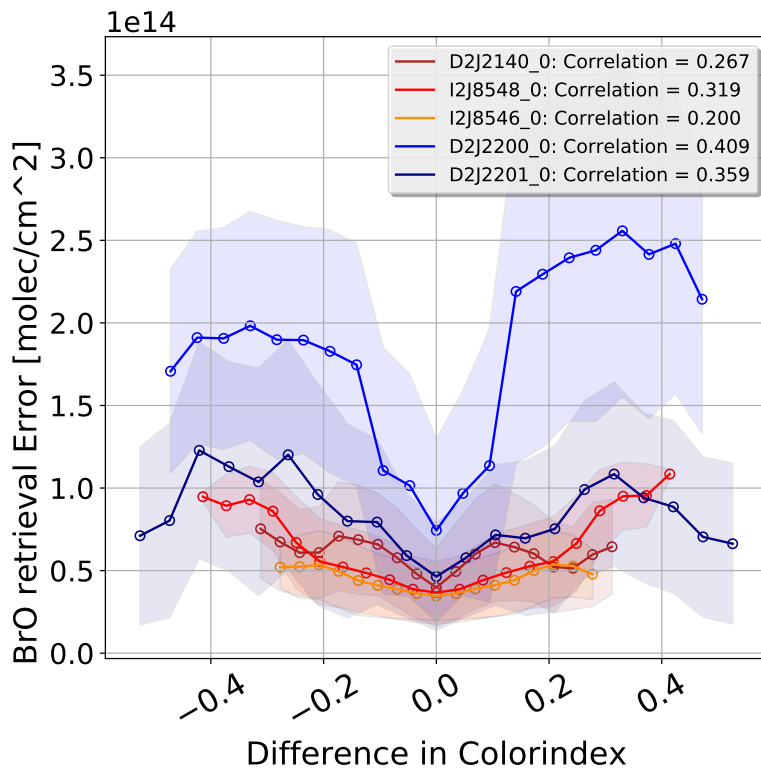


Figure 6.9: The BrO measurement error as a function of the difference of colorindex between the reference and the plume is shown for each of the individual instruments at Tungurahua and Nevado del Ruiz. To evaluate the plume spectra all reference spectra with a temporal distance of no longer than two weeks are used. An increase of the BrO error with the absolute difference in colorindex is observable. This is quantified by a correlation between the BrO retrieval error and the absolute difference in colorindex. The plots reveal a symmetry around axis with zero colorindex difference.

Instrument	D2J2140_0	I2J8546_0	I2J8548_0	D2J2200_0	D2J2201_0
Slope	5.07e+12	1.40e+12	3.77e+12	2.04e+13	1.38e+13
Correlation	0.340	0.156	0.310	0.538	0.631
Zero point	3.43e+13	3.39e+13	3.28e+13	4.01e+13	2.24e+13
ΔDT_2	6.8	24.2	8.7	1.9	1.62

Table 6.4: The BrO measurement error as a function of the difference of daytime between the reference and the plume is fitted with a first order polynomial for each of the individual instruments at Tungurahua and Nevado del Ruiz. This table shows the fitting parameters slope and zero point. Moreover, the correlation between the BrO error and the absolute daytime difference is shown. In the ΔDT_2 row the daytime difference for which the error doubles compared to a daytime difference of zero is shown.

tified by several measurement quantities that they influence. As Mie scattering is dominant in clouds the wavelength of the light that is scattered is different than the Rayleigh sky. Thus, clouds can be easily identified by their white color. Therefore, the cloudiness of the sky can be quantified in a scalar measure defined by the ratio of the measured intensity at two wavelengths, the so-called colour index. Wagner et al. (2014) showed that for a zenith-looking instrument the measured radiation intensity is enhanced by clouds. Thus, clouds can cause large errors for the retrieved gas column density and the corresponding uncertainties. Cloud effects are especially severe if the cloudiness for the recorded plume and reference spectra strongly defer. Also for broken clouds the described effect can be observed as measurements at some elevation angles might be influenced by clouds while others are not. In this work the Colour Index (CI) is the ratio between the intensities at 320nm and 360 nm. These two wavelengths are as far apart as the filter used for stray-light prevention in the spectrometers allows. On the other hand, the lower wavelength avoids the deep UV range where SO₂ and O₃ absorption plays a dominant role. The Mie scattering in the clouds is responsible for the higher amount of radiation from larger wavelengths. This results in a decrease of the CI (Lübecke, 2014).

We evaluated the CI at the zenith. To increase the stability of the fit we add 10 intensities. Using always the zenith to evaluate the colour index makes the colour index more comparable, but if broken clouds occur, the CI of the reference and the plume could differ from the calculated CI of the zenith. This could be a reason for the large deviations of the mean BrO error as function of the colour index (see Figure 6.9)

In Figure 6.9 the BrO error is plotted against the colorindex difference between the plume and the reference spectrum. The plot is done similar to the plots for the temperature. The plots mostly reveal a symmetry around the zero colorindex difference-axis. Thus, the absolute colorindex can be used for the fitting which is done equivalently to the analysis of the temperature and the daytime. The computed

Instrument	D2J2140_0	I2J8546_0	I2J8548_0	D2J2200_0	D2J2201_0
Mean	72.0/85.1%	147.4/90.0%	198.4/91.4%	275.0/96.8%	205.8/91.2%
Std	31.87/89.0%	32.0/107.0%	71.0/109.5%	70.8/101.8%	50.1/121.6%
Min	6/75.0%	58/51.3%	91/93.8%	54/84.4%	45/71.4%
Max	160/94.7%	214/100%	399/100%	433/100%	297/100%

Table 6.5: This table shows the absolute amount and the ratio (to Table 6.1) of remaining references if restricting the daytime difference to the mean ΔDT_2 over all instruments except I2J8546_0 due to the large uncertainty ($Mean(\Delta DT_2) = 4.75h$). Here in the "Mean" and "Std" row for each instrument the average restriction is shown with the corresponding standard deviation. The "Min" and "Max" rows show the extend of restriction in the extreme cases (minimum and maximum amount of available references / restriction ratio).

fitting parameters slope and zero point for each instrument are shown in table 6.6. The zero points at Tungurahua vary from $3.36 \cdot 10^{13} \frac{molec}{cm^2}$ to $4.01 \cdot 10^{13} \frac{molec}{cm^2}$. The variation at Nevado del Ruiz ranges from $4.74 \cdot 10^{13} \frac{molec}{cm^2}$ to $7.21 \cdot 10^{13} \frac{molec}{cm^2}$.

The correlation is as well calculated and ranges from 0.2 for the instrument I2J8546_0 to 0.409 for D2J2200_0.

The ΔCI_2 row in the table shows the colorindex difference for which the error doubles compared to a colorindex difference of zero.

Instrument	D2J2140_0	I2J8546_0	I2J8548_0	D2J2200_0	D2J2201_0
Slope	2.30e+14	7.92e+13	1.17e+14	5.42e+14	1.91e+14
Correlation	0.267	0.200	0.319	0.409	0.359
Zero point	4.01e+13	3.36e+13	3.47e+13	7.21e+13	4.74e+13
ΔCI_2	0.174	0.424	0.297	0.133	0.248

Table 6.6: The BrO measurement error as a function of the difference of colorindex between the reference and the plume is fitted with a first order polynomial for each of the individual instruments at Tungurahua and Nevado del Ruiz. This table shows the fitting parameters slope and zero point. Moreover, the correlation between the BrO error and the absolute colorindex difference is shown. In the ΔCI_2 row the colorindex difference for which the error doubles compared to a colorindex difference of zero is shown.

If restricting the colorindex difference to the mean $Mean(\Delta CI_2) = 0.255$ over all instruments the amount of possible references decrease very little as can be seen in

Instrument	D2J2140_0	I2J8546_0	I2J8548_0	D2J2200_0	D2J2201_0
Mean	84.6/100%	163.7/100%	215.6/99.3%	275.4/97.0%	219.4/97.3%
Std	35.8/100%	29.9/100%	65.4/101%	67.8/97.6%	49.86/121%
Min	8/100%	113/100%	97/100%	61/95.3%	28 /44.4%
Max	169/100%	214/100%	399/100%	421/97.2%	297/100%

Table 6.7: This table shows the absolute amount and the ratio (to Table 6.1) of remaining references if restricting the colorindex difference to the mean ΔCI_2 over all instruments ($Mean(\Delta CI_2) = 0.2553$). Here in the "Mean" and "Std" row for each instrument the average restriction is shown with the corresponding standard deviation. The "Min" and "Max" rows show the extend of restriction in the extreme cases (minimum and maximum amount of available references / restriction ratio).

Table 6.7.

6.1.5 Elevation Angle

Instrument	D2J2140_0	I2J8546_0	I2J8548_0	D2J2200_0	D2J2201_0
Slope	1.73e+8	1.55e+10	-9.00e+9	2.92e+11	-3.96e+10
Correlation	0.000	-0.010	0.012	0.065	-0.034
Zero point	4.77e+13	4.23e+13	3.78e+13	8.37e+13	6.44e+13

Table 6.8: The BrO measurement error as a function of the difference of elevation angle between the reference and the plume is fitted with a first order polynomial for each of the individual instruments at Tungurahua and Nevado del Ruiz. This table shows the fitting parameters slope and zero point. Moreover, the correlation between the BrO error and the absolute elevation angle difference is shown.

The elevation angle describes the angle between the horizon and the zenith. When using the plume spectrum and the reference spectrum of the same time, the difference in elevation angle cannot be zero, since the location of the plume does not coincide with the location of the reference.

In fig. 6.10 the BrO error is plotted as a function of the elevation angle. Obviously no significant correlation between the two parameters can be identified. This is not surprising because other than the previously discussed parameters we do not expect a more precise measurements for a difference of zero. Only the data of the D2J2200_0 instrument significantly varys with the elevation angle. The observable

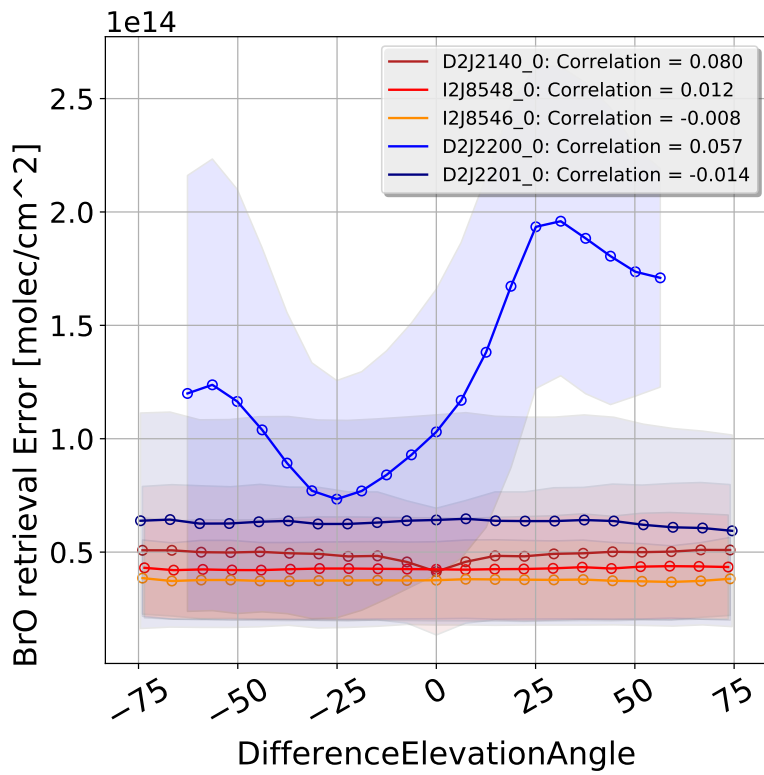


Figure 6.10: The BrO measurement error as a function of the difference of elevation angle between the reference and the plume is shown for each of the individual instruments at Tungurahua and Nevado del Ruiz. To evaluate the plume spectra all reference spectra with a temporal distance of no longer than two weeks are used. The plots do not reveal a symmetry around axis with zero elevation angle difference for all instruments. The D2J2200_0 instrument at Nevado del Ruiz is not symmetric around zero.

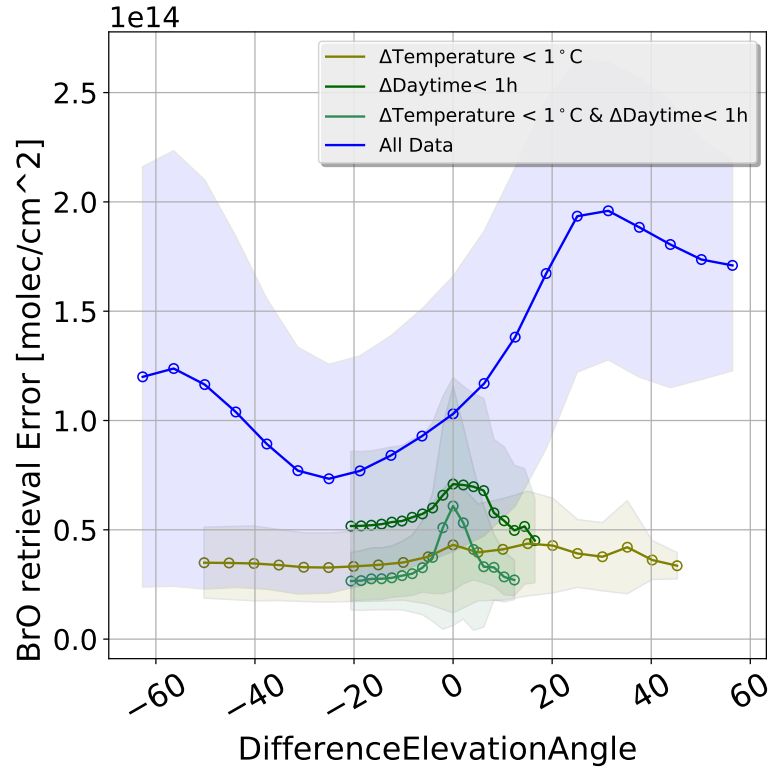


Figure 6.11: The BrO measurement error as a function of the difference of elevation angle between the reference and the plume for the D2J2200_0 instrument. To evaluate the origin of the behavior of the BrO retrieval error of the D2J2200_0 instrument as a function of the difference in elevation angle, the data are analysed on its temperature and daytime dependence. The same dependence is shown with restriction to a difference in temperature ($\Delta\text{Temperature}$) of below 1°C or restriction on a daytime difference of below 1h ($\Delta\text{Daytime} \pm 1\text{h}$). The curves are marked with different green color tones, as it is shown in the legend. The blue line shows the BrO error as function of the elevation angle, when using all data for comprehension.

variation of the BrO error with the elevation angle differs from the symmetric dependence of all other external parameter, the minimum BrO error can be found at a difference in elevation angle of -20°. This curve is a result of the solar altitude over the day which can be obtained if only using data of the same day time. Such a plot can be seen in Figure 6.11. Figure 6.11 shows the BrO retrieval error as function of the difference elevation angle for the D2J2200_0 instrument at the Nevado del Ruiz volcano. The blue line is equivalent to the results which are shown in Figure 6.10 for comparison. The green lines show data, with a maximal difference in temperature of 1°C or maximal difference in daytime of 1h. If restricting the data to just small differences in temperature or/and daytime, the dependency between the BrO retrieval and elevation angle appears to be not significant. Whereas the maximum of the BrO error can be found at an difference in elevation angle of zero.

Since the BrO error does not depend significantly on the elevation angle no restriction on difference of the elevation angle is needed.

6.1.6 Exposure time

The exposure time is the length of time the sensor of the NOVAC instrument is exposed to light. In one scan the exposure time is set constant to the exposure time of the first scan, the pre reference. The amount of light that reaches the film or image sensor is proportional to the exposure time. The exposure time is adjusted in the way that the maximum intensity does not overly the capacity of the sensor. Thus, the exposure time can be used as a degree of sky lightness.

We can observe a small dependency of the BrO error on the exposure time at Tungurahua and Nevado del Ruiz as it is shown in Figure 6.12. The BrO error as a function of the difference in exposure time is also symmetric around zero for all instruments. Thus the absolute difference in the exposure time is sufficient for the evaluation.

The instruments at Tungurahua do not show a significant dependence (correlation coefficient between 0.067 and 0.251) on the exposure time, even though there is always a minimum of the BrO error at a difference of the Exposure Time of 0ms.

Nevado del Ruiz shows a stronger correlation between the BrO error and the exposure time.

Table 6.9 shows the slope, correlation, zero point and the ΔET_2s . The differences in exposure time where the BrO error increases by a factor of two compared to the difference of exposure time of zero. Restrictions of the exposure time to the mean of the ΔET_2s of all instruments which is 632.25 ms leads to an average decrease compared to table 6.1 of data of 98.78%. The results for each instrument can be found in table 6.10.

Section 6.1.6 shows the amount of possible references if the only data are considered which do not exceed the thresholds in each external parameter. The average

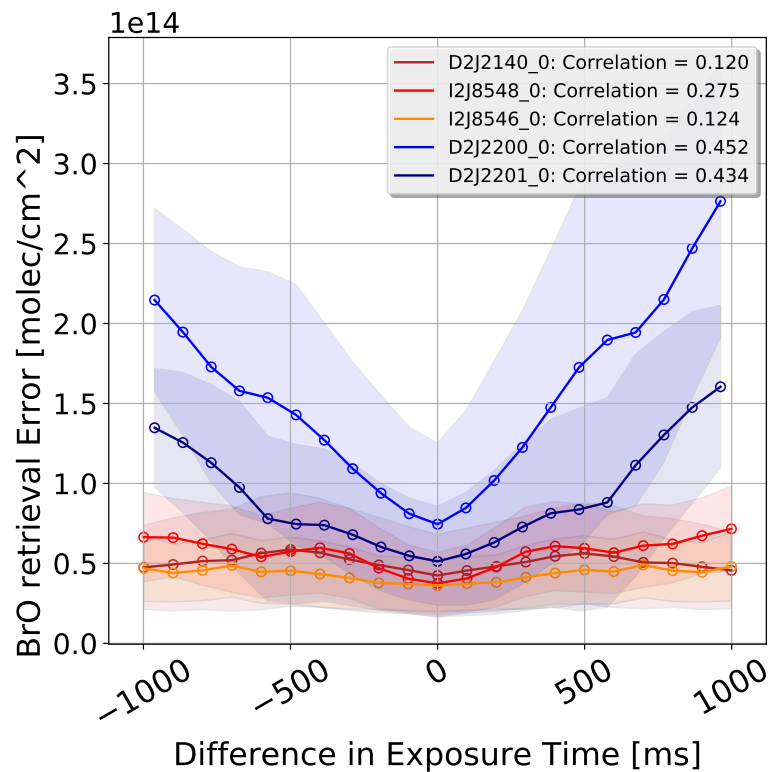


Figure 6.12: The BrO measurement error as a function of the difference of exposure time between measuring the reference and the plume are shown. To evaluate the plume spectra all reference spectra with a temporal distance of no longer than two weeks are used. An increase of the BrO error with the distance in exposure time is observable.

Instrument	D2J2140_0	I2J8546_0	I2J8548_0	D2J2200_0	D2J2201_0
Slope	5.54e+9	1.54e+10	3.04e+10	1.72e+11	9.37e+10
Correlation	0.067	0.121	0.251	0.452	0.434
Zero point	4.63e+13	3.58e+13	3.87e+13	6.88e+13	4.68e+13
ΔT_2	8357	662	1273	95	499

Table 6.9: The BrO measurement error as a function of the difference of exposure time between the reference and the plume is fitted with a first order polynomial for each of the individual instruments at Tungurahua and Nevado del Ruiz. This table shows the fitting parameters slope and zero point. Moreover, the correlation between the BrO error and the absolute exposure time difference is shown.

Instrument	D2J2140_0	I2J8546_0	I2J8548_0	D2J2200_0	D2J2201_0
Mean	81.7/96.5%	162.8/99.4%	212.8/98.0%	284.0/100%	225.6/100%
Std	35.3/98.6%	30.1/101%	64.5/99.5%	69.5/100%	41.2/100%
Min	8/100%	113/100%	95/97.9%	64/100%	63/100%
Max	167/98.8%	214/100%	395/99.0%	433/100%	297/100%

Table 6.10: Amount of possible references when restricting the difference in exposure time between plume and reference to differences below 632.25 ms.

amount of available references per plume decreases to 64%. While the performance decreases as by **xy percent. this will be explained later.**

Dependency of external parameters on each other

In all discussions on the impact of the external parameter on the retrieved BrO error the dependency of the external parameter on each other are neglected. It is plausible that the temperature correlates with the cloudiness or the lightness due to sunlight. Therefore the correlation of the exposure time with the BrO error could be a result of the correlation of the temperature with the BrO error. Figure 6.13 shows an example of the dependency of external parameters on each other. The difference in temperature as a function of the difference in exposure time. The BrO error is color-coded.

All correlations between the external parameters are shown in Figure 6.14. Figure 6.14 shows discrete correlation values from 0.3 to 1. Correlations below 0.3 are ignored. Small plus and minus signs indicate whether the correlation is negative or positive. The temperature depends on the daytime, due to the dependence of the temperature on the sun, thus a correlation between the difference in temperature

Instrument	D2J2140_0	I2J8546_0	I2J8548_0	D2J2200_0	D2J2201_0
Mean	36.0/42.6%	112.9/69.0%	148.9/68.6%	217.0/76.4%	140.4/62.2%
Std	22.35/62.4%	50.6/169.2%	75.9/117.1%	82.1/118.1%	71.0/172.3%
Min	1/12.5%	8/7.1%	12/12.4%	3/4.7%	6/9.5%
Max	127/75.1%	212/99.1%	382/95.7%	398/91.9%	283/95.3%

Table 6.11: Amount of possible references while restricting the difference in colorindex between plume and reference to differences above 0.255. maximal Time difference is $3.358^{\circ}C$, maximal daytime difference is 4.75h without Exposure Time between plume and reference to differences below 632.25 ms.

and the difference in daytime (Correlation of ≈ 0.5) can be observed. Since the temperature depends on the intensity of the sun, it also correlates with the difference in exposure time (Correlation of ≈ 0.4). The difference in temperature also slightly correlates with the difference in colorindex, due to the dependency of temperature on the cloudiness (Correlation of ≈ 0.3). The low correlations could appear due to the uniform cloudiness near to the equator. The correlation between the temperature difference to the temporal difference (Correlation of ≈ 0.3) probably occurs due to long term changes in temperature. Furthermore the difference in exposure time correlates with the daytime and the colorindex (Correlation of ≈ 0.4) as a result of the dependency on the sun intensity.

To eliminate the correlation between the external parameters the BrO error dependency on one external parameter where calculated by keeping the differences in the other external parameters constant. Hereby only parameters were kept constant, where the correlation is above 0.3. Thus, when looking at the temperature, only the difference in temperature need to be constant, since the temporal distance does not correlate with the other considered external parameter. The results can be seen in Figure 6.15 to Figure 6.18.

Figure 6.15 shows the BrO retrieval error as a function of the temporal difference between the reference and the plume spectrum. All differences in temperature are below one degree. Compared to the correlations, calculated without eliminating the dependence on the temperature, the correlations increase. The dependence of the instruments installed at Tungurahua are still significant higher. From the results can be interpreted that the temporal difference between the time when measuring the plume and the reference has an impact on the fit quality, but this impact is smaller as the impact of the instrument temperature.

Figure 6.16 shows the dependency of the BrO retrieval error on the difference in exposure time for all considered instruments. Hereby, only data are used, where the difference in temperature is below 1 degree, the difference in colorindex is below 0.05 and the difference in daytime is below one hour. The temporal difference and

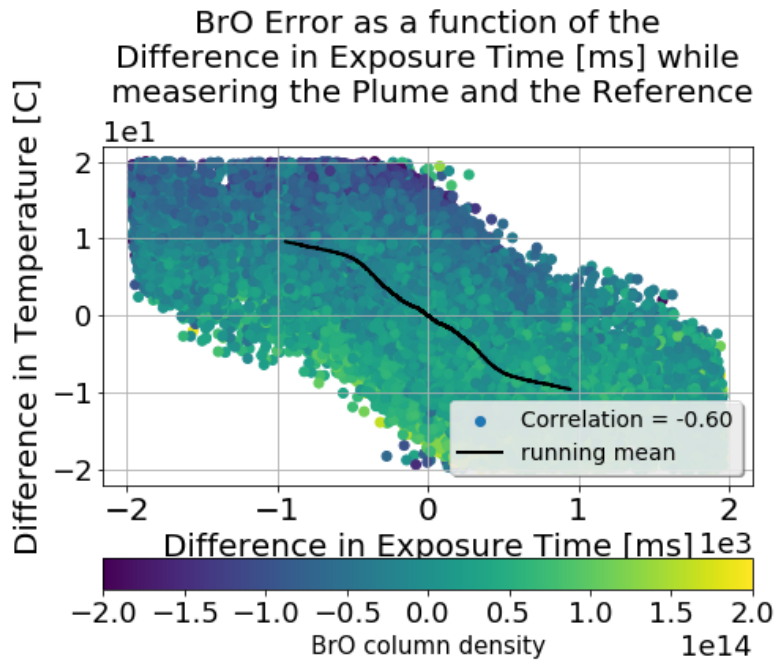


Figure 6.13: An example of the dependency of external parameters on each other. The difference in temperature as a function of the exposure time. data from Tungurahua.

the difference in elevation angle are not kept constant, since we could not observe a relation between the exposure time and the temporal difference or the elevation angle. The correlations between the BrO error and the difference in exposure time decrease for each instrument if the temperature, daytime and colorindex are kept constant. Even though, the correlations at Nevado Del Ruiz are still higher as the correlations at Tungurahua.

Figure 6.17 shows the BrO retrieval error as a function of the difference in colorindex for all instruments. The temperature and the exposure time shows a dependency on the colorindex as it can be seen in Figure 6.14. Both are kept constant, the difference in temperature is below 1 degree and the difference in exposure time is below 100 ms. The correlations decrease compared to Figure 6.9. Especially the correlation of the D2J2201_0 instrument decreases.

Figure 6.18 shows the BrO retrieval error as a function of the difference in daytime for all considered instruments. As it can be seen in fig. 6.14 the exposure time and the temperature need to be kept constant. The difference in temperature is below 1 degree, the difference in exposure time belwo 100 ms. A general decrease of the correlations compared to Figure 6.8 is observable.

Restricting the data, to where the temperature difference is kept below one degree, leads to an distortion of the data. Thus the results plotted in Figure 6.15 to Figure 6.18 could also have systematic errors.

When comparing the correlations of the data from ?? and ?? to the correlations

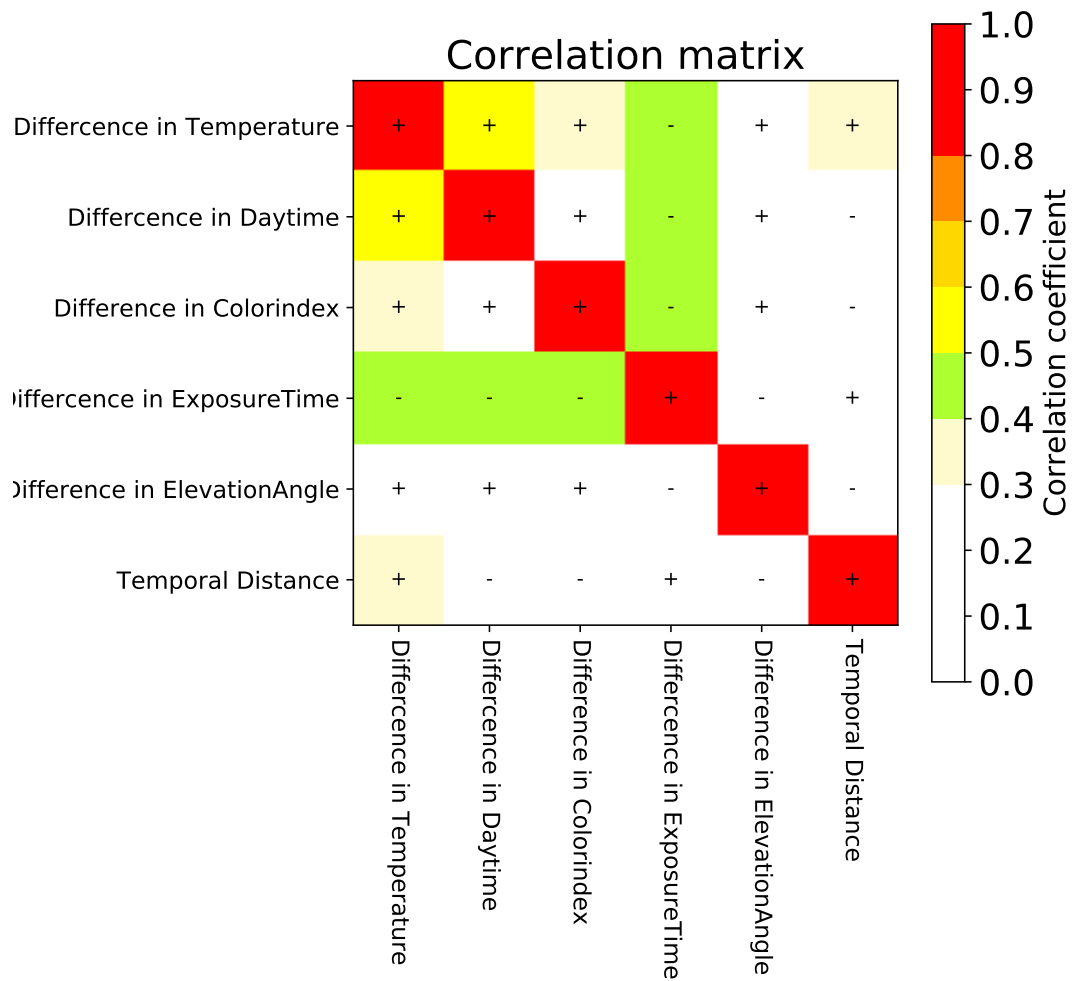


Figure 6.14: Correlation matrix of the external parameters. The correlation is discrete colour coded. Positive correlation is labeled with a plus whereas negative correlation is labeled with a minus. The correlation matrix is calculated using the data from D2J2140_0.

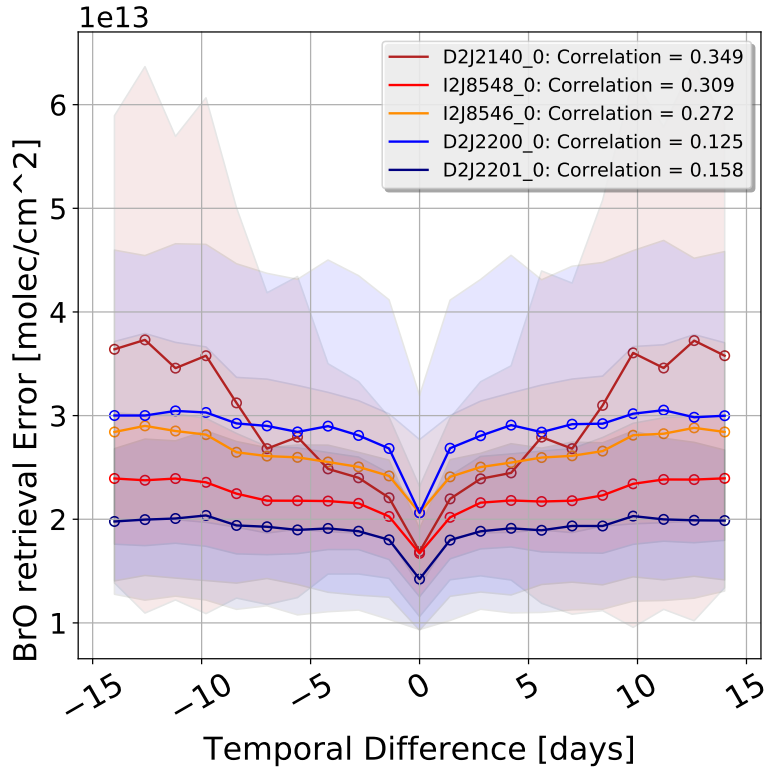


Figure 6.15: The BrO measurement error as a function of the temporal difference between measuring the reference and the plume are shown. Therefor, the reference spectra are restricted such that the maximal temperature difference between reference and plume is 1°C .

of Figure 6.6 to Figure 6.12 a large reduction of the correlation is obvious. Only the difference in temperature still shows a significant correlation to the BrO error. However, the minimal BrO error coincidence in almost all cases with a difference in external parameters of zero. A dependency of the BrO error on the external parameter can still be seen even tough the correlation is very small.

Excluding of the external parameters due to the rather low correlation leads to a worse quality of the results, since the effects of the single parameter add up to a not negligible amount. However, note that the added impact of all external parameter except for the temperature are less important than the temperature. **Wäre super wenn du diese Behauptung durch Zahlen beweisen kannst. Wie viel besser ist die Trefferquote wenn du alle parameter berücksichtigst im vergleich zu temperatur weg lassen?**

For the final evaluation of contaminated data we use the results of Figure 6.6 to Figure 6.9. Since the correlations between the external parameters are considered in the final 4 dimensional fit.

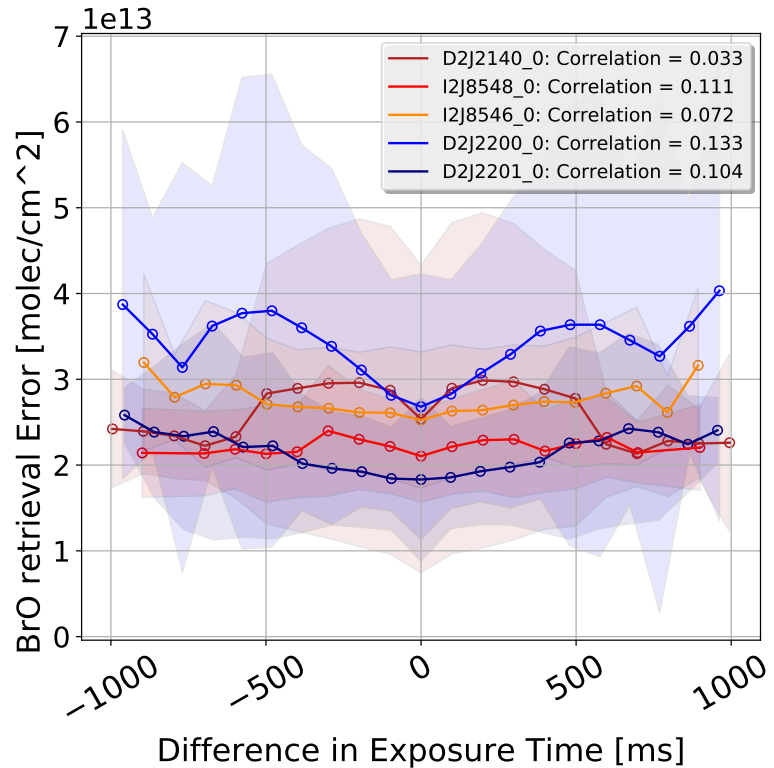


Figure 6.16: The BrO measurement error as a function of the exposure time difference between measuring the reference and the plume are shown. Therefor, the reference spectra are restricted such that the maximal color index difference between reference and plume is 0.05. The maximal daytime difference is 1h.

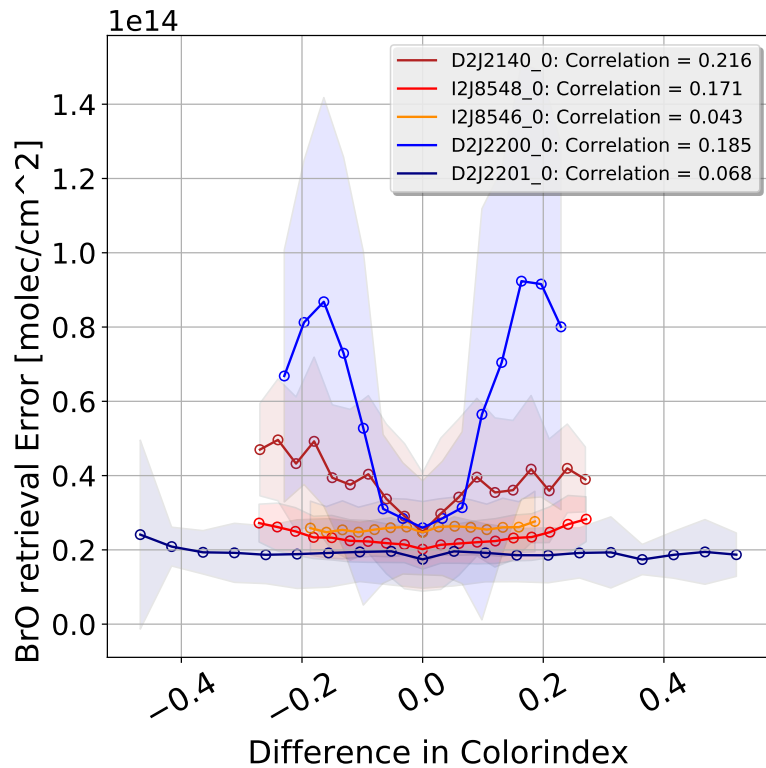


Figure 6.17: The BrO measurement error as a function of the color index difference between measuring the reference and the plume are shown. Therefor, the reference spectra are restricted such that the maximal temperature difference between reference and plume is $1^{\circ}C$. The maximal exposure time difference is $100ms$.

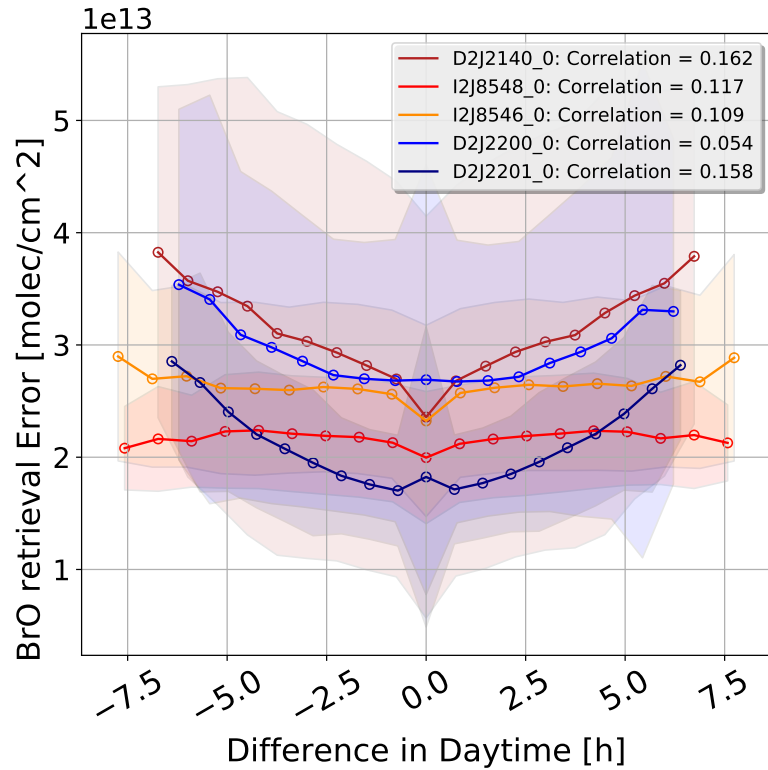


Figure 6.18: The BrO measurement error as a function of the daytime difference between measuring the reference and the plume are shown. Therefor, the reference spectra are restricted such that the maximal temperature difference between reference and plume is 1°C . The maximal exposure time difference is 100ms .

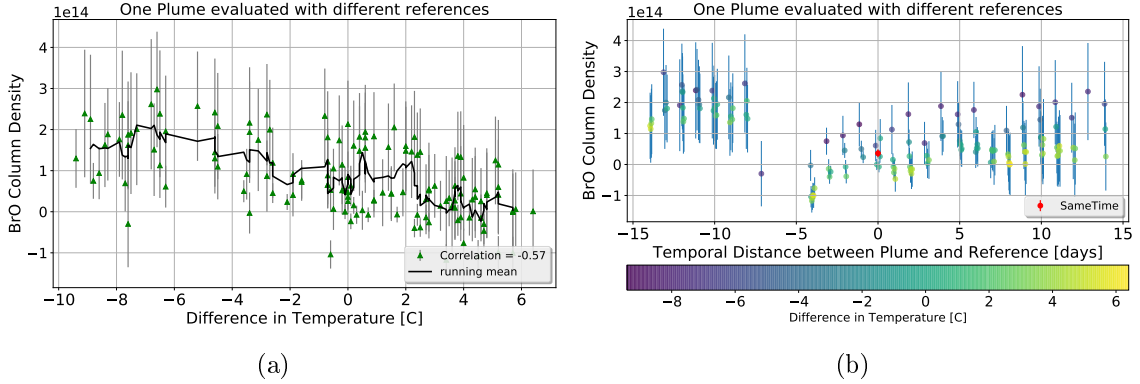


Figure 6.19: One plume is evaluated by using different references. The plume is recorded at Tungurahua volcano with the D2J2140_0 instrument. The recording time was the 03.12.2008 at 16:46 o'clock. The y axis shows the BrO column density difference between the NOVAC method and contamination based method. (a) The difference in BrO is plotted as a function of the temperature difference between the plume and the references. Every data point indicates one reference. (b) The difference in BrO is plotted as a function of the temporal difference between the one plume and the different references.

6.2 BrO dependence on external parameters

The external parameters not only influence the fit quality but also the evaluation of the gas amount. A high difference in certain external parameter could distort the calculated BrO column density. Figure 6.19 shows the evaluation of one plume with respect to different references. The temporal difference between the references and the plume do not exceed two weeks. In theory we expect that the choice of the reference should not make a difference, therefore all BrO column densities resulting from the evaluation should be equivalent. But we can see a high variation if choosing different references. The variability of the BrO column density depends as well on the external parameters, when looking at the temperature dependency a mean decrease of the BrO column density with an increasing temperature can be observed. Figure 6.19 is a result of an exemplary evaluation of one plume. An examination of all several plumes evaluated by different references is shown in Figure 6.20. The plots are equivalent to the plots for BrO error (for an example see fig. 6.6). The BrO SCDs vary strongly with the differences in external parameters. It is observable, that the BrO SCDs recorded by the instruments at Nevado Del Ruiz vary in a larger range than for the BrO SCDs recorded by instruments at Tungurahua. This can also be observed for the BrO retrieval errors. The absolute BrO SCDs increase with the difference in external parameters.

(a) Temporal difference: For the temporal difference no significant correlation can be observed. (b) Difference in color index: The correlations differ for every instrument

even for instruments of the same volcano. The correlations vary from -0.368 to 0.446. (c) Difference in daytime: For the instruments at Nevado Del Ruiz the BrO SCD correlates strongly with the difference in daytime. This can be a result of the dependence on the temperature, since the correlations are very similiar, only the correlations are a little bit stronger for the difference in temperature. (d) The strange dependence which can be seen between the BrO error and the difference in elevation angle for the D2J2200 instrumnt can be seen in this plot as well. The other instruments do not show any correlation between the BrO SCD and the difference in elevation angle.(e) The correlations for the difference in exposure time are opposite to the correlations in daytime.

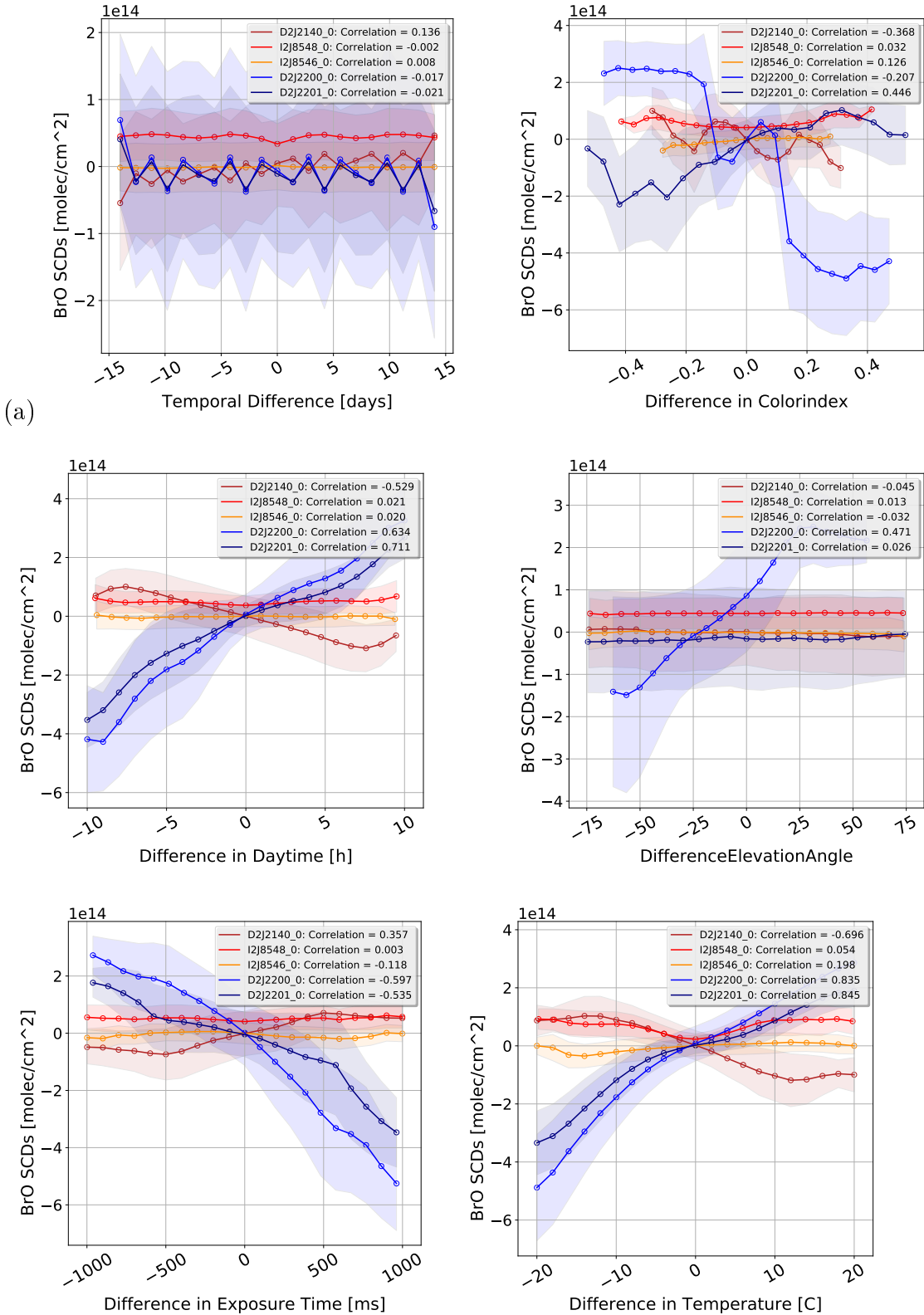


Figure 6.20: The BrO measurement value as a function of the difference of the external parameters between measuring the reference and the plume are shown.

Summary

This chapter examines the influence of external on the precision of the BrO evaluation. Herby the following parameter are considered: temporal difference, temperature, daytime, colorindex, elevation angle, exposure time. The findings are based on the data of three instruments installed at the Tungurahua volcano and two instruments at the Nevado Del Ruiz volcano. The maximal temporal difference between measuring the plume and the reference is set to 14 days to prevent large uncertainties in the BrO evaluation. Due to the mechanical influence on the wavelength to pixel mapping the temperature for all analysed instruments has the most significant impact on the BrO evaluation for all considered external parameters. The elevation angle does not seem to influence the evaluation for all examined instruments thus the elevation is excluded from the evaluation. The influence of the other external parameter change at every instrument. So a relatively strong impact of the exposure time can be seen at the D2J2201_0 instrument at Nevado Del Ruiz, while the exposure time does not seem to significantly influence the evaluation of the data from the I2J8548_0 at Tungurahua.

7 Contamination based method

Based on the findings about the influence of external parameters on the BrO error we propose an algorithm which is able to pick an appropriate volcanic-trace-gas free reference.

The first step is, to evaluate every reference with solar atlas spectrum, to check for contamination.

If the reference is contaminated:

- We have a list of possible references where all references are not contaminated and the temporal distance to the plume date is no longer than 14 days.
- For all possible references we calculate the differences in the external parameters
- We use the analysis of external parameters as described above to estimate the BrO error of all references
- We choose the reference with the smallest estimated BrO error as new reference
- We evaluate the plume spectra with the new reference.

The assumption is, that the BrO error ϵ_{BrO} can be described as the sum of ϵ_0 and the deviation of ϵ_{BrO} with respect to all external parameters. ϵ_0 is the BrO error when evaluate the plume spectrum with the "same-time-Reference". It is determined due to the accurateness of the NOVAC-instruments.

$$\epsilon_{BrO} = \epsilon_0 + \frac{d\epsilon}{dt} + \frac{d\epsilon}{d^\circ} + \frac{d\epsilon}{dT} + \frac{d\epsilon}{ddt} + \frac{d\epsilon}{dc} + \mathcal{O}(OP) \quad (7.1)$$

$$\rightarrow \Delta\epsilon_{BrO} = \epsilon_{BrO} - \epsilon_0 = \underbrace{\frac{d\epsilon}{dt}}_{=0} + \frac{d\epsilon}{d^\circ} + \frac{d\epsilon}{dT} + \frac{d\epsilon}{ddt} + \frac{d\epsilon}{dc} + \mathcal{O}(OP) \quad (7.2)$$

Here the parameter t stands for the time between plume-time and reference-time. The parameter T is the difference in temperature. The parameters dt and c are the differences in the daytime and the colorindex. The term (*OP*) accounts for other excluded external parameters. The task occurring at this stage is to find the best representation for the deviations. An then find the reference which minimize $\Delta\epsilon_{BrO}$

The easiest way is to just calculate the BrO error of all possible references for every plume by using the DOASIS routine. If this method is used it is possible to

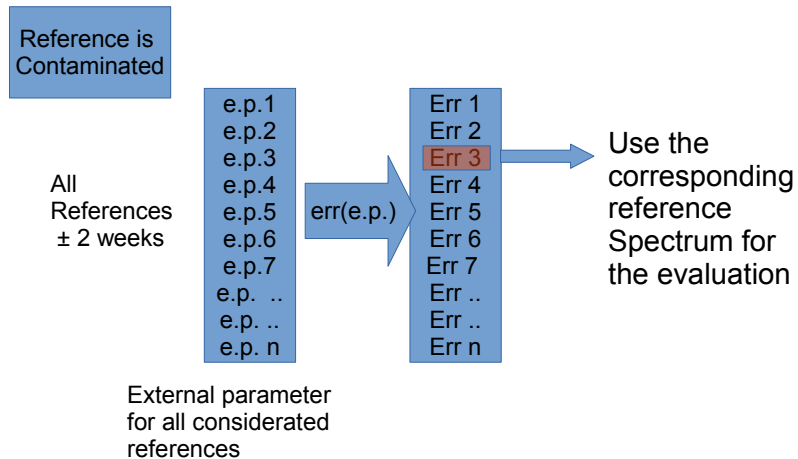


Figure 7.1: Visualization of the contamination based Method. If the reference is contaminated a list of possible references is available, where the temporal difference between the plume and the reference is not longer than two weeks. For every possible reference, the estimated BrO error is calculated by considering the corresponding difference in important external parameters. The reference with the so calculated minima BrO error is used for the evaluation.

choose the reference for which the BrO error is minimal. However this takes too much computation time since the evaluation time would be proportional to the number of possible references because the evaluation needs to be done for $\mathcal{O}(n)$ with n as the number of potential reference spectra. Doing this evaluation for every plume-reference pair makes it impossible to do the evaluation in real, or near real time. In this thesis a novel approach of identifying an ideal reference spectrum, by considering external parameters, is introduced. This way a much faster estimation with constant complexity $\mathcal{O}(1)$ is reached. But the above described optimal evaluation is used to rate new approach and compare them among each other. The optimal evaluation always choose the reference with the smallest absolute error. We don't use the relative error due to his vulnerability. Using the relative error leads to a less precision since the references with the highest BrO column density is preferred. The results of the algorithm which chooses the reference automatically are described relative to an optimal evaluation. If the relative error is larger than 5 the data are excluded from the evaluation.

In the following we examine several methods for choosing the best reference based on the analysis of external parameters.

7.1 Fit data

The following chapter analyses fitting the data with a first order polynomial. Figure 6.6 to Figure 6.12 show the BrO error as a function of external parameters. Hereby, the curves are symmetric around zero difference in the respective external parameter. Therefore, it is not necessary to distinguish between positive or negative deviations from the equal surrounding conditions. Thus, the absolute differences can be utilized.

A linear approximation of the BrO error as function of the considered external parameters leads to a variation of Equation (7.2) : With linear differentiations of the BrO error with respect to the respective external parameters Equation (7.2) can be written as:

$$\Delta\epsilon_{BrO} = a_t \cdot \Delta t + a_{ET} \cdot \Delta ET + a_T \cdot \Delta T + a_{dt} \cdot \Delta dt + a_c \cdot \Delta c + \mathcal{O}(OP) \quad (7.3)$$

To determine the coefficients a_x (Equation (7.3)) the data visualized in Figure 6.6-6.12 where used. The fitting is done with an ordinary least square linear regression. In particular we used the python function Linear Regression from the library sklearn ([SKI](#)).

As it can be seen in Section 6.1 the impact of the different external parameters change for every instrument depending on the location and the instrument themselves. While the BrO error does not show any dependence on some external parameters for some instruments, the error has very strong dependence on the same external parameter at an other instrument. An example is the correlation between BrO error and the difference in daytime of 0.6 for D2J2201_0 (Nevado Del Ruiz) and a correlation of 0.16 for I2J8546_0 at the Tungurahua volcano. To get a more stable algorithm less external parameter are preferable. Thus, we need to distinguish between the stability of the fit, which improves with less external parameters and quality of the fit, which improves with more external parameters. A preferable strategy is, to find a solution which is valid for all instruments. Moreover, utilizing less external parameters saves computation time. One possibility is to use all external parameters where the correlation is above a certain value. Since we want to get a selection valid for all instruments there are two possibilities: The first one is that we decide by using the mean correlation of all instruments. The second option is to use the highest correlation.

To answer this question quantitatively for the fitting routine we evaluated data of Tungurahua and Nevado Del Ruiz with different combinations of the external parameter described in Section 6.1. Since we could not observe any correlation between the BrO error and the elevation angle the external parameter elevation angle was neglected in this analysis. To rate the results for the single instruments (three at Tungurahua and two at Nevado Del Ruiz) the difference to the "optimal evaluation" (explained in ??) is used. Hereby the factor X , a quantity which describes

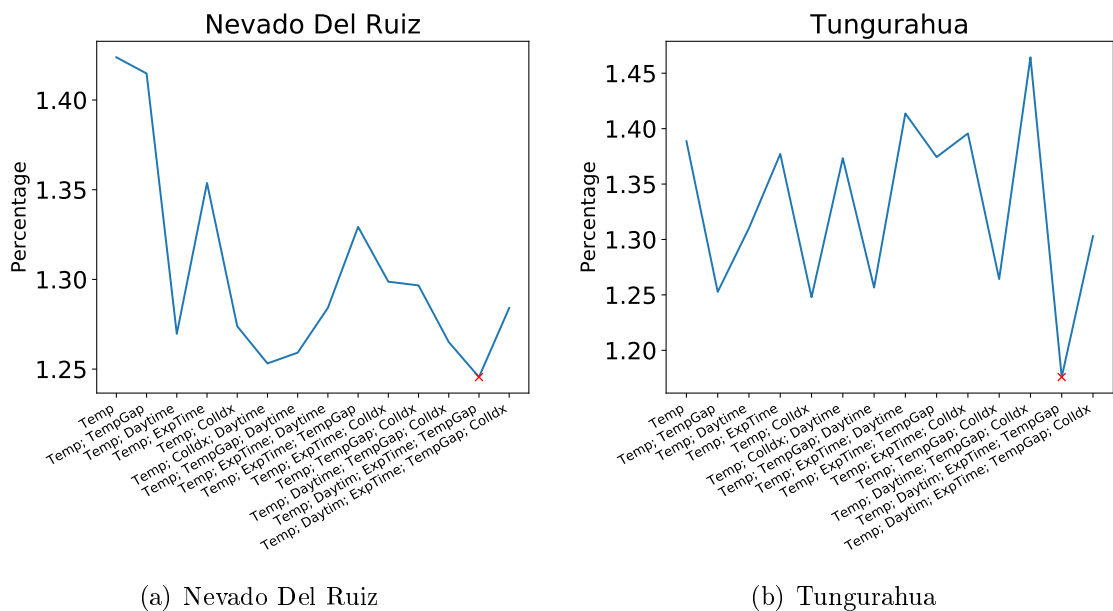


Figure 7.2: Deviation from the "optimal evaluation" as a function of the selection of differences in external parameters which are used for the evaluation. Here the utilized combination of external parameters are plotted on the x-axis and the deviation on the y-axis. The ideal combination (lowest deviation) is marked with a red cross.

	Mean Correlation	-	Highest Correlation	-
Temperature	0.798		0.92	
Colorindex	0.3108		0.409	
Exposure time	0.265		0.452	
Elevation Angle	0.02		0.067	
Daytime	0.395		0.631	

Table 7.1: The correlation coefficients between the BrO measurement error and the different external parameters. As a correlation value both the average and the maximum correlation is given.

the distinction between the optimal-Method and the contamination based method, serves as a indicator:

$$X = \frac{1}{n} \sum_k^n \frac{EContBased_k}{EOpt_k} \quad (7.4)$$

n is the total amount of contaminated spectra, $EOpt$ is the BrO error, in the optimal-evaluation, $EContBased$ is the BrO error, in the contamination based-evaluation. Figure 7.2 shows the X factor for the Tungurahua and the Nevado Del Ruiz volcano. The y-axis shows the factors X averaged over all instrument at the volcanoes. The factors X change from instrument to instrument. The results for every instrument can be seen in the appendix (Figure .1). The factors X range from 1.18 to 1.42.

Single references-plume pairs result in a very high BrO error, which has a very high impact on the calculation of the X factors. As it can be seen in Figure 7.2 for both volcanoes the X factor is minimal for the combination of the following external parameters:

- Temperature • Daytime • Colorindex • Temporal Difference

For the final algorithm this combination of external parameters is used. The coefficients a_x are calculated for each instrument at Nevado Del Ruiz and Tungurahua. Furthermore, the coefficients a_x are calculated with the combined data from all instruments installed at one volcano. The results for the Nevado Del Ruiz volcano can be found in Section 7.1 and for the Tungurahua volcano in Table 7.3.

As it can concluded from Figure 7.2 The best results are found if all parameters are used with a mean correlation above 0.3 (see Section 7.1)

	(b) Data of Nevado Del Ruiz D2J2201_0		(c) Data of Nevado Del Ruiz D2J2200_0		(d) Data of Nevado Del Both Instruments	
Constant	value	import	value	import	value	import
a_T	7.505e+12	0.866	1.179e+13	0.925	1.07e+13	0.973
a_{CI}	3.482e+13	0.048	1.024e+14	0.046	3.48e+10	0.070
a_t	-3.2e+09	0.0	-1.6e+09	0.0	-9.1e+08	0.0
a_{dt}	1.869e+12	0.095	1.054e+12	0.033	1.52e+11	0.006
					-6.81e+13	-0.047

Table 7.2: The results of the fitting with a first order polynomial. The constants of Equation (7.3) are calculated. The value shows the actual number. The importance, referred to as import, indicates the relative impact on the evaluation. (a)Data from Nevado Del Ruiz from the D2J2201_0 instrument. (b)Data from Nevado Del Ruiz from the D2J2200_0 instrument. Data from Nevado Del Ruiz from both instrument.

7.2 Other approaches

Fitting is not the only possibility of finding the optimal reference out of the list of all possible references.

In the following two additionally possibilities are presented. Both are based on the findings in section 6.1.

7.2.1 Nearest neighbor approach

Beside linear regression also the nearest neighbor approach can be utilized to estimate the BrO error for the evaluation with a potential reference spectrum. The nearest neighbor search describes an optimization problem for a given point $m \in \mathbb{R}^n$ and a set $S \subset \mathbb{R}^n$:

$$\bar{s}(m) = \min_{s \in S} d(m, s) \quad (7.5)$$

Here $d(\cdot, \cdot)$ is a distance function that computes the dissimilarity between the two input arguments. Typical distance metrics are the L1 distance $d_{L1}(m, s) = ||m - s||^2$ or the L2 (also euclidean) distance function $d_{L2}(m, s) = ||m - s||$.

In many cases not only one nearest neighbor but a set M of k nearest neighbors is of interest. In this case the optimization problem of Eq. 7.5 must be modified to

$$\bar{S}_k(m) = \min_{S_k \subset S} \sum_{s \in S_k, m \in M} d(s, m) \quad (7.6)$$

	(b) Data of Tungurahua D2J2140_0		(c) Data of Tungurahua I2J8548_0		(d) Data of Tungurahua I2J8546_0	
Constant	value	import	value	import	value	import
a_T	3.732e+12	0.664	6.459e+12	0.920	3.939e+12	0.850
a_{CI}	6.982e+13	0.078	2.760e+13	0.066	-1.521e+13	-0.042
a_t	3.5e+10	0.2	1.2e+10	0.13	2.0e+10	0.2
a_{dt}	7.797e+11	0.069	-6.049e+11	-0.055	1.158e+11	0.017

(e) Data of Tungurahua I2J8546_0	
value	import
5.055e+12	0.838
2.534e+13	0.057
1.8e+10	0.117
-1.109e+11	-0.012

Table 7.3: The results of the fitting with a first order polynomial. The value shows the actual number. The importance, referred to as import, indicates the relative impact on the evaluation. The constants of Equation (7.3) are calculated. (a)Data from Tungurahua from the instrument. (b)Data from Tungurahua from the instrument. (c) Data from Tungurahua averaged over all instrument. both instruments Tungurahua

In many cases the nearest neighbor search is used to estimate a target variable y_m for a feature vector $m \in \mathbb{R}^n$. This method assumes a given set feature vectors S for which the target variables y_S are known. Then the target variable y_m for a given m can be estimated by:

$$y_m = \frac{1}{k} \sum y_S \quad (7.7)$$

Advantages of the nearest neighbor approach

The main advantage of the nearest neighbor method is that there is no need for a pre-assumption of a fitting method. The fitting method assumes that the BrO error depends linearly on the external parameter. As it can be seen in Figure 6.6-Figure 6.12 this does not need to be the case. Thus, the nearest neighbor method is able to approximate the BrO error as a function of the external data in a more variable way.

Disadvantages of the nearest neighbor approach

Compared to fitting the data, the nearest neighbor is much slower. The reason for this is, the vast amount of comparison operations that is necessary for each computation. Thus, the calculation time increases with the amount of learning data.

To normalize the distances d , the normalization function needs to be chosen and therefore pre-assumptions about feature importance are required. Including the fact, that the results of the nearest neighbor method are a little worse compared to the fitting method **hier sagen wie der faktor X für die nearest neighbor methode ist**, the disadvantages of the nearest neighbor method outweigh the advantages.

7.2.2 Iterative approach

The idea of the iterative method is, that the importance of the individual external parameters are very different, that means if we have the list of possible references, we take all references where the temperature difference is minimal, so we get a new, much smaller list of possible references. From this list we choose all references where the next external parameter for example the daytime is minimal and again get a new list. We proceed this way with the following external parameters. We experiment with the sequence of the parameters, to increase the success of the method. The final sequence is:

Temperature • Daytime • Colorindex • Temporal Difference • Exposure time

Advantages of the iterative approach

The advantages of the iterative approach is the simple calculation and thus the short calculation time. Since the temperature is by far the external impact with the largest impact on the evaluation it is reasonable to look at first at the temperature, and after that on the other parameters.

Another advantage is, that the external conditions of the resulting references, are in an well-defined framework, similar to the conditions of the plume. Therefore the systematic errors resulting from the effects on the BrO SCDs (see Figure 6.20) can be kept small.

Disadvantages of the iterative approach

The iterative approach leads to a rigid evaluation of the data. References, which have very similar conditions as the plume could be excluded of the evaluation due to a large difference in one external parameter. The decision for the best suited reference is based on one by one parameter. Thus it is impossible to look at all parameters by the same time. This could lead to a less optimal evaluation when looking at the BrO error. As a result the iterative method has a worse X factor compared to the nearest neighbour and the fitting method.

8 Comparison with NOVAC evaluation

This chapter shows and discuss the difference of the BrO, SO₂ and BrO/SO₂ ratio data when evaluating with the NOVAC-Method, or with the contamination based method. The aim is to discover the systematic differences between the different retrievals and to discuss the reliability of the data.

To obtain the reference with minimal expected BrO error the calculation of Equation (7.3) and the corresponding coefficients from Table 7.3 (Tungurahua) and Section 7.1 (Nevado Del Ruiz) were used. For the retrieval only "Multi Add" data were used. The maximal temporal difference between measuring the reference and the plume is two weeks.

We restricted non of the external parameter due to the higher x factor as it can be seen in ...

Furthermore we do not distinguish between the individual instruments. ????????????

Figure 8.1 shows a comparison of the results of contaminated data for performing the evaluation with the NOVAC-method and the contamination based method. The x-axis shows the column density of BrO respectively SO₂ calculated with NOVAC-method, the y-axis shows the column density calculated with the contamination based method. Only data are used where the corresponding SO₂ column density lies above the plume limit ($SO_2_SCD > 7 \cdot 10^{17}$). Meaning the column densities evaluated with the contamination based method. The corresponding SO₂ SCD's evaluated with NOVAC could be below $7 \cdot 10^{17}$. The plots at the left side (Figure 8.1(a) and 8.1(c)) show the results from the Tungurahua volcano while the plots at the right side (Figure 8.1(b) and 8.1(d)) show the results from Nevado Del Ruiz volcano. The black solid line shows a linear fit of the data, the dotted line indicates where the both evaluation are equivalent.

Figure 8.1(a) respectively 8.1(b) show the results for the BrO retrieval:

- The BrO column densities retrieved due to the contamination based method have become larger on average compared to the NOVAC method.
- An almost constant offset of $1.2 \cdot 10^{13}$ (Tungurahua) and $2.0 \cdot 10^{13}$ (Nevado Del Ruiz) can be seen.

The constant offset between the results from the contamination based method and the NOVAC-method leads to the assumption, that (Erklärung)

Figure 8.1(c) respectively 8.1(d) show the results for the SO₂ retrieval:

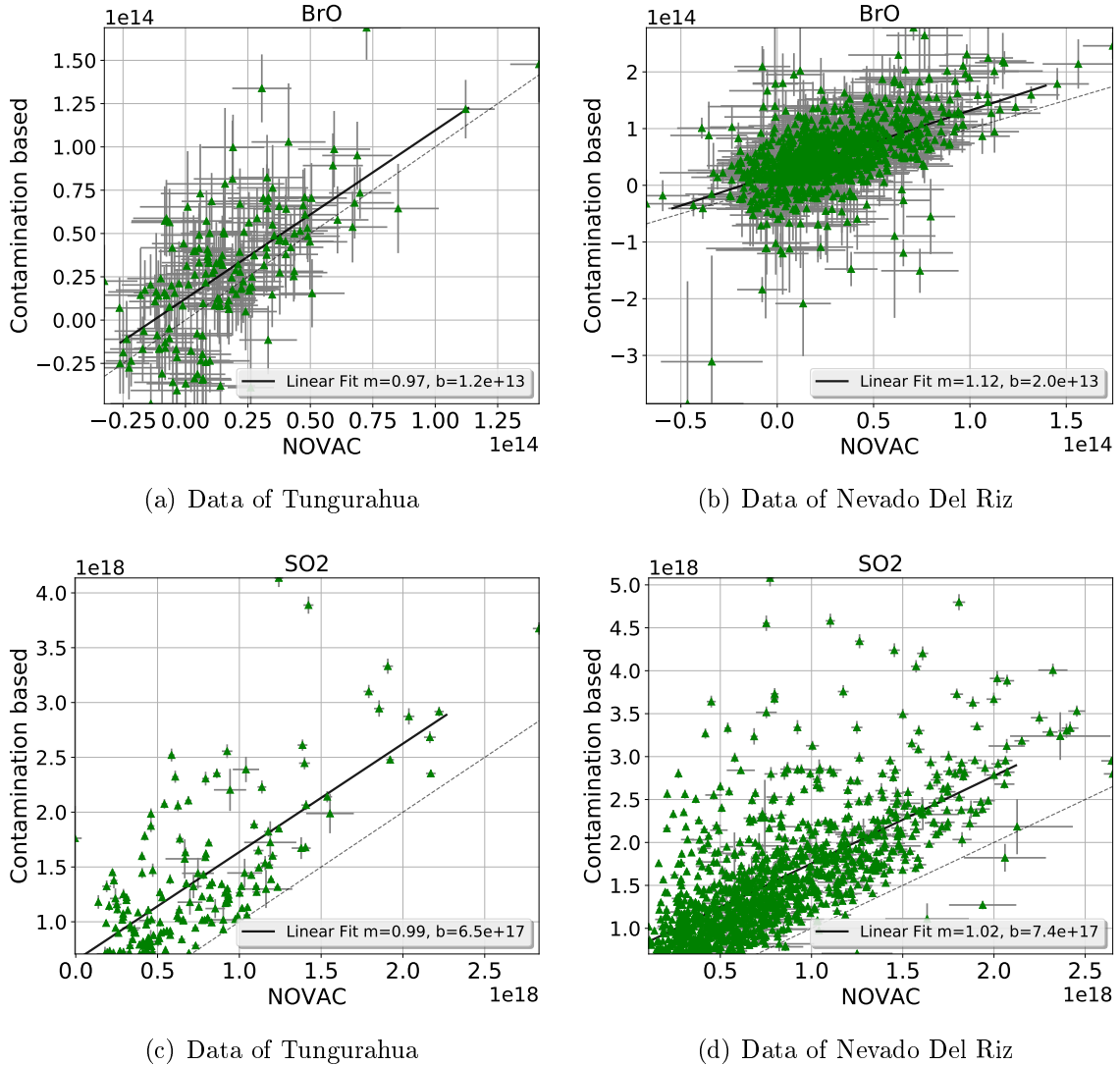


Figure 8.1: Comparison of the results of contaminated data for performing the evaluation with the NOVAC-method and the contamination based method. Only data are used where the corresponding SO₂ column density (retrieved from the contamination based method) lies above the plume limit of $SO_2_SCD > 7 \cdot 10^{17}$. The black solid line shows a linear fit of the data, the dotted line indicates where the both evaluation are equivalent. (a) Results for the BrO column densities from Tungurahua; (b) Results for the BrO column densities from Nevado Del Ruiz; (c) Results for the SO₂ column densities from Tungurahua; (d) Results for the SO₂ column densities from Nevado Del Ruiz

- The SO₂ column densities retrieved due to the contamination based method have become larger for almost every measurement compared to the NOVAC

method.

- An almost constant offset of $6.5 \cdot 10^{17}$ (Tungurahua) and $7.4 \cdot 10^{17}$ (Nevado Del Ruiz) can be seen.

Figure 8.2 shows the difference of the ratio when performing the evaluation with the NOVAC method or the contamination based method. The results for Tungurahua are visualized at the left side (Figure 8.2(a), 8.2(c)) and the results for Nevado Del Ruiz are shown at the right side (Figure 8.2(b), 8.2(d)). Figure 8.2(a) and 8.2(b) show the results of the contamination based method plotted against the results of the NOVAC method. Figure 8.2(c) and 8.2(d) show the actual difference between both methods. The column density calculated with NOVAC was subtracted from the corresponding column density retrieved with the contamination based method. The black valid line indicates a linear fit of the data, the dotted grey line shows where the difference is zero, that means both evaluations lead to the same ratio.

- For low BrO/SO₂ ratios approximately below zero, the ratios calculated with the contamination based method are higher than the ratios retrieved with the NOVAC method. For higher BrO/SO₂ ratios (approximately above zero) the ratios calculated with the NOVAC method are larger.
- The absolute difference between both evaluation methods increases with the increase of the absolute ratio

Due to the increase of the SO₂ column density when performing the evaluation with the contamination based method more SO₂ SCD lie above the plume limit of $7 \cdot 10^{17} \frac{\text{molec}}{\text{cm}^2}$. This leads to an increase of the amount of reliable data.

In the following we will discuss the results for the Tungurahua volcano and the Nevado Del Ruiz.

8.1 Tungurahua

In the considered timespan from June 2008 to August 2009, 6500 multi add spectra are recorded.

Using the conventional NOVAC-method to perform the evaluation with ignoring contamination results in an amount of SO₂ column densities within the plume limit of 6.7 percent. Thus 6.7 percentage of the data can be used for the examination of the volcanic gas emissions in this timespan.

6.0 percentage of all spectra are found as contaminated and thus needs to be excluded from the conventional NOVAC-evaluation. From the remaining data, if the contaminated spectra would be excluded, only 5.5 percent of the SO₂ column densities are above the plume limit (see Table 8).

A higher amount of spectra within the SO₂ limits can be found within the contaminated data even if the contaminated data are evaluated with the NOVAC-method.

	Tungurahua	Nevado Del Ruiz			
Total Amount of Data	6500	14005			
Total amount of Data above Plume Limit	6.7%	12.8%			
Contaminated Data	0.060	0.099			
Contaminated data		Not contaminated data			
	Tungu rahua	Nevado Del Ruiz		Tungu rahua	Nevado Del Ruiz
Within Plume-limit	NOVAC Cont based	0.192 0.419	0.399 0.779	Within Plume-limit	0.055 0.088
not analysable	0.025	0.078			

Here the percentage of data in the plume-limit is: 19.2. Therefore the contaminated data are 2.86 times more frequently above the detection limit. This lead to the presumption, that the possibility of getting contaminated data increases with the gas amount leaving the volcano.

The following paragraph deals only with the contaminated data: When performing the evaluating of the contaminated data with the contamination based method 41.9 percent of the resulting SO₂ column densities are in the plume limit. Thus the reliable amount of contaminated data increase by 118.7 percentage while the total amount of data increase by 45.2 percent. Thus 7.986 percent of all data are above plume limit when consider contamination.

Due to using trace gas free references instead of contaminated references about 45.2 percent more data are available.

Due to the very small amount of BrO column densities above the detection limit often the daily mean of the BrO/SO₂ ratios is used. Hereby at least tree to four "Multi Adds" per day in the plume limit need to be recorded. Thus performing the evaluation of contaminated data with the contamination based method leads to more data. Some days which had less than tree to four valid data points could then have four or more multi adds. 12.5 percent more daily mean data can be retrieved when using the contamination based method. The amount of daily means increases less than the total amount of data, this effect can be explained due to a higher occurrence of contamination if the SO₂ column densities are high, thus more data are retrieved for days with high SO₂ amount.

8.2 Nevado Del Ruiz

At Nevado Del Ruiz a larger time span where examined thus there is a higher amount of "Multi Add" Data of: 14005. When ignoring contamination and evaluate all spectra by the NOVAC-method 12.8 percenage of the SO₂ SCDs are above the plume limit.

The total amount of contamination data is 1392 this is equivalent to 9.9% of all data. Evaluating the contaminated data with the NOVAC-method yields in 39.9% of the SO₂ SCDs within the plume limit. As at Tungurahua the occurence of data above the plume limit within the contaminated data is larger as for not contaminated data (by a factor of 3.4).

The following paragraph deals only with the contaminated data: If using the contamination based method 77.9 percent of the SO₂ column densities are above the detection limit. Thus an increase of SO₂ SCDs above the plume limit within the contaminated data of 95% is observable. In total the amount of SO₂ SCDs above the plume limit increases by 68.8%. percent. As a result 12.8 percent of all data are above the plume limit.

For the same reasons as described for the Tungurahua volcano we are also interested in the daily means: In total we get 22.6 percent more daily means in the Timespan at Nevado Del Ruiz.

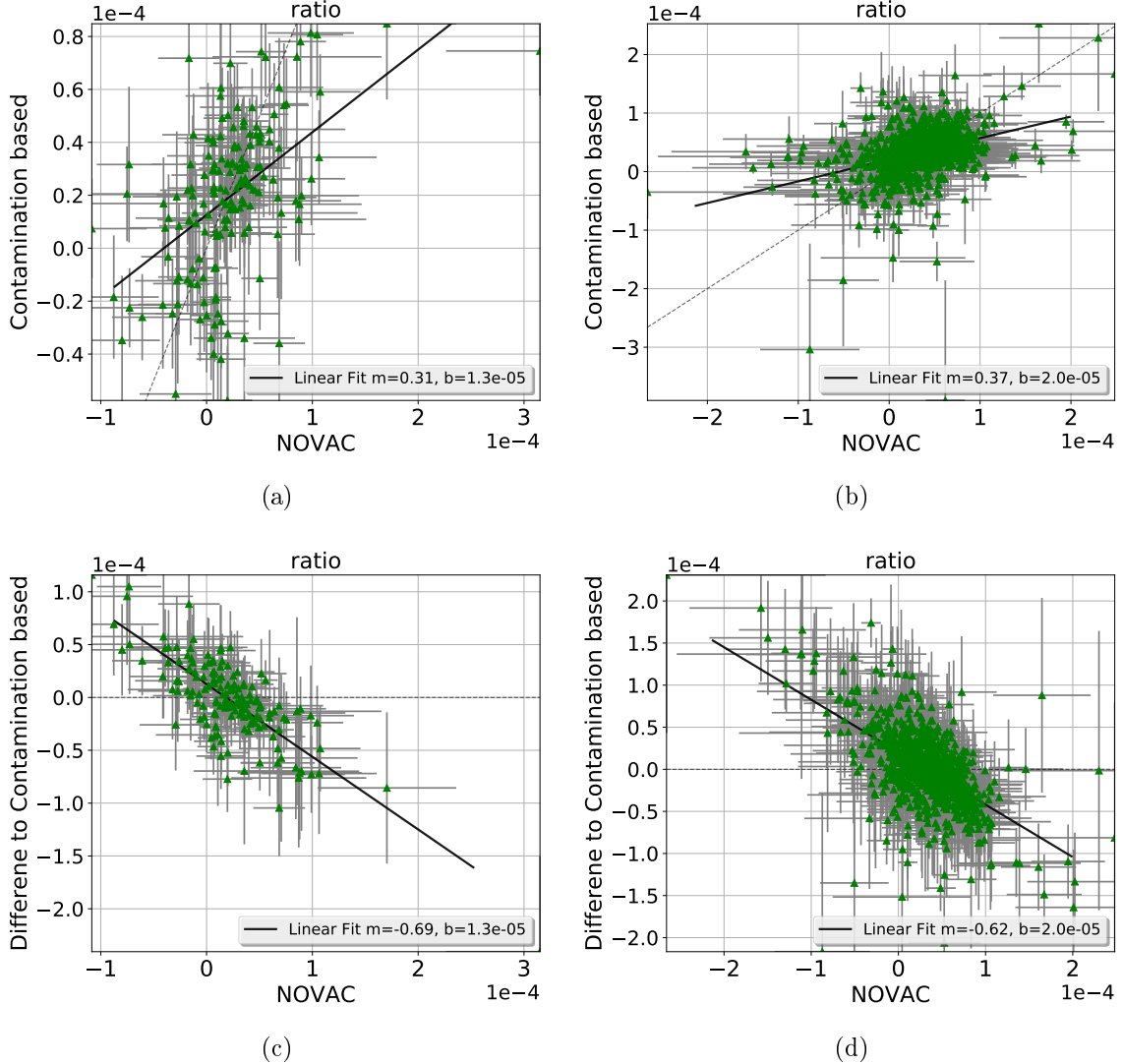


Figure 8.2: Comparison of the results of contaminated data for performing the evaluation with the NOVAC-method and the contamination based method. Only data are used where the corresponding SO₂ column density (retrieved from the contamination based method) lies above the plume limit of $SO_2_SCD > 7 \cdot 10^{17}$. (a)+(b): The black solid line shows a linear fit of the data, the dotted line indicates where the both evaluations are equivalent. (a) Results for the BrO /SO₂ column densities from Tungurahua; (b) Results for the BrO /SO₂ column densities from Nevado Del Ruiz. (c) +(d) The column density calculated with NOVAC was subtracted from the corresponding column density retrieved with the contamination based method. The black valid line indicates a linear fit of the data, the dotted grey line shows where the difference is zero, that means both evaluations lead to the same ratio. (c) Tungurahua (d) Nevado Del Ruiz

8.3 BrO/SO₂ time series

This section presents the final time series of SO₂, BrO and BrO/SO₂ for Tungurahua and Nevado Del Ruiz.

Figure 8.3 shows the results for the Nevado del Ruiz volcano. The plot at the top of Figure 8.3 shows the results for SO₂. The SO₂ SCDs below the plume limit are coloured in blue, data points above the plume limit are coloured in green, the red circles show the SO₂ SCDs where the same time reference was contaminated, thus the contamination based evaluation was used for those plume spectra. The contaminated data points are only marked in red, if the SO₂ SCD is above the plume limit. Contaminated data below the detection limit are not particularly marked. If the contaminated data would be excluded from the evaluation only the green data points can be used for the evaluation of the time series.

The middle plot of Figure 8.3 shows the corresponding BrO time series. The green data points indicates BrO SCDs where the corresponding SO₂ amount is above the detection limit, while the red BrO SCDs show contaminated data above the detection limit.

The plot at the bottom of Figure 8.3 show the BrO/SO₂ ratio time series, the red, blue and green coloured data points have the same meaning as for BrO and SO₂. Figure 8.4 shows the equivalent plot for the Tungurahua volcano.

Figure 8.5 shows a time series of Daily means of the BrO/SO₂ ratio. The minimum amount of valid data point within one day is above 4. Days where 3 or less valid data where recorded are not considered in this figure. Thus all considered ratios have an SO₂ SCD above the plume limit. The red marked ratios shows data which are only able to use, if the contaminated data are used as well.

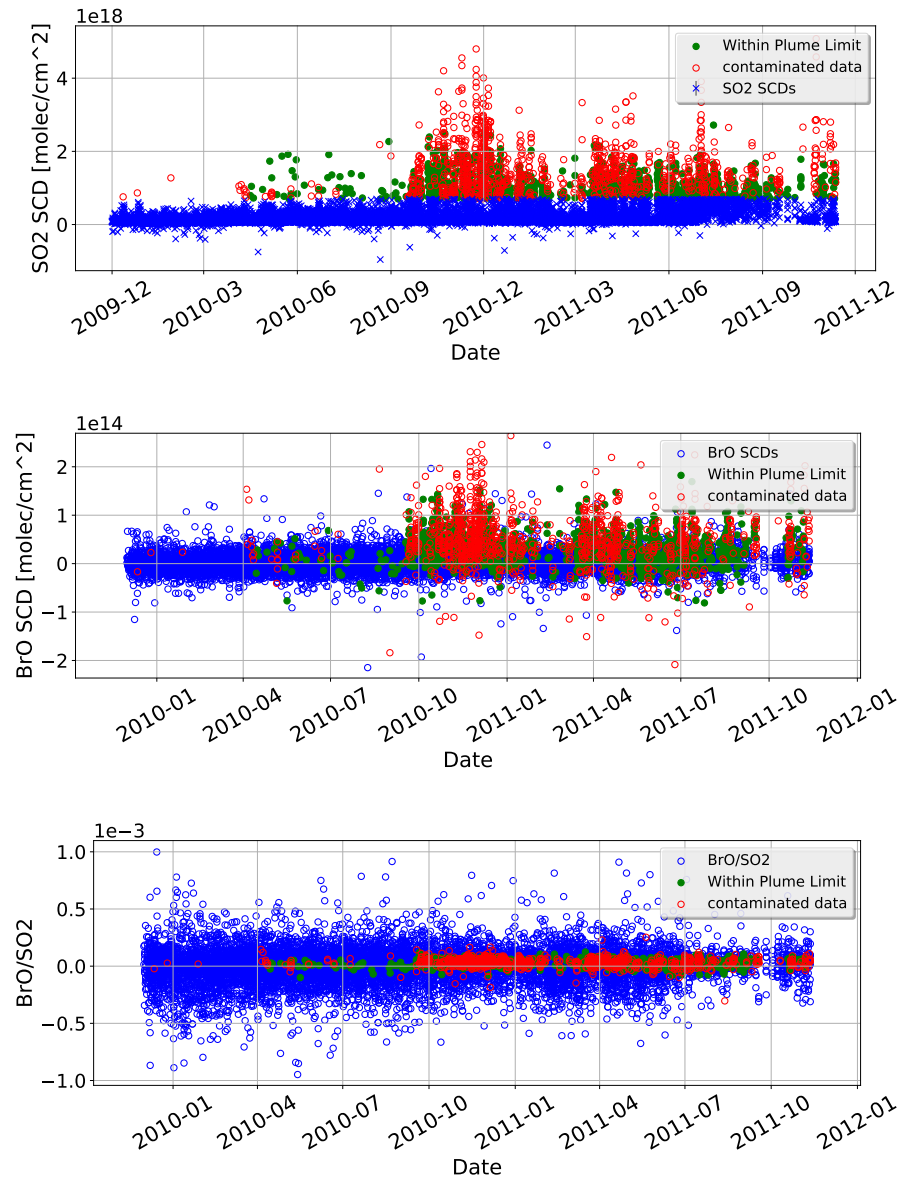


Figure 8.3: Time series of the BrO/SO₂ ratios for Nevado del Ruiz . The contaminated data are evaluated by using the contamination based method. Blue data points are below the detection limit, green data points are not contaminated, valid SO₂ SCDs. Red data points are contaminated data, evaluated with the contamination based method.

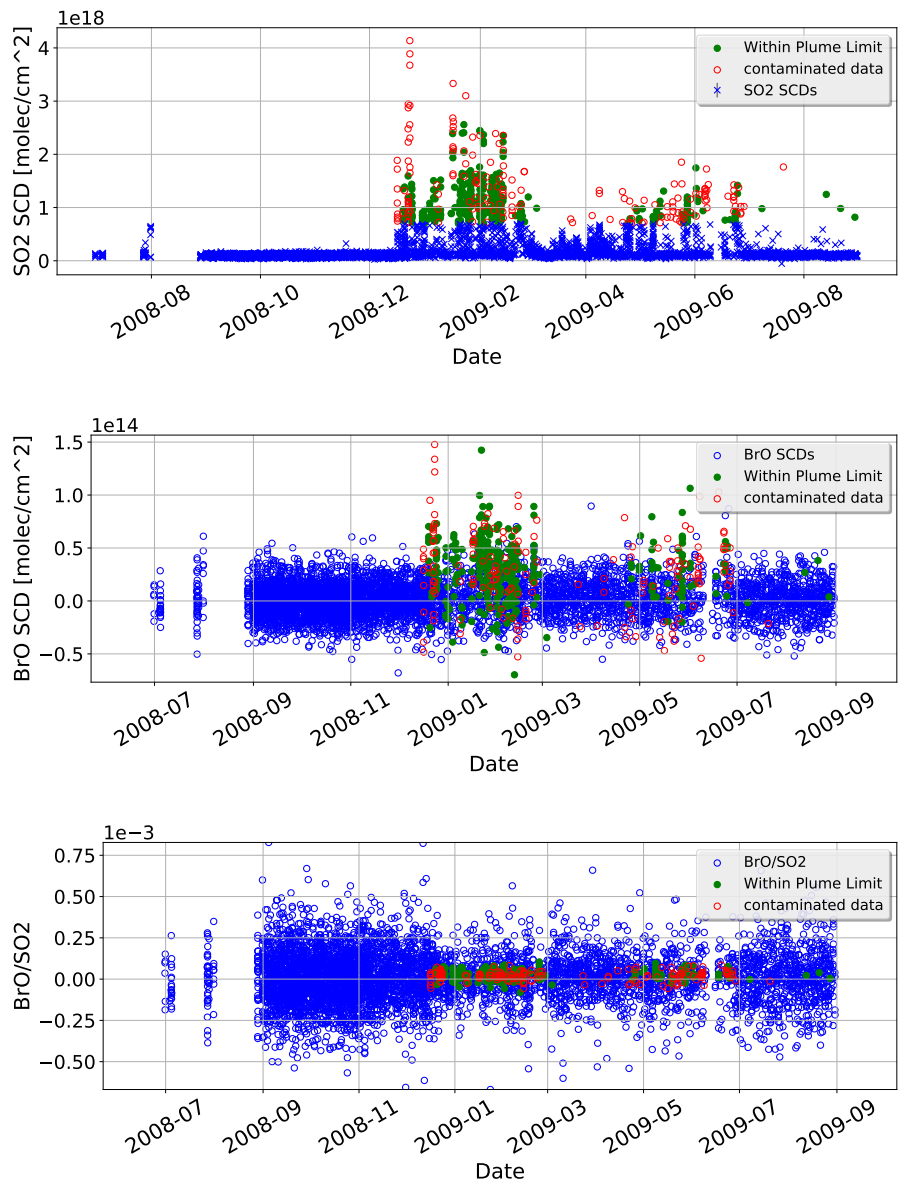


Figure 8.4: Time series of the BrO/SO₂ ratios for Tungurahua. The contaminated data are evaluated by using the contamination based method. Blue data points are below the detection limit, green data points are not contaminated, valid SO₂ SCDs. Red data points are contaminated data, evaluated with the contamination based method.

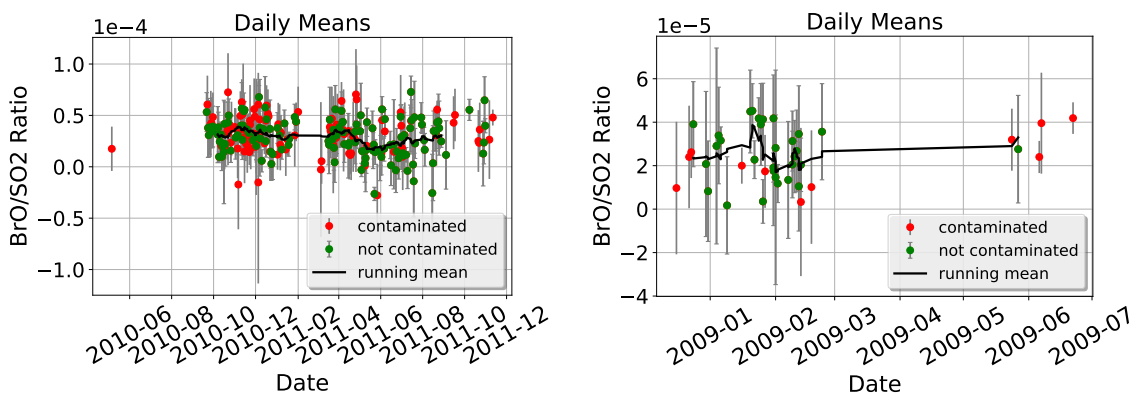


Figure 8.5: BrO/SO₂ ratio daily mean time series for Nevado del Ruiz (left) and Tungurahua (right). SO₂ SCDs used for this plot are above the plume limit of $7 \cdot 10^{17}$. The minimum amount of data per day are four. Days where less than four valid ratios are recorded are not considered in this plot. As a result of using the contaminated data as well more daily means are available, since more days have an amount of valid data's above four. Those dates are marked with red. The other data are colored in green.

9 Issues of our method

The presented method is questionable since we did not consider contamination of the plume due to a lack of information. And we did not consider the different lifetimes of SO₂ and BrO. This leads to a faster

9.1 Contamination of the plume

As discussed above it might occur, that, the plume is contaminated as well. This might be the case if the volcanic gas of the volcano is not taken away by the wind, but accumulates at the instrument. If this is the case, using an contamination free reference of another time would lead to an overestimation of the column density of gases.

The contamination of the plume is visualized in Figure 9.1. This is one possible occurrence of contamination. As it can be seen gas of the old plume affected the measurement of the reference and the plume. However for this example the influence on the measurement of the reference is much larger since the light path trough the old plume (coloured orange in Figure 9.1) is longer for the reference than for the measurement of the volcanic plume. Thus we underestimate the Gas amount if we do not use an gas free reference, but overestimate if we do so. The real gas amount might be between the measured amount with and without using a reference measured at another time.

The contamination set up could differ from Figure 9.1. This would lead to different results. However the reference region is in most of the time at a larger elevation angle than the plume, thus, the assumption that the light pass trough the old plume is on the average longer for the reference, of both reference and plume are contaminated.

With the data retrieved by the NOVAC instruments it is very difficult up to impossible to discover whether the plume is contaminated or not.

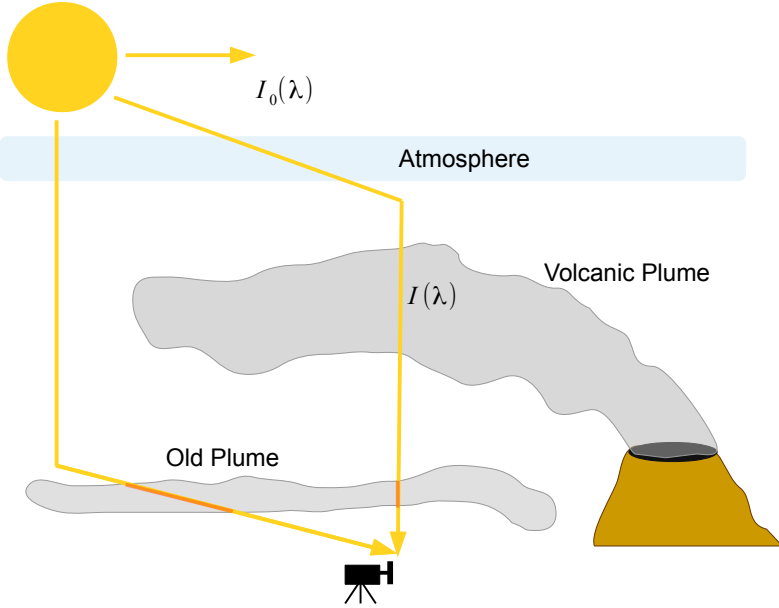


Figure 9.1: Visualization of the contamination of the plume. An old plume of the day before. Due to a lack of wind the plume sinks down and accumulates above the instrument. The light path through the old plume is longer when recording the reference spectra (orange).

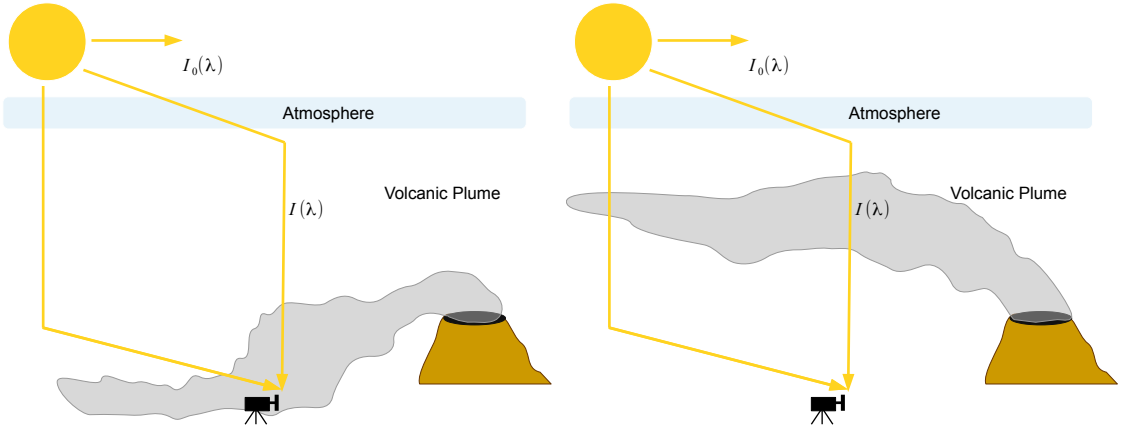


Figure 9.2: Visualization of possible scenarios for contamination. Left: the plume sinks in the way that the instrument is within the plume, therefore, all elevation angles will contain volcanic trace gases, while the plume is not additionally contaminated. Right: the plume covers the hole sky, thus all elevation angles "see" volcanic trace gases.

10 Conclusion

The Network for Observation of Volcanic and Atmospheric Change provides a very large of longtime timeseries. This treasure of the data contains a hge amount of informations about volcanoes, which could give an intresting insight of the physically foundations on volcanic activity.

The evaluation of the volcanoes is is in particular based on the assumption that the atmospheric background of the volcanic trace gases SO₂ and BrO is negligible. This is important to assure since the evaluation calculates the dSCDs because the DOAS method only gets the difference in gas amount between the background, the reference and the signal, the plume spectra.

Lübcke et al. (2014) found by using a solar atlas spectrum as reference that the reference provided by the NOVAC-Instrument is not always gas free. As a result some references are contaminated with volcanic trace gases. If that is the case the contaminated data eather needs to be excluded from the evaluation or the contaminated reference need to replaced by a gas free reference. If we want to keep the contaminated data we need to find an appropriate gasfree reference. A solar atlas spectrum can not be taken for the BrO evlautuon due to the low amount of BrO and the increase of the BrO error if using a solar atlas spectrum. Thus a gasfree reference recorded by the same instrument is a possible choice.

There are more than one gasfree reference of the same instrument available. Due to the low accuracy of the BrO retrieval it is reasonably to choose the reference with respect to the BrO error. An analysis of the BrO error as function of difference external parameter as: Temporal difference between measuring the plume and the reference; Temperature; Colorindex; Exposure time; Elevation angle; Daytime, is presented. Differences in those parameters between the reference spectrum an the plume spectrum influence the evaluation. If both, the the reference and the plume a recorded at the same time all those external parameter are identical and therefore do not need to be considered in the evaluation. The dependence of the BrO column density on external parameters was discussed as well.

The result of this analysis, was, that in general the retrieved BrO error is minimal, if the considered parameter are similar for the plume and reference. Only the elevation angle does not seem to influence the retrieval. From the considered parameter the temperature has the most significant impact of 60% up to 97% compared to the other parameter, at all observed instruments at Tungurahua as well as at the Nevado Del Ruiz volcano. The importance of the other instruments are different for every instrument, depending on the location of the instrument and the instrument itself.

Based on this findings an algorithm is introduced to automatically find the alterna-

tive reference if a reference need to be replaced due to contamination of the reference which was measured at the same time as the plume spectrum.

Fitting the data with an four dimensional first order polynomial turned out to give the best results.

The evaluation of th contaminated data with the here invented algorithm showed that BrO as well as SO₂ was underestimated by ignoring the contamination problem. We showed that the contamination based method gives BrO SCDs with an on the average 1.2e+13 at Tungurahua (2.0e13 Nevado Del Ruiz) higher column density, while the SO₂ amount increases as well with an on the average constant amount of 6.5e17 at Tungurahua (7.4e17 Nevado Del Ruiz) . Thus the results for the BrO/SO₂ ratio calculated with the contamination based method changed compared to the conventional method in the way, that low ratios increases, while high ratios decreases.

A further advantage of the new calculation is, that due to the higher amount of the SO₂ SCDs the amount of data above the plume limit increases. Using the contamination based method leads to an total increase of 45 % (Tungurahua) and 87% (Nevado Del Ruiz) of data.

?? made investigations on the lifetime of SO₂ and BrO. The lifetime of SO₂ can reach to several weeks, while the decay of BrO proceed in faster times. As a result we should observe a lower contamination of BrO. This could be observed in our results. In theory it could be that due to the smaller lifetimes of BrO contamination only influences the SO₂ evaluation, if that is the case, the best option would be to use a high defined solar atlas spectrum as reference for the SO₂ evaluation, but an reference recorded with the same instrument at the same time for the BrO evaluation, since BrO could not be retrieved using an high defined

Part III

Appendix

Dependency external parameters on each other

Difference of Temperature on Difference of exposure time

$$\Delta T = -26.32 \cdot \Delta ExpTime + 2 \cdot 10^{-15} \quad (.1)$$

Difference of Temperature on Difference of colorindex

$$\Delta T = 0.0022 \cdot \Delta ColIdx + 2 \cdot 10^{-19} \quad (.2)$$

Difference of Temperature on Difference of Day time

$$\Delta T = 0.262 \cdot \Delta daytime - 4 \cdot 10^{-17} \quad (.3)$$

Difference of Temperature on Difference of Elevation angle

$$\Delta T = 1.08 \cdot \Delta ElevAngle - 1 \cdot 10^{-16} \quad (.4)$$

Difference of Exposure on Difference of Col Idx

$$\Delta Exposure = -6.22 \cdot 10^{-5} \Delta ColIdx + 1 \cdot 10^{-18} \quad (.5)$$

Difference of Exposure on Difference of Day time

$$\Delta Exposure = -0.004 \cdot \Delta daytime - 1 \cdot 10^{-17} \quad (.6)$$

Difference of Exposure on Difference of Elevation angle

$$\Delta Exposure = -0.047 \cdot \Delta ElevAngle + 3 \cdot 10^{-16} \quad (.7)$$

Difference of Colorindex on Difference of Day time

$$\Delta ColIdx = 4.51 \cdot \Delta daytime - 1.2 \cdot 10^{-15} \quad (.8)$$

Difference of Colorindex on Difference of Elevation angle

$$\Delta ColIdx = -52 \cdot \Delta ElevAngle + 1.45 \cdot 10^{-14} \quad (.9)$$

Difference of Colorindex on Difference of Elevation angle

$$\Delta ColIdx = 3.5 \cdot \Delta ElevAngle - 6 \cdot 10^{-16} \quad (.10)$$

Figures to more plumes to one ref

Evaluation of the dependence of the BrO SCD on external dependence

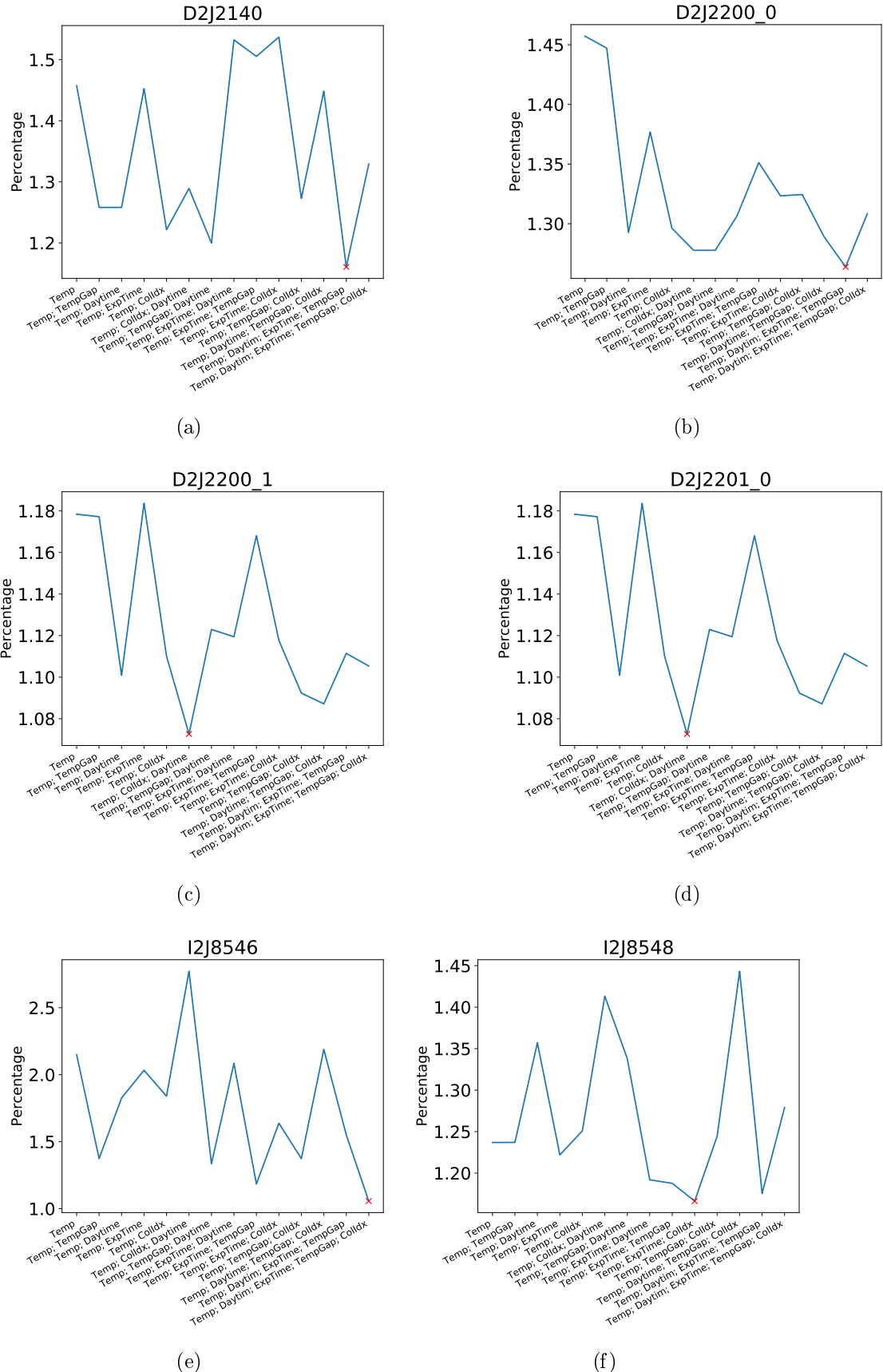


Figure .1:

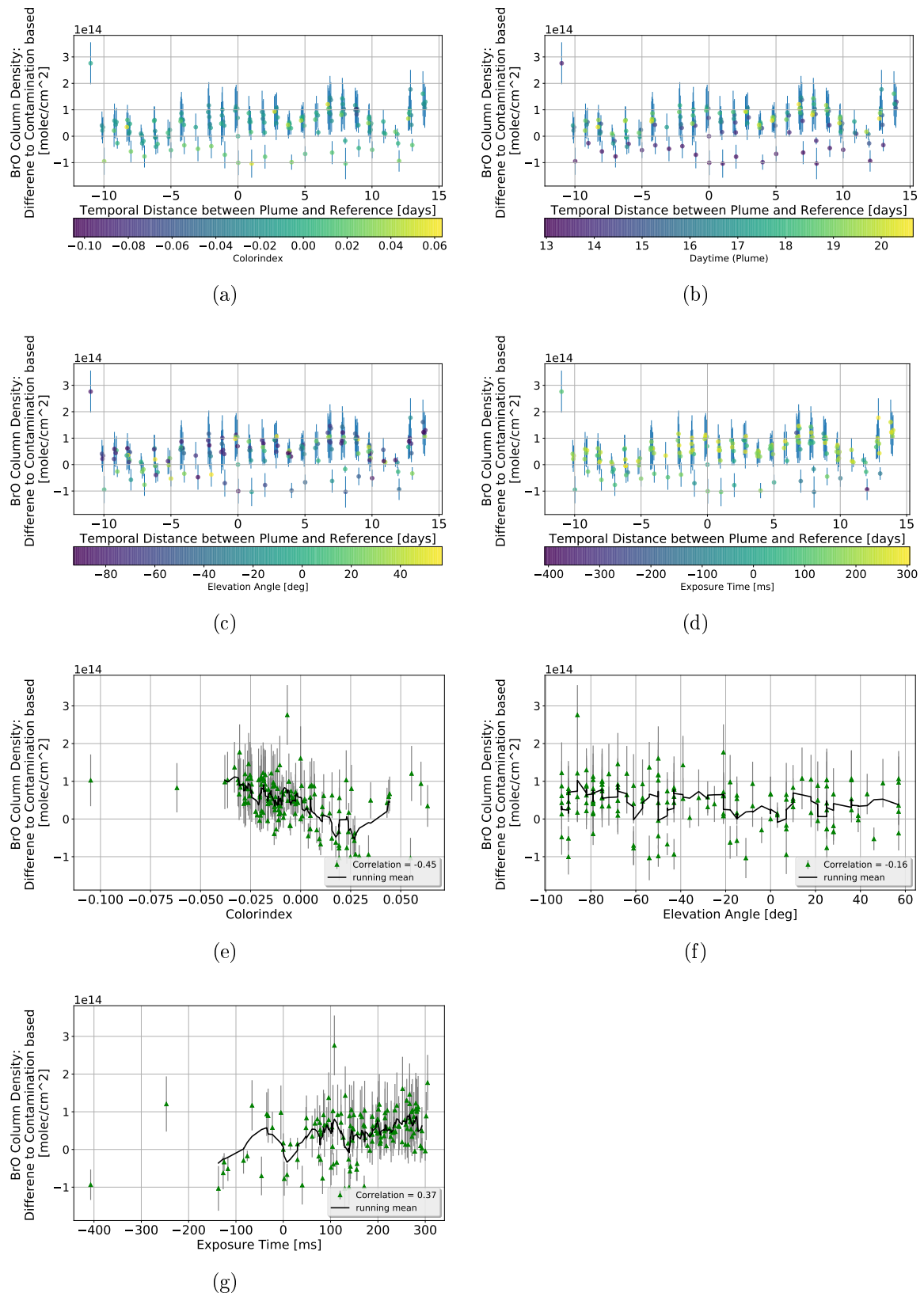


Figure .2:

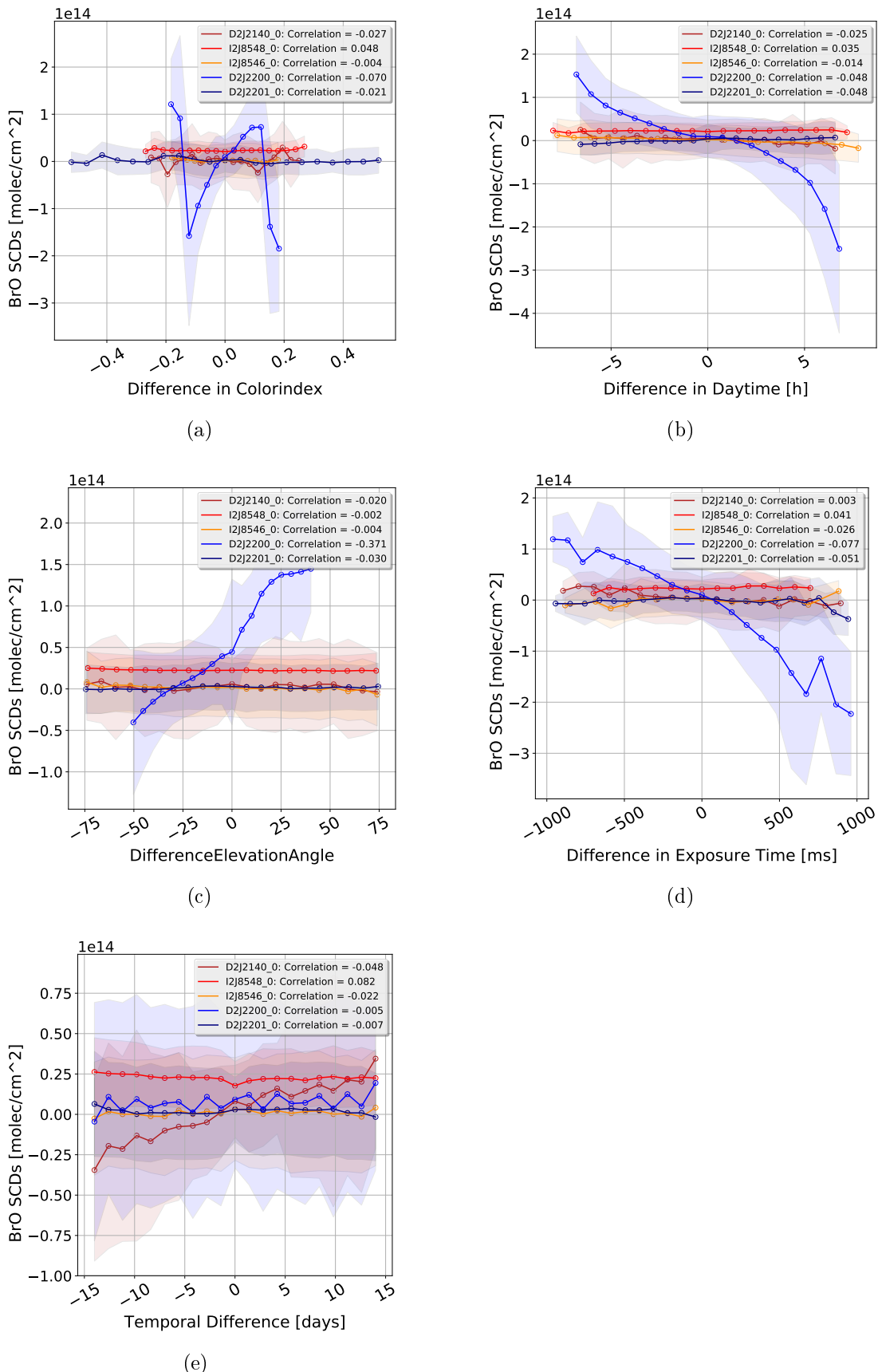


Figure .3:

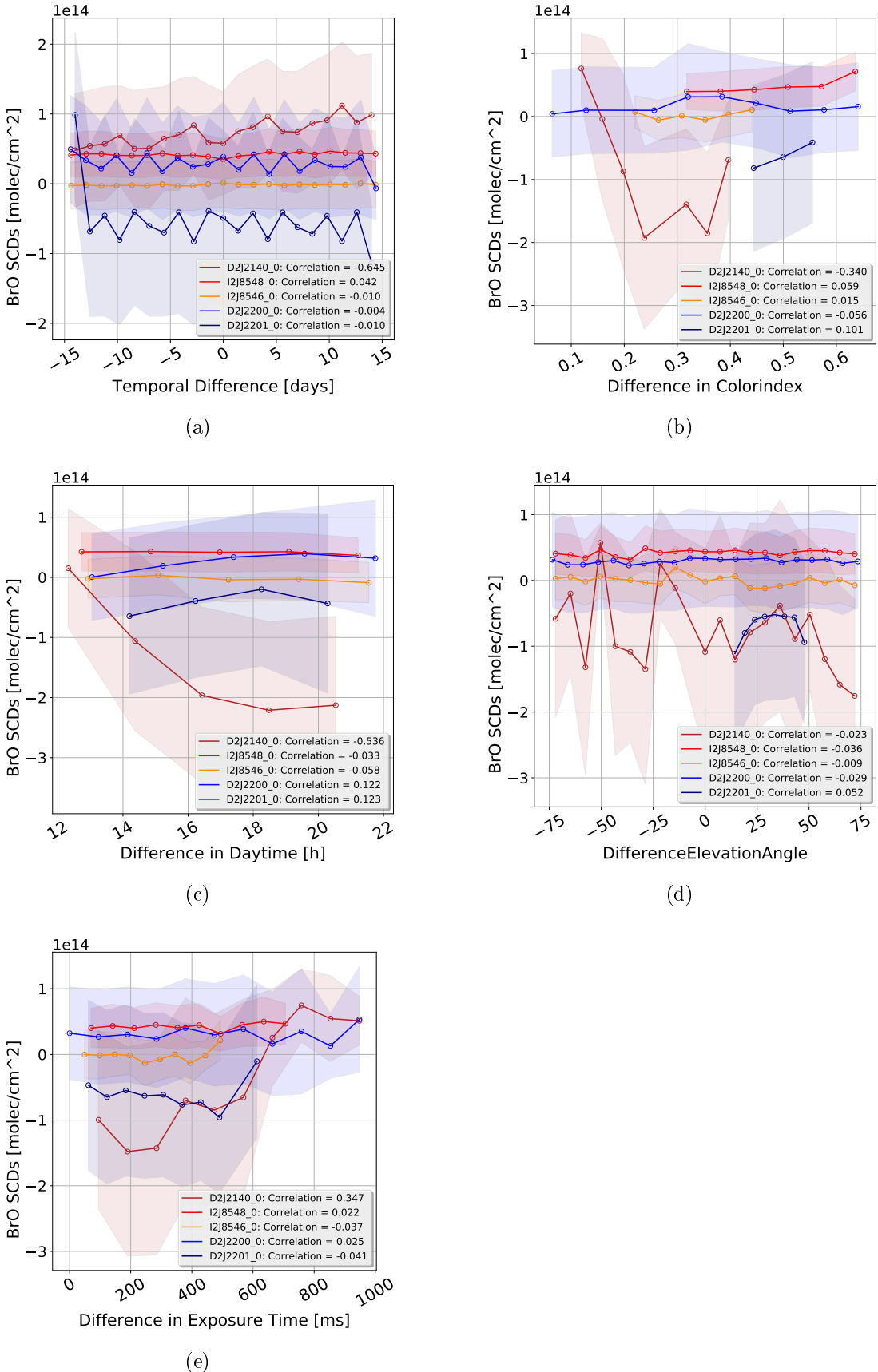


Figure .4:

A Lists

A.1 List of Figures

2.1	Influence of volcanic eruptions and quiet degassing on earth climate. Redrawn on the basis of Robock (2000)	11
2.2	schematic sketch of a Bromine Explosion. Release of HBr at the volcanic vent. Mixing with ambient air in the effective source region leads to Br formation. This resulting Bromine species react to BrO with ozone from the plume. Adapted from Bobrowski et al. (2007) . .	14
2.3	BrO/SO ₂ ratio as a function of the distance from the volcanic vent with a constant wind speed of 10 m/s. From Lübcke (2014)	15
2.4	Bromine reactions inside of a volcanic vent. The release of HBr at the volcanic vent is drawn in orange. Inside of aerosols heterogeneous dissociation with HOBr forms Br ₂ . Then Br ₂ splits photolytically into single Br radicals. BrO results through a reaction with O ₃ upon mixing with ambient air. Reactions with H ₂ O forms HOBr creating an autocatalytic cycle. The reaction cycle along the blue lines are called Bromine explosion. From Warnach (2015)	16
2.5	Dependency of the ratios of different volcanic trace gases on depth. Data originate from Stromboli volcano. From Lübcke (2014) repro- duced from Burton et al. (2007)	17
3.1	Schematic sketch of the DOAS measurement of volcanic plume con- stituents. The column density of the plume constituent of interest is retrieved by comparing the spectrum $I(\lambda)$ which is measured through the plume with the spectrum $I'_0(\lambda)$ measured outside of the plume. .	22
3.2	Basic idea of the DOAS principle: Light attenuate due to broad band and narrow band effects. The broad band extinction is caused by aerosols and Raylight scattering ($I_0 \rightarrow I'$). The measured intensity I is formed by narrow band effects due to differential absorption struc- tures by trace gases with the optical density τ' . Adapted from Kern (2009)	23
4.1	Global map of the volcanoes monitored by NOVAC. Used with friendly permission of Santiago Arellano.	28
4.2	schematic sketch of a NOVAC instrument. From Galle et al. (2010) .	29

4.3	Topographig Map of the Tungurahua Volcano. The predominant plume direction is shaded in yellow. Four NOVAC stations are shown as red squares, the corresponding scanning geometry is sketched with black lines. From Hidalgo et al. (2015)	30
5.1	(a) SO ₂ SCD as a function of the elevation angle with error bars computed by the DOASIS fitting routin. (b) BrO SCD as a function of the elevation angle with error bars computed by the DOASIS fitting routine. Taken from Warnach (2015)	34
5.2	NOVAC Evaluation: (a) Measurement at the volcano (b) Evaluation of the spectral data with the DOAS routine using the absorption cross sections of BrO and SO ₂ . (c) Finding the location of the plume and reference (d) (taken from Warnach (2015)) Computation of the ratios BrO/SO ₂ at Tungurahua. Bild noch ändern, letztes bild andere stil, verwechseln SO₂ und BrO absorbtion	34
5.3	(a) SO ₂ SCD as a function of the elevation angle. The co-added plume region is marked with red diamonds, and the co added reference region with green stars. From Warnach (2015). (b) Flow chart of the BrO and SO ₂ evaluation. From Lübcke (2014).	36
5.4	The decrease of the amount of data above the plume limit as a function of the plume limit. The plume limits below the actual plume limit of $7 \cdot 10^{17}$ are marked with a yellow shade. noch dazu: In Prozent sieht das in der Tat schrecklich aus, relevant für eine Zeitreihenanalyse ist aber eher die (absolute) Anzahl der Tage mit (Multi-Scan-)Daten. Vielleicht als zweites Bild daneben?!	37
5.5	Scan with a contaminated reference spectrum from April 2011. From Warnach (2015)	38
5.6	The strength of contamination as function of the mean SO ₂ amount of the day before. The strength of contamination is defined as the difference in SO ₂ SCD when evaluation with an alternative reference, or neglect the contamination. Left: data from Tungurahua. Right: data from Nevado Del Ruiz. Wie wurde mean SO₂ bestimmt? Wie sieht es bei max SO₂ aus? (Und eigentlich müsse man ja eher die SO₂ Emissionen anschauen. Die wir aber nicht (so einfach) kennen.)	41
6.1	BrO error distribution shown for all instruments considered in this thesis. The left plot shows the BrO distribution for the "same time retrieval", the left plot shows the BrO error distribution for the evaluation with a reference from another time, where the temporal difference between plume and reference is not longer than two weeks. The peaks for the single instrument are located at: D2J2140_0: 1.2e+13; I2J8548_0: 1.3e+13; I2J8546_0: 1.4e+13; D2J2200_0: 1.4e+13; D2J2201_0: 1.1e+13	43

6.2	Wavelength shift over the time. The shift is shown for six NOVAC-instruments from Tungurahua. The red and yellow dots show the running mean over 20 days. Red line indicates a temperature independent long term polynomial. Source: Warnach (2015)	45
6.3	The BrO error as a function of the temporal difference shown for the Pillate instrument from Tungurahua (2008-2009). (a) Temporal differences up to 400 days. (b) Temporal differences up to 120h. The periodical BrO error evolution indicates the impact of the daytime	46
6.4	Histogram showing the frequency of getting the best reference as function of the temporal difference between plume and reference measuring. A Gaussian-like distribution is retrieved. The red dotted line visualizes a Gaussian fit for the shown histogram.	48
6.5	The BrO measurement error as a function of the temporal difference in days between the reference and the plume is shown for each of the individual instruments at Tungurahua and Nevado del Ruiz. The instruments at Nevado del Ruiz are coloured in blue, while the instruments at Tungurahua are coloured in red colour tones. To evaluate the plume spectra all reference spectra with a temporal distance of no longer than two weeks are used. An increase of the BrO error with the absolute difference in temperature is observable. This is quantified by a correlation between the BrO retrieval error and the absolute temporal difference. The plots reveal a symmetry around the axis with zero temperature difference.	49
6.6	The BrO measurement error as a function of the difference of temperature between the reference and the plume is shown for each of the individual instruments at Tungurahua and Nevado del Ruiz. To evaluate the plume spectra all reference spectra with a temporal distance of no longer than two weeks are used. An increase of the BrO error with the absolute difference in temperature is observable. This is quantified by a correlation between the BrO retrieval error and the absolute difference in temperature. The plots reveal a symmetry around the axis with zero temperature difference.	50
6.7	Short term wavelength as a function of the instrument temperature for Pillate 1. The coloring of the scatter points indicate the temporal evolvement. (a) initial period prior to January 2010 (b) after 2010. Source: Warnach (2015).	51

6.13 An example of the dependency of external parameters on each other. The difference in temperature as a function of the exposure time. data from Tungurahua.	65
6.14 Correlation matrix of the external parameters. The correlation is discrete colour coded. Positive correlation is labeled with a plus whereas negative correlation is labeled with a minus. The correlation matrix is calculated using the data from D2J2140_0.	66
6.15 The BrO measurement error as a function of the temporal difference between measuring the reference and the plume are shown. Therefor, the reference spectra are restricted such that the maximal temperature difference between reference and plume is 1°C.	67
6.16 The BrO measurement error as a function of the exposure time difference between measuring the reference and the plume are shown. Therefor, the reference spectra are restricted such that the maximal color index difference between reference and plume is 0.05. The maximal daytime difference is 1h.	68
6.17 The BrO measurement error as a function of the color index difference between measuring the reference and the plume are shown. Therefor, the reference spectra are restricted such that the maximal temperature difference between reference and plume is 1°C. The maximal exposure time difference is 100ms.	69
6.18 The BrO measurement error as a function of the daytime difference between measuring the reference and the plume are shown. Therefor, the reference spectra are restricted such that the maximal temperature difference between reference and plume is 1°C. The maximal exposure time difference is 100ms.	70
6.19 One plume is evaluated by using different references. The plume is recorded at Tungurahua volcano with the D2J2140_0 instrument. The recording time was the 03.12.2008 at 16:46 o clock. The y axis shows the BrO column density difference between the NOVAC method and contamination based method. (a) The difference in BrO is plotted as a function of the temperature difference between the plume and the references. Every data point indicates one reference. (b) The difference in BrO is plotted as a function of the temporal difference between the one plume and the different references.	71
6.20 The BrO measurement value as a function of the difference of the external parameters between measuring the reference and the plume are shown.	73

7.1	Visualization of the contamination based Method. If the reference is contaminated a list of possible references is available, where the temporal difference between the plume and the reference is not longer than two weeks. For every possible reference, the estimated BrO error is calculated by considering the corresponding difference in important external parameters. The reference with the so calculated minima BrO error is used for the evaluation.	76
7.2	Deviation from the "optimal evaluation" as a function of the selection of differences in external parameters which are used for the evaluation. Here the utilized combination of external parameters are plotted on the x-axis and the deviation on the y-axis. The ideal combination (lowest deviation) is marked with a red cross.	78
8.1	Comparison of the results of contaminated data for performing the evaluation with the NOVAC-method and the contamination based method. Only data are used where the corresponding SO ₂ column density (retrieved from the contamination based method) lies above the plume limit of $SO_2_SCD > 7 \cdot 10^{17}$. The black solid line shows a linear fit of the data, the dotted line indicates where the both evaluation are equivalent. (a) Results for the BrO column densities from Tungurahua; (b) Results for the BrO column densities from Nevado Del Ruiz; (c) Results for the SO ₂ column densities from Tungurahua; (d) Results for the SO ₂ column densities from Nevado Del Ruiz . . .	84
8.2	Comparison of the results of contaminated data for performing the evaluation with the NOVAC-method and the contamination based method. Only data are used where the corresponding SO ₂ column density (retrieved from the contamination based method) lies above the plume limit of $SO_2_SCD > 7 \cdot 10^{17}$. (a)+(b): The black solid line shows a linear fit of the data, the dotted line indicates where the both evaluation are equivalent. (a) Results for the BrO /SO ₂ column densities from Tungurahua; (b) Results for the BrO /SO ₂ column densities from Nevado Del Ruiz. (c) +(d) The column density calculated with NOVAC was substracted from the corresponding column density retrieved with the contamination based method. The black valid line indicates a linear fit of the data, the dotted grey line shows where the difference is zero, that means both evaluations lead to the same ratio. (c) Tungurahua (d) Nevado Del Ruiz	88
8.3	Time series of the BrO/SO ₂ ratios for Nevado del Ruiz . The contaminated data are evaluated by using the contamination based method. Blue data points are below the detection limit, green data points are not contaminated, valid SO ₂ SCDs. Red data points are contaminated data, evaluated with the contamination based method.	90

8.4	Time series of the BrO/SO ₂ ratios for Tungurahua. The contaminated data are evaluated by using the contamination based method. Blue data points are below the detection limit, green data points are not contaminated, valid SO ₂ SCDs. Red data points are contaminated data, evaluated with the contamination based method.	91
8.5	BrO/SO ₂ ratio daily mean time series for Nevado del Ruiz (left) and Tungurahua (right). SO ₂ SCDs used for this plot are above the plume limit of $7 \cdot 10^{17}$. The minimum amount of data per day are four. Days where less than four valid ratios are recorded are not considered in this plot. As a result of using the contaminated data as well more daily means are available, since more days have an amount of valid data's above four. Those dates are marked with red. The other data are colored in green.	92
9.1	Visualization of the contamination of the plume. An old plume of the day before. Due to a lack of wind the plume sinks down and accumulates above the instrument. The light path through the old plume is longer when recording the reference spectra (orange).	94
9.2	Visualization of possible scenarios for contamination. Left: the plume sinks in the way that the instrument is within the plume, therefore, all elevation angles will contain volcanic trace gases, while the plume is not additionally contaminated. Right: the plume covers the hole sky, thus all elevation angles "see" volcanic trace gases.	94
.1	99
.2	100
.3	101
.4	102

A.2 List of Tables

2.1	Volcanic gas constituents at the emission vent and global estimated source strength. Adapted from Textor et al. (2004)	12
2.2	Technical data of the instruments installed at the Tungurahua volcano.	19
2.3	Technical data of the instruments installed at the Nevado Del Ruiz volcano.	20
6.1	Amount of possible references when restricting the time span between plume and reference to two weeks. Here in the "Mean" and "Std" row for each instrument the average restriction is shown with the corresponding standard deviation. The "Min" and "Max" rows show the extend of restriction in the extreme cases (minimum and maximum amount of available references / restriction ratio).	47

6.2	The BrO measurement error as a function of the difference of temperature between the reference and the plume is fitted with a first order polynomial for each of the individual instruments at Tungurahua and Nevado del Ruiz. This table shows the fitting parameters slope and zero point. Moreover, the correlation between the BrO error and the absolute temperature difference is shown. For the temperature difference this correlation with an average of 0.797 is the highest compared to the other external parameters. In the ΔT_2 row the temperature difference for which the error doubles compared to a temperature difference of zero is shown. This is already the case for a difference of $3.3^\circ C$	52
6.3	This table shows the absolute amount and the ratio (to Table 6.1) of remaining references if restricting the temperature difference to the mean ΔT_2 over all instruments ($Mean(\Delta T_2) = 3.3^\circ C$). Here in the "Mean" and "Std" row for each instrument the average restriction is shown with the corresponding standard deviation. The "Min" and "Max" rows show the extend of restriction in the extreme cases (minimum and maximum amount of available references / restriction ratio).	54
6.4	The BrO measurement error as a function of the difference of daytime between the reference and the plume is fitted with a first order polynomial for each of the individual instruments at Tungurahua and Nevado del Ruiz. This table shows the fitting parameters slope and zero point. Moreover, the correlation between the BrO error and the absolute daytime difference is shown. In the ΔDT_2 row the daytime difference for which the error doubles compared to a daytime difference of zero is shown.	56
6.5	This table shows the absolute amount and the ratio (to Table 6.1) of remaining references if restricting the daytime difference to the mean ΔDT_2 over all instruments except I2J8546_0 due to the large uncertainty ($Mean(\Delta DT_2) = 4.75h$). Here in the "Mean" and "Std" row for each instrument the average restriction is shown with the corresponding standard deviation. The "Min" and "Max" rows show the extend of restriction in the extreme cases (minimum and maximum amount of available references / restriction ratio).	57
6.6	The BrO measurement error as a function of the difference of colorindex between the reference and the plume is fitted with a first order polynomial for each of the individual instruments at Tungurahua and Nevado del Ruiz. This table shows the fitting parameters slope and zero point. Moreover, the correlation between the BrO error and the absolute colorindex difference is shown. In the ΔCI_2 row the colorindex difference for which the error doubles compared to a colorindex difference of zero is shown.	57

6.7 This table shows the absolute amount and the ratio (to Table 6.1) of remaining references if restricting the colorindex difference to the mean ΔCI_2 over all instruments ($Mean(\Delta CI_2) = 0.2553$). Here in the "Mean" and "Std" row for each instrument the average restriction is shown with the corresponding standard deviation. The "Min" and "Max" rows show the extend of restriction in the extreme cases (minimum and maximum amount of available references / restriction ratio).	58
6.8 The BrO measurement error as a function of the difference of elevation angle between the reference and the plume is fitted with a first order polynomial for each of the individual instruments at Tungurahua and Nevado del Ruiz. This table shows the fitting parameters slope and zero point. Moreover, the correlation between the BrO error and the absolute elevation angle difference is shown.	58
6.9 The BrO measurement error as a function of the difference of exposure time between the reference and the plume is fitted with a first order polynomial for each of the individual instruments at Tungurahua and Nevado del Ruiz. This table shows the fitting parameters slope and zero point. Moreover, the correlation between the BrO error and the absolute exposure time difference is shown.	63
6.10 Amount of possible references when restricting the difference in exposure time between plume and reference to differences below 632.25 ms.	63
6.11 Amount of possible references while restricting the difference in colorindex between plume and reference to differences above 0.255. maximal Time difference is $3.358^\circ C$, maximal daytime difference is 4.75h without Exposure Time between plume and reference to differences below 632.25 ms.	64
7.1 The correlation coefficients between the BrO measurement error and the different external parameters. As a correlation value both the average and the maximum correlation is given.	79
7.2 The results of the fitting with a first order polynomial. The constants of Equation (7.3) are calculated. The value shows the actual number. The importance, referred to as import, indicates the relative impact on the evaluation. (a)Data from Nevado Del Ruiz from the D2J2201_0 instrument. (b)Data from Nevado Del Ruiz from the D2J2200_0 instrument. Data from Nevado Del Ruiz from both instrument.	80

7.3	The results of the fitting with a first order polynomial. The value shows the actual number. The importance, referred to as import, indicates the relative impact on the evaluation. The constants of Equation (7.3) are calculated. (a)Data from Tungurahua from the instrument. (b)Data from Tungurahua from the instrument. (c) Data from Tungurahua averaged over all instrument. both instruments Tungurahua	81
-----	---	----

B Bibliography

Smithsonian Institution global volcanism program. <https://volcano.si.edu/>. Accessed: 2018-03-20.

NOVAC novac-site. <http://www.novac-project.eu/>. Accessed: 2018-01-29.

Python scikit-learn.org. http://scikit-learn.org/stable/modules/generated/sklearn.linear_model.LinearRegression.html. Accessed: 2018-01-19.

N Bobrowski and G Giuffrida. Bromine monoxide/sulphur dioxide ratios in relation to volcanological observations at mt. *Etna*, 2009:433–445, 2006.

N Bobrowski and U Platt. So₂/bro ratios studied in five volcanic plumes. *Journal of Volcanology and Geothermal Research*, 166(3-4):147–160, 2007.

N Bobrowski, G Hönninger, B Galle, and U Platt. Detection of bromine monoxide in a volcanic plume. *Nature*, 423(6937):273, 2003.

Nicole Bobrowski, R Von Glasow, A Aiuppa, S Inguaggiato, I Louban, OW Ibrahim, and U Platt. Reactive halogen chemistry in volcanic plumes. *Journal of Geophysical Research: Atmospheres*, 112(D6), 2007.

JP Burrows, A Richter, A Dehn, B Deters, S Himmelmann, S Voigt, and J Orphal. Atmospheric remote-sensing reference data from gome—2. temperature-dependent absorption cross sections of o₃ in the 231–794 nm range. *Journal of quantitative spectroscopy and radiative transfer*, 61(4):509–517, 1999.

Mike Burton, Patrick Allard, Filippo Muré, and Alessandro La Spina. Magmatic gas composition reveals the source depth of slug-driven strombolian explosive activity. *Science*, 317(5835):227–230, 2007.

Markus Bussemer. Der ring-effekt: Ursachen und einfluß auf die spektroskopische messung stratosphärischer spurenstoffe. *Diplomathesis, University of Heidelberg*, 1993.

K Chance and RL Kurucz. An improved high-resolution solar reference spectrum for earth's atmosphere measurements in the ultraviolet, visible, and near infrared. *Journal of quantitative spectroscopy and radiative transfer*, 111(9):1289–1295, 2010.

Oliver C Fleischmann, Matthias Hartmann, John P Burrows, and Johannes Orphal. New ultraviolet absorption cross-sections of bro at atmospheric temperatures measured by time-windowing fourier transform spectroscopy. *Journal of Photochemistry and Photobiology A: Chemistry*, 168(1-2):117–132, 2004.

Bo Galle, Mattias Johansson, Claudia Rivera, Yan Zhang, Manne Kihlman, Christoph Kern, Thomas Lehmann, Ulrich Platt, Santiago Arellano, and Silvana Hidalgo. Network for observation of volcanic and atmospheric change (novac)—a global network for volcanic gas monitoring: Network layout and instrument description. *Journal of Geophysical Research: Atmospheres*, 115(D5), 2010.

TM Gerlach. Volcanic sources of tropospheric ozone-depleting trace gases. *Geochemistry, Geophysics, Geosystems*, 5(9), 2004.

Hans-F Graf, Johann Feichter, and Bärbel Langmann. Volcanic sulfur emissions: Estimates of source strength and its contribution to the global sulfate distribution. *Journal of Geophysical Research: Atmospheres*, 102(D9):10727–10738, 1997.

Minard L Hall, Claude Robin, Bernardo Beate, Patricia Mothes, and Michel Monzier. Tungurahua volcano, ecuador: structure, eruptive history and hazards. *Journal of Volcanology and Geothermal Research*, 91(1):1–21, 1999.

Martina M Halmer, H-U Schmincke, and H-F Graf. The annual volcanic gas input into the atmosphere, in particular into the stratosphere: a global data set for the past 100 years. *Journal of Volcanology and Geothermal Research*, 115(3-4): 511–528, 2002.

C Hermans, AC Vandaele, S Fally, M Carleer, R Colin, B Coquart, A Jenouvrier, and M-F Merienne. Absorption cross-section of the collision-induced bands of oxygen from the uv to the nir. In *Weakly interacting molecular pairs: unconventional absorbers of radiation in the atmosphere*, pages 193–202. Springer, 2003.

Silvana Hidalgo, Jean Battaglia, Santiago Arellano, Alexander Steele, Benjamin Bernard, Julie Bourquin, Bo Galle, Santiago Arrais, and Freddy Váscone. So₂ degassing at tungurahua volcano (ecuador) between 2007 and 2013: Transition from continuous to episodic activity. *Journal of Volcanology and Geothermal Research*, 298:1–14, 2015.

IPCC. *Summary for Policymakers*, book section SPM, page 1–30. Cambridge University Press, Cambridge, United Kingdom and New York, NY, USA, 2013. ISBN ISBN 978-1-107-66182-0. doi: 10.1017/CBO9781107415324.004. URL www.climatechange2013.org.

Christoph Kern. *Spectroscopic measurements of volcanic gas emissions in the ultraviolet wavelength region*. PhD thesis, 2009.

Stefan Kraus. *DOASIS: A framework design for DOAS*. Shaker, 2006.

Peter Lübcke. *Optical remote sensing measurements of bromine and sulphur emissions: Investigating their potential as tracers of volcanic activity.* PhD thesis, 2014.

Peter Lübcke, Nicole Bobrowski, S Arellano, Bo Galle, G Garzón, Leif Vogel, and U Platt. Bro/so 2 molar ratios from scanning doas measurements in the novac network. *Solid Earth*, 5(1):409, 2014.

Richard Meller and Geert K Moortgat. Temperature dependence of the absorption cross sections of formaldehyde between 223 and 323 k in the wavelength range 225–375 nm. *Journal of Geophysical Research: Atmospheres*, 105(D6):7089–7101, 2000.

Kimio Noguchi and Hiroshi Kamiya. Prediction of volcanic eruption by measuring the chemical composition and amounts of gases. *Bulletin Volcanologique*, 26(1): 367–378, 1963.

Maddalena Pennisi and Marie-Françoise Le Cloarec. Variations of cl, f, and s in mount etna’s plume, italy, between 1992 and 1995. *Journal of Geophysical Research: Solid Earth*, 103(B3):5061–5066, 1998.

D Perner and U Platt. Detection of nitrous acid in the atmosphere by differential optical absorption. *Geophysical Research Letters*, 6(12):917–920, 1979.

G Pinardi, MV Rozendaal, and C Fayt. The influence of spectrometer temperature variability on the data retrieval of so2. *NOVAC second annual activity report, NOVAC consortium*, 44:48, 2007.

U Platt and N Bobrowski. Quantification of volcanic reactive halogen emissions. *Volcanism and Global Change*, eds A. Schmidt, K. Fristad, L. Elkins-Tanton, Cambridge University Press, Cambridge, UK, ISBN, 1466525386, 2015.

Ulrich Platt and Jochen Stutz. Differential absorption spectroscopy. *Differential Optical Absorption Spectroscopy*, pages 135–174, 2008.

Alan Robock. Volcanic eruptions and climate. *Reviews of Geophysics*, 38(2):191–219, 2000.

GG Salerno, MR Burton, C Oppenheimer, T Caltabiano, VI Tsanev, and N Bruno. Novel retrieval of volcanic so2 abundance from ultraviolet spectra. *Journal of Volcanology and Geothermal Research*, 181(1-2):141–153, 2009.

A Schmidt and A Robock. Volcanism, the atmosphere and climate through time. *Volcanism Glob. Environ. Chang*, pages 195–207, 2015.

Anja Schmidt, Kirsten Fristad, and Linda T Elkins-Tanton. Volcanism and global environmental change, 2015.

Hans-Ulrich Schmincke. *Vulkanismus*. Wissenschaftliche Buchgesellschaft, 3 edition, 2000.

S Solomon, RW Portmann, RR Garcia, W Randel, F Wu, R Nagatani, J Gleason, L Thomason, LR Poole, and MP McCormick. Ozone depletion at mid-latitudes: Coupling of volcanic aerosols and temperature variability to anthropogenic chlorine. *Geophysical research letters*, 25(11):1871–1874, 1998.

Susan Solomon, Arthur L Schmeltekopf, and Ryan W Sanders. On the interpretation of zenith sky absorption measurements. *Journal of Geophysical Research: Atmospheres*, 92(D7):8311–8319, 1987.

Christiane Textor, Hans-F Graf, Claudia Timmreck, and Alan Robock. Emissions from volcanoes. In *Emissions of Atmospheric Trace Compounds*, pages 269–303. Springer, 2004.

Thorvaldur Thordarson and Stephen Self. Atmospheric and environmental effects of the 1783–1784 laki eruption: A review and reassessment. *Journal of Geophysical Research: Atmospheres*, 108(D1), 2003.

S Twomey. Pollution and the planetary albedo. *Atmospheric Environment (1967)*, 8(12):1251–1256, 1974.

Ann Carine Vandaele, Christian Hermans, Paul C Simon, Michel Carleer, Réginald Colin, Sophie Fally, Marie-France Merienne, Alain Jenouvrier, and Bernard Coquart. Measurements of the no₂ absorption cross-section from 42 000 cm⁻¹ to 10 000 cm⁻¹ (238–1000 nm) at 220 k and 294 k. *Journal of Quantitative Spectroscopy and Radiative Transfer*, 59(3-5):171–184, 1998.

Ann Carine Vandaele, Christian Hermans, and Sophie Fally. Fourier transform measurements of so₂ absorption cross sections: II.: Temperature dependence in the 29 000–44 000 cm⁻¹ (227–345 nm) region. *Journal of Quantitative Spectroscopy and Radiative Transfer*, 110(18):2115–2126, 2009.

Leif Vogel. *Volcanic plumes: Evaluation of spectroscopic measurements, early detection, and bromine chemistry*. PhD thesis, 2011.

T Wagner, A Apituley, S Beirle, S Dörner, U Friess, J Remmers, and R Shaiganfar. Cloud detection and classification based on max-doas observations. *Atmospheric Measurement Techniques*, 7(5):1289–1320, 2014.

Simon Warnach. Improvements of bro and so₂ retrievals of novac data - tungurahua volcano as a case study. Master's thesis, 2015.

Erklärung:

Ich versichere, dass ich diese Arbeit selbstständig verfasst habe und keine anderen als die angegebenen Quellen und Hilfsmittel benutzt habe.

Heidelberg, den (Datum)